“Crosstalk between the MEK5/ERK5 and PKB/FoxO pathways: underlying mechanism and its relevance for vasoprotection and tumorigenesis”

~ ~ ~

“Interaktion zwischen dem MEK5/ERK5-Signalweg und der PKB/FoxO Signalkaskade: zugrunde liegender Mechanismus und seine Relevanz für Gefäßerhalt und Tumorgenese”

Doctoral thesis for a doctoral degree at the Graduate School of Life Sciences

Julius-Maximilians-Universität Würzburg

Section Biomedicine

Submitted by

Lorenza Fusi

From Gavardo (BS) - Italy

Würzburg, 2022

This document is licensed under the Creative Commons Attribution 4.0 International License (CC BY 4.0):
http://creativecommons.org/licenses/by/4.0 This CC license does not apply to third party material (attributed to another source) in this publication.

Submitted on: _____

Office stamp

MEMBERS OF THE THESIS COMMITTEE

Chairperson: Prof. Dr. Manfred Gessler

Primary Supervisor: Prof. Dr. Marc Schmidt

Supervisor (Second): Prof. Dr. Elke Butt-Dörje

Supervisor (Third): Dr. David Schrama

Date of Public Defence: _____

Date of Receipt of Certificates: _____

AFFIDAVIT

I hereby confirm that my thesis entitled "Crosstalk between the MEK5/ERK5 and PKB/FoxO pathways: underlying mechanism and its relevance for vasoprotection and tumorigenesis" is the result of my own work. I did not receive any help or support from commercial consultants. All sources and/or materials applied are listed and specified in the thesis.

Furthermore, I confirm that this thesis has not yet been submitted as part of another examination process neither in identical nor in similar form.

Place, Date

Signature

EIDESSTATTLICHE ERKLÄRUNG

Hiermit erkläre ich an Eides statt, die Dissertation „Interaktion zwischen dem MEK5/ERK5-Signalweg und der PKB/FoxO Signalkaskade: zugrunde liegender Mechanismus und seine Relevanz für Gefäßerhalt und Tumorgenese" eigenständig, d.h. insbesondere selbständig und ohne Hilfe eines kommerziellen Promotionsberaters, angefertigt und keine andere als die von mir angegebenen Quellen und Hilfsmittel verwendet zu haben.

Ich erkläre außerdem, dass die Dissertation weder in gleicher noch in ähnlicher Form bereits in einem anderen Prüfungsverfahren vorgelegen hat.

Ort, Datum

Unterschrift

TABLE OF CONTENTS

MEMBERS OF THE THESIS COMMITTEE - 3 -

AFFIDAVIT - 5 -

EIDESSTATTLICHE ERKLÄRUNG - 5 -

TABLE OF CONTENTS - 7 -

FIGURES AND TABLES LIST - 11 -

FIGURES AND SUPPLEMENTARY FIGURES - 11 -

TABLE AND SUPPLEMENTARY TABLES - 11 -

LIST OF ABBREVIATIONS - 12 -

SUMMARY - 15 -

ZUSAMMENFASSUNG - 16 -

INTRODUCTION - 18 -

THE FORKHEAD BOX O TRANSCRIPTION FACTORS - 18 -

THE FORKHEAD BOX TRANSCRIPTION FACTORS SUPERFAMILY - 18 -

THE FOXOS: FROM THE WORMS TO THE HUMANS - 18 -

THE REGULATION OF FOXO PROTEINS - 20 -

THE ROLE OF FOXO PROTEINS IN THE ENDOTHELIUM - 23 -

THE FOXO TRANSCRIPTION FACTORS IN PATHOLOGICAL CONDITIONS - 24 -

THE FOXOS AS TRANSCRIPTION FACTORS: TISSUE-SPECIFIC GENE CONTROLLERS? - 25 -

THE FOXO SYSTEM IN THE PRACTICAL LABORATORY ROUTINE - 27 -

THE MEK5/ERK5 CASCADE - 28 -

THE MITOGEN-ACTIVATED PROTEIN KINASE FAMILY - 28 -

THE UNICITY OF MEK5/ERK5 CASCADE - 28 -

THE ROLE OF THE MEK5/ERK5 CASCADE IN CELLS AND TISSUES - 29 -

THE ENDOTHELIUM AND THE MEK5/ERK5 SIGNALLING WAY - 30 -

First evidence of FoxO3 negative regulation by the MEK5/ERK5 cascade - 31 -

Scope of the project - 33 -

Results - 34 -

The antagonism between FoxOs and the MEK5/ERK5 pathway - 34 -

A new FoxO3 construct suitable for interaction studies and its functional validation - 34 -

The effect of the MEK5/ERK5 activation on FoxO3 localization - 36 -

The modulation of FoxO3-interactome by the MEK5/ERK5 pathway - 38 -

The interaction of FoxO factors with TRRAP - 41 -

TRRAP and the histone acetyltransferase complexes - 41 -

Nuclear interaction between FoxO3 and TRRAP in HUVEC and HEK293 - 42 -

TRRAP binds to other FoxO family members in HEK293 - 44 -

TRRAP is required for FoxO3 transcriptional activity in HUVEC - 46 -

FoxO3-dependent apoptosis and cell cycle arrest depend on TRRAP expression - 48 -

FoxO3 transcriptional activity is promoted by TRRAP in osteosarcoma cells - 50 -

Discussion and outlook - 51 -

Materials - 56 -

Materials and buffers - 56 -

Cloning - 56 -

Agarose gel electrophoresis - 56 -

Cell culture - 57 -

Cell manipulation - 58 -

Calcium-Phosphate transfection - 59 -

DEAD-Dextran transfection - 59 -

DNA analysis - 59 -

RNA analysis - 60 -

Immunofluorescence - 60 -

Protein analysis - 61 -

Western Blot - 62 -

Immunoprecipitation - 64 -

Mass spectrometry - 64 -

TRRAP status definition - 65 -

Commercial kits and consumables - 66 -

TECHNICAL EQUIPMENT - 67 -

SOFTWARE - 68 -

METHODS - 69 -

CLONING OF NEW PLASMIDS - 69 -

CLONING OF 3XHA.FOXO3.A3.ER AND 3XHA.FOXO3.A3.ER(H212R) - 69 -

BACTERIA TRANSFORMATION AND PLASMIDIC DNA ISOLATION - 72 -

CELL CULTURE - 72 -

THAWING OF CELLS - 72 -

PASSAGING, COUNTING, AND RESEEDING OF CELLS - 72 -

FREEZING OF CELLS - 73 -

CULTURING CONDITIONS - 73 -

CELL TRANSDUCTION AND TRANSFECTION - 74 -

GENERATION OF STABLE RETROVIRUS-PRODUCING CELL LINES - 74 -

RETROVIRAL TRANSDUCTION - 74 -

DEAD-DEXTRAN TRANSFECTION - 74 -

CALCIUM-PHOSPHATE TRANSFECTION - 75 -

TRANSFECTION OF SIRNA - 75 -

CELL CYCLE AND APOPTOSIS ANALYSIS - 76 -

MRNA EXPRESSION ANALYSIS: TWO-STEP REAL-TIME PCR - 77 -

FIRST STEP: MRNA EXTRACTION AND CDNA SYNTHESIS - 77 -

SECOND STEP: QUANTITATIVE REAL-TIME PCR - 77 -

APPLICATION OF LSS - 78 -

IMMUNOFLUORESCENT STAINING - 79 -

PROTEIN EXTRACTION - 79 -

TOTAL CELL LYSIS - 79 -

EXTRACTION OF NUCLEAR AND CYTOPLASMIC FRACTIONS - 80 -

DETERMINATION OF PROTEIN CONCENTRATION - 80 -

WESTERN BLOT - 80 -

IMMUNOPRECIPITATIONS - 81 -

ANALYSIS OF FOXO3-NUCLEAR-INTERACTOME - 82 -

LUCIFERASE ASSAY - 84 -

GDNA EXTRACTION AND TRRAP STATUS DETERMINATION - 84 -

STATISTICAL EVALUATION - 85 -

SUPPLEMENTARY MATERIAL - 86 -

REFERENCES - 90 -

ACKNOWLEDGEMENTS - 98 -

PUBLICATIONS LIST - 101 -

CURRICULUM VITAE - 103 -

FIGURES AND TABLES LIST

Figures and supplementary figures

Figure 1: Representation of FoxO proteins and their most important domains in H. sapiens..... - 19 -
Figure 2: Illustration of the main mechanism of FoxO regulation.....- 20 -
Figure 3: Cartoon explaining the inducible system established to study FoxO functions. .....- 27 -
Figure 4: Schematic representation of the MEK5/ERK5 pathway. .....- 29 -
Figure 5: The effect of MEK5/ERK5 activity on FoxO3-dependent apoptosis and transcription in HUVEC.....- 32 -
Figure 6: 3xHA.FoxO3.A3.ER activation causes apoptosis and is counteracted by the MEK5/ERK5 cascade. .....- 35 -
Figure 7: The MEK5/ERK5 pathway does not affect FoxO3 localization. .....- 37 -
Figure 8: Analysis of FoxO3-interactome in absence and presence of MEK5D. ..... - 40 -
Figure 9: FoxO3 interacts with TRRAP in the nucleus in both HUVEC and in HEK293. .....- 43 -
Figure 10: TRRAP interacts with FoxO4 in HEK293 and does not bind to the FoxO-DB domain. .- 45 -
Figure 11: TRRAP augments FoxO3 transactivation.....- 47 -
Figure 12: FoxO3-TRRAP interaction is essential for FoxO3 to trigger apoptosis..... - 49 -
Figure 13: TRRAP binds to FoxO3 and sustains FoxO3-dependent transcription in UTA-6.....- 50 -
Figure 14: Illustration of the new potential regulatory mechanism of FoxO proteins.....- 54 -
Figure 15: Determination of TRRAP status in melanoma cell lines.....- 55 -
Figure 16: Cartoon describing the cloning process of pBP-3xHA.FoxO3.A3.ER.....- 70 -
Figure 17: Representation of the cloning history of pBP-3xHA.FoxO3.A3.ER(H212R)..... - 71 -

Suppl. Figure 1: Density controls for the phase contrast pictures in Figure 6B. ..... - 86 -
Suppl. Figure 2: Negative controls for the IF in Figure 7A..... - 86 -

Table and supplementary tables

Table 1: Summary of the main PTMs of FoxOs and the responsible enzymes.....- 22 -

Suppl. Table 1: Enriched nuclear FoxO3-binding proteins without and with MEK5D.....- 87 -
Suppl. Table 2: Potential FoxO3-interacting proteins differentially regulated by MEK5D..... - 89 -

LIST OF ABBREVIATIONS

4-OHT: 4-hydroxytamoxifen

AMPK: Adenosine monophosphate-activated protein kinase

ANGPT2: Angiopoietin 2

APS: Ammonium persulfate

ATM: Ataxia-telangiectasia mutated

ATR: Ataxia- and Rad3-related

BCL2L11: BCL2-like protein 11 (or BIM)

BMK1: Big MAP kinase 1 (or ERK5)

BSA: Bovine serum albumin

CBP: CREB-binding protein

CDKN1B: Cyclin-dependent kinase inhibitor 1B (or $p27^{kip1}$)

cDNA: Complementary DNA

C_t: Threshold cycle

CUL1: Cullin-1

DB domain: DNA-binding domain

DBE: DAF-16 binding element

DMAP1: DNA methyltransferase 1-associated protein 1

DMEM: Dulbecco's modified eagle medium

DMSO: Dimethyl sulfoxide

DNA-PK: DNA-dependent protein kinase

dsDNA: Double strand DNA

DTT: Dithiothreitol

ECL: Enhanced chemiluminescence

ECs: Endothelial cells

EDTA: Ethylenediaminetetraacetic acid

EGFP: Enhanced green fluorescent protein

EGTA: Ethylene glycol-bis(β-aminoethyl ether)-N,N,N′,N′-tetra acetic acid

ELB: E1A lysis buffer

eNOS: Endothelial nitric oxide synthase

EP400: E1A-binding protein p400

ER: Oestrogen receptor

ERK: Extracellular signal-regulated kinase

FANCD2: Fanconi anaemia complementation group D2

FBS: Foetal bovine serum

FDR: False discovery rate

Fox: Forkhead box

FOX domain: "Forkhead" or "Winged-helix" domain

FoxO: Forkhead box O

FoxOs: FoxO1, FoxO3 and FoxO4

FREs: FoxO responsive elements

gDNA: Genomic DNA

GF: Growth factor

HA: Human influenza hemagglutinin

HAT: Histone acetyltransferase

HAUSP: Herpes-virus-associated ubiquitin specific protease (or USP7)

HEPES: 4-(2-hydroxyethyl)-1-piperazineethanesulfonic acid

HIF1: Hypoxia-inducible factor 1

HUVEC: Human umbilical vein endothelial cells

IFs: Immunofluorescent stainings

IGF1: Insulin-like growth factor 1

IGFBP1: IGF binding protein 1

IP: Immunoprecipitation

IRE: Insulin-responsive element

JNK: Jun-N-terminal kinase

KLF2 and 4: Krüppel-like factors 2 and 4

LAP-tag: Localization and purification tag

LB: Lysogeny broth

LFQ: Label-free quantification

LSS: Laminar shear stress

MAPKKKs: MAPK kinase kinases

MAPKKs: MAPK kinases

MAPKs: Mitogen-activated protein kinases

MEK5: MAPK/ERK kinase 5

MEK5D: Constitutively active mutant of MEK5

MDM2: MDM2 proto-oncogene

MS: Mass spectrometry

MST1: Mammalian sterile 20-like kinase 1

mTOR: Mammalian target of rapamycin

NanoLC-MS/MS: Nano-liquid chromatography-tandem MS

NES: Nuclear export signal

NF-κB: Nuclear factor kappa B

NLS: Nuclear localization signal

OD: Optical density, a measurement of absorbance

PAIMP: Phorbol-12-myristate-13-acetate-induced protein 1 (or NOXA)

PARP1: Poly(ADP-ribose) polymerase 1

PB1 domain: Phox and Bem1 domain

PBS: Phosphate-buffered saline

PCR: Polymerase chain reaction

PI: Propidium iodide

PI3K: Phosphoinositide-3-kinase

PIKKs: PI3K-related kinases

PKB: Protein kinase B (or AKT)

PMSF: Phenylmethylsulphonyl fluoride

PRMT1: Protein arginine methyltransferase 1

PTMs: Post-translational modifications

PVDF: Polyvinylidene fluoride

qPCR: Quantitative real-time PCR

ROS: Reactive oxygen species

RPMI: Roswell Park Memorial Institute 1640 medium

SD: Standard deviation

SDS: Sodium dodecyl sulphate

SETD7: SET domain containing 7, histone lysine methyltransferase (or SET9)

SGK: Serum and glucocorticoid-induced kinase

SIRT1 and 2: Sirtuin 1 and 2

siSCR: Scrambled siRNA

siTRRAP: Pool of two siRNAs against *TRRAP* gene

SKP2: S-phase kinase associated protein 2

SMG1: Suppressor of morphogenesis in genitalia 1

TA: Transactivation domain

TBS: Tris buffered saline

TEMED: Tetramethylethylenediamine

TEV: Tobacco etch virus

TFs: Transcription factors

TNF: Tumour necrosis factor

TRRAP: Transformation/Transcription domain-associated protein

VCAM1: Vascular cell adhesion molecule 1

VEGF: Vascular endothelial growth factor

SUMMARY

Forkhead box O transcription factors are a family of proteins involved in cellular processes downstream of the Insulin-PI3K-PKB pathway. In response to extra- or intracellular stresses, for example starvation or oxidative stress, FoxOs are required to direct cell cycle progression and apoptosis. In endothelial cells, they induce apoptosis, and their deregulation is linked to diseases involving the insulin pathway, such as diabetes. FoxOs also exhibit a complex role in tumour transformation: here their main function is to suppress tumorigenesis. In both physiological and cancer contexts, FoxO activation leads to the transcription of some general targets, such as $p27^{kip1}$ or IGFBP1. The FoxOs can also induce tissue-specific genes, as ANGPT2 and BIM in the endothelium.

In endothelial cells, another pathway with a pivotal function is the MEK5/ERK5 MAPK signalling way. Its activation promotes cell survival and proliferation in stressful conditions, e.g., when blood vessels are exposed to the shear forces exerted by the blood stream. Furthermore, recent data described ERK5 as a kinase directing tumour resistance upon therapy-induced stress.

Comparing their reported roles in various tumours and in the endothelium, FoxO proteins and the MEK5/ERK5 MAPK cascade appear to exert opposite functions. First non-published data confirmed the hypothesis that FoxO factors are subject to a negative modulation by the MEK5/ERK5 pathway. Hence, one goal of this PhD project was to further characterise this crosstalk at molecular level. The major mechanism of FoxO regulation is the balance among several post-translational modifications, such as phosphorylation, acetylation, and ubiquitination. Most importantly, the PKB-dependent phosphorylation of FoxOs negatively controls their activity, and it is critical for their subcellular localization. Therefore, the regulation of FoxO localization as mechanism of ERK5-dependent suppression was studied, but the results presented in this thesis argue against this hypothesis. However, additional experiments are required to explore the impact of ERK5 activity on FoxO post-translational modifications.

FoxO activity can also be modulated by the interaction with other proteins, which in turn could explain general- and tissue-specific gene expression. Thus, another objective of this work was to investigate FoxO3-interactome in endothelial cells and the impact of MEK5/ERK5 activation on it. As published in (Fusi et al. 2022) and presented here, this analysis unveiled TRRAP as new FoxO-bound protein in several cell types. Moreover, the interaction did not rely on the capacity of the FoxOs to bind their consensus DNA sequences at the promoter of target genes. Functional data demonstrated that TRRAP is required for FoxO-dependent gene transcription in endothelial and osteosarcoma cells. In addition, TRRAP expression in the endothelium is important for FoxO-induced apoptosis. In summary, the interaction between FoxO factors and TRRAP revealed a new regulatory mechanism of FoxO-dependent gene transcription. It remains to be analysed whether the MEK5/ERK5 cascade may exert its suppressive effect on FoxO activity by interfering with their binding to TRRAP and whether such a mechanism may be relevant for tumorigenesis.

ZUSAMMENFASSUNG

Forkhead-Box-O-Proteine sind eine Familie von Transkriptionsfaktoren, die an verschiedenen zellulären Prozessen stromabwärts des Insulin-PI3K-PKB-Signalwegs beteiligt sind. Als Reaktion auf extra- oder intrazelluläre Stressfaktoren, wie Wachstumsfaktorentzug oder oxidativen Stress, werden die FoxOs benötigt, um Zellzyklusprogression und Apoptose zu regulieren. In Endothelzellen induzieren sie Apoptose und ihre Fehlregulation ist mit Krankheiten, bei denen der Insulinsignalweg involviert ist, wie etwa *Diabetes mellitus*, verbunden. FoxOs spielen auch eine komplexe Rolle bei der Tumortransformation: Hier besteht ihre Hauptfunktion darin, die Tumorentstehung zu unterdrücken. Sowohl im physiologischen als auch im Kontext von Krebs führt die FoxO-Aktivierung zur Transkription verschiedener allgemeiner Zielgene, wie $p27^{kip1}$, BIM oder IGFBP1. Die FoxOs können aber auch gewebespezifische Gene, wie zum Beispiel ANGPT2 im Endothel, induzieren.

Ein weiterer Signalweg mit wichtiger Funktion in Endothelzellen ist der MEK5/ERK5-MAPK Signalweg. Seine Aktivierung fördert das Überleben und Wachstum von Zellen unter Stressbedingungen, wie z. B. wenn Blutgefäße durch den Blutstrom Schubspannungskräften ausgesetzt sind. Darüber hinaus zeigen neuere Daten, dass ERK5 auch an der Tumorresistenzentwicklung unter therapieinduziertem Stress beteiligt ist.

Ein Vergleich der bekannten Rolle beider Signalwege im Endothel und bei der Tumorgenese, impliziert eine mutmaßlich gegensätzliche Funktion von FoxO Proteinen und der MEK5/ERK5-MAPK Kaskade. Erste unveröffentlichte Daten stützen die Hypothese, dass FoxO Faktoren einer Negativregulation durch MEK5/ERK5 unterliegen. Ein Ziel dieses Promotionsprojekts, war es daher diesen Zusammenhang auf molekularer Ebene näher zu charakterisieren. Die FoxO-Regulierung ist primär das Zusammenspiel mehrerer posttranslationaler Modifikationen wie Phosphorylierung, Acetylierung und Ubiquitinierung. Der wichtigste Regulationsmechanismus ist dabei die inhibitorische Phosphorylierung durch die Kinase PKB, welche die transkriptionelle FoxO-Aktivität hemmt und deren subzelluläre Lokalisierung ins Zytoplama fördert. Daher wurde zunächst der Einfluss von ERK5 auf die FoxO-Lokalisierung untersucht. Die Daten dieser Arbeit sprechen gegen einen Einfluss von der ERK5 Aktivität auf FoxO Lokalisation, doch sind zusätzliche Experimente erforderlich, um dessen Wirkung auf das Muster der posttranslationalen Modifikation der FoxOs zu klären.

FoxO-Aktivität kann auch durch die Interaktion mit anderen Proteinen moduliert werden, die wiederum auch die allgemeine und gewebespezifische Genexpression steuern könnten. Ein weiteres Ziel dieser Arbeit war es daher, das FoxO3-Interaktom in Endothelzellen und den Einfluss forcierter MEK5/ERK5-Aktivierung darauf zu untersuchen. Wie in (Fusi et al. 2022) gezeigt und hier vorgestellt, führte diese Analyse zur Identifikation von TRRAP als neuem generellen FoxO-Bindepartner. Die zelltypunabhängige Interaktion beider Proteine beruhte dabei nicht auf

der Fähigkeit der FoxOs direkt an ihre Konsensus-DNA-Sequenzen in den Promotoren ihrer Zielgene zu binden. Funktionelle Daten zeigten nachfolgend, dass TRRAP entscheidend zur FoxO-abhängigen Gentranskription in Endothel- und Osteosarkomzellen beiträgt. Darüber hinaus ist TRRAP im Endothel für die effiziente Apoptoseinduktion durch FoxOs wichtig. Zusammenfassend offenbarte die Interaktion zwischen FoxO-Faktoren und TRRAP einen neuen Regulationsmechanismus der FoxO-abhängigen Gentranskription. Es bleibt zu prüfen, ob die MEK5/ERK5 Kaskade FoxOs dadurch hemmt, dass sie die Bindungsfähigkeit von FoxO an TRRAP stört, und ob die beobachtete FoxO-TRRAP Interaktion auch im Kontext der Tumorgenese von Bedeutung ist.

INTRODUCTION

The Forkhead box O transcription factors

The Forkhead box transcription factors superfamily

The superfamily of Forkhead box (Fox) proteins is a large group of transcription factors (TFs) involved in the regulation of several biological functions, such as metabolism, stress response, differentiation, cell proliferation and apoptosis, longevity, migration, and invasion (Myatt and Lam 2007). The Fox family in humans comprises fifty factors distributed in nineteen subfamilies, from FoxA to FoxS (Lam et al. 2013). All these proteins share a ca. 100-amino-acids-long evolutionary conserved DNA-binding region termed "Forkhead" or "Winged-helix" domain (FOX domain), which gives the name to the family. Homologous proteins are found in many other organisms, from the lower orders, e.g., the worm *C. elegans*, to the mammals, through the fruit fly *D. melanogaster* (Myatt and Lam 2007).

Despite the presence of the highly conserved FOX domain, the single Fox transcription factors show quite heterogeneous tissue-specific functions. It is worth mentioning FoxA, a factor controlling tissue development, FoxM1, a master regulator of G2-M cell cycle progression, and FoxP, a protein contributing to neuronal or T cell development and differentiation (Golson and Kaestner 2016). Due to the importance of the processes they control, it is not surprising that deregulation of Fox proteins has been associated with the onset and progression of several types of cancers (Myatt and Lam 2007). This work focuses on the function and the regulation of one of the best-studied Fox subfamilies, the Forkhead box O (FoxO) subgroup and their activity in the endothelium, a tissue where they have relevant physiological functions, will be analysed.

The FoxOs: from the worms to the humans

The FoxO TFs were first discovered in model organisms: dFOXO as a single gene in *D. melanogaster* (Weigel et al. 1989) and the protein DAF-16 in *C. elegans* (Lin et al. 1997). The fruit fly dFoxO acts downstream of the Insulin/Insulin-like growth factor 1 (IGF1) signalling pathway as merging element that reacts to several environmental stresses (e.g., nutrient deprivation or abundance, Reactive oxygen species (ROS) or UV light) (Puig and Mattila 2011). In nematodes DAF-16 is similarly controlled by the Insulin/IGF1 cascade and it promotes longevity and the formation of the so-called "*Dauer*" quiescent state. The active DAF-16 modulates transcription not only of genes involved in aging and survival, but also of genes implicated in metabolism, protection from pathogens and stress resistance (Tullet 2015).

In *H. sapiens* the FoxO subfamily comprises four members: FoxO1, 3, 4 and 6. FoxO1 (also known as FKHR), FoxO3 (or FKHRL1), and FoxO4 (alternatively called AFX) are the most common transcription factors of the family collectively termed "FoxOs" in this work. They have overlapping

functions, and they regulate the cellular fate in stress-dependent contexts, for instance upon Growth factor (GF) deprivation, exposure to oxidative and genotoxic stress, or during aging (Gui and Burgering 2021). Instead, FoxO6 expression is mainly limited to the brain, where it shows a specific spatial and temporal regulation (Jacobs et al. 2003), and to the liver, where it controls glucose and lipid metabolism (Lee and Dong 2017). Furthermore, two other isoforms, FoxO2 and FoxO5, were discovered: the first proved to be homologous to FoxO3, while the latter was found to be only expressed in *D. rerio* (Eijkelenboom and Burgering 2013).

The human FoxOs share the characteristic FOX domain of the Fox protein (for simplicity, from here on the FOX domain of the FoxOs is referred to as "DNA-binding domain" or "DB domain"), which identifies and binds the so-called FoxO responsive elements (FREs). The FREs are two specific DNA sequences: the DAF-16 binding element (DBE) and Insulin-responsive element (IRE) and they are present in the promoter region of most of their regulated genes (Calissi, Lam, and Link 2021). In addition, FoxOs contain three other preserved domains, essential for their functionality: the Transactivation domain (TA), important for their transcriptional activity, the Nuclear localization signal (NLS) and the Nuclear export signal (NES), central for the coordination of their subcellular localization (Figure 1) (Calissi, Lam, and Link 2021).

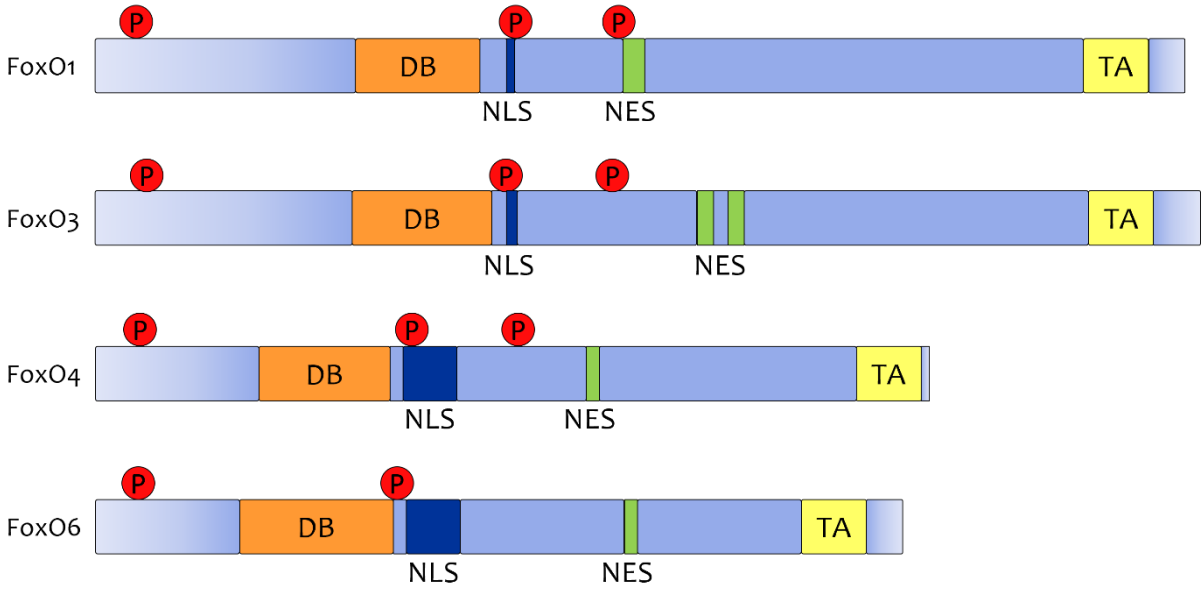

Figure 1: Representation of FoxO proteins and their most important domains in *H. sapiens*.

Schematic picture of the four members of FoxO family in humans (FoxO1, 3, 4 and 6). The most important domains for FoxO functionality and regulation are highlighted. Orange: DNA-binding domain (DB); dark blue: Nuclear localization signal (NLS); green: Nuclear export signal (NES); yellow: Transactivation domain (TA); red circles: sites phosphorylated by PKB (P). *Adapted from (Calissi, Lam, and Link 2021).*

The regulation of FoxO proteins

FoxO location to the nucleus is essential because it enables them to bind the promoters of the target genes and to control gene expression. Thus, nuclear/cytoplasmic shuttling is a fine-tuning mechanism principally guided by the Phosphoinositide-3-kinase (PI3K)/Protein kinase B (PKB, also known as AKT) pathway. In presence of insulin or IGFs, the cascade becomes active and the effector kinase PKB phosphorylates the FoxO proteins at three conserved amino acid residues (Figure 1) (Biggs et al. 1999; Brunet et al. 1999; Kops et al. 1999). This phosphorylation has an inhibitory effect on FoxOs, as it fosters the binding with the chaperone protein 14-3-3 and leads to FoxO nuclear export and sequestration in the cytoplasm. The binding with 14-3-3 triggers a conformational change, which hides the DB and the NLS domains of FoxOs (Obsilova et al. 2005; Tzivion, Dobson, and Ramakrishnan 2011). This promotes the separation of FoxOs from the DNA and their shuttling out of the nucleus, supporting the cytosolic retention of FoxOs and their inhibition. The slackening of the negative phosphorylation by PKB allows FoxOs to relocate back to the nucleus and to become again functional (Figure 2) (Calnan and Brunet 2008).

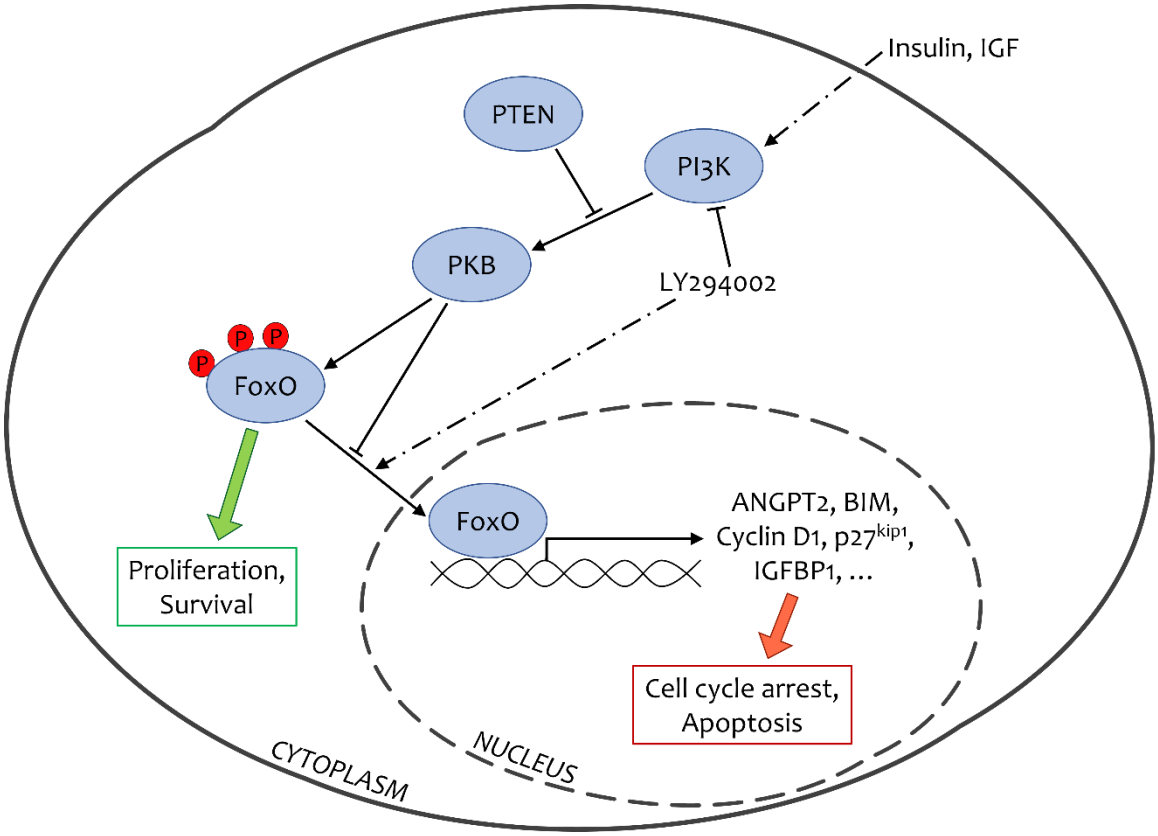

Figure 2: Illustration of the main mechanism of FoxO regulation.

Schematic representation of the PI3K/PKB cascade and of the regulation of FoxO factors. In the graphic the main outcomes of FoxO activation or inhibition are also described (red and green transparent boxes). Moreover, pharmacological (LY294002) and physiological (PTEN) inhibitors of the PI3K/PKB pathway are indicated. PTEN, which is often downregulated in tumour entities, leads to constitutive PKB activation and suppression of FoxO activity (Nakamura et al. 2000).

Apart from this major regulation mechanism, FoxO activity is influenced by the phosphorylation initiated by other enzymes. The Serum and glucocorticoid-induced kinase (SGK) phosphorylates FoxO transcription factors at the same sites as PKB, similarly causing the cytoplasmic accumulation of FoxOs in response to GFs (Brunet et al. 2001). Another kinase with an inhibitory effect on FoxOs is the Extracellular signal-regulated kinase 1/2 (ERK1/2). The direct phosphorylation by ERK1/2 promotes the degradation of FoxO proteins and therefore it reduces their activity (Boccitto and Kalb 2011). Phosphorylation of FoxOs can also have a positive impact on its transcriptional capacity. For instance, Adenosine monophosphate-activated protein kinase (AMPK) phosphorylates FoxOs on six residues in response to high levels of ROS, leading to an increased accumulation of FoxOs in the nucleus (Wang, Yu, and Huang 2016). Elevated amounts of oxidative stress also induce the activity of the Mammalian sterile 20-like kinase 1 (MST1) and the Jun-N-terminal kinase (JNK), which can both phosphorylate the FoxO proteins, steering their localization towards the nucleus (Calnan and Brunet 2008).

Besides phosphorylation, other post-translational modifications (PTMs) regulate FoxO proteins stability, activity, and degradation. Acetylation of FoxOs by CREB-binding protein (CBP)/p300 reduces the DNA-binding capacity of FoxOs and therefore it inhibits their transcriptional activity (Boccitto and Kalb 2011). Deacetylation of FoxO factors is mainly guided by Sirtuin 1 and 2 (SIRT1 and 2). So far, it is not fully clear if SIRT1 and 2 act as positive or negative regulators of FoxOs, as evidences for both increased and decreased transcriptional activity upon deacetylation by SIRT1 or SIRT2 were reported (summarised in (Wang, Yu, and Huang 2016)).

As for many other proteins, FoxO turnover is regulated by E3 ubiquitin ligases, but addition or removal of a single ubiquitin molecule rather affects their localization (Wang, Yu, and Huang 2016). In this context the MDM2 proto-oncogene (MDM2) has an important role in FoxO activation as it attaches a single ubiquitin to FoxO4, and thus it augments its nuclear localization (Brenkman et al. 2008). This effect is counteracted by the Herpes-virus-associated ubiquitin specific protease (HAUSP, also called USP7), that removes ubiquitin residues and prevents FoxO4 re-localization to the nucleus (van der Horst et al. 2006). FoxO1 was also shown to be controlled by polyubiquitination. Here S-phase kinase associated protein 2 (SKP2) ubiquitin ligase induces FoxO1 degradation, thereby inhibiting its transcriptional activity and restoring cell growth and survival (Huang et al. 2005).

Another critical PTM of FoxO proteins is methylation, which was shown to mainly affect Arg and Lys residues. The Protein arginine methyltransferase 1 (PRMT1) methylates Arg amino acids of FoxO1 in the phosphorylation consensus motif of PKB. This directly abrogates PKB-dependent phosphorylation of FoxO1 and results in FoxO1 nuclear accumulation (Yamagata et al. 2008). The histone lysine methyltransferase SET domain containing 7 (SETD7, known also as SET9) was shown to have a controversial role in the Lysin-methylation of FoxO3. On one hand Calnan and colleagues reported that SETD7-dependent methylation decreases FoxO3 stability, but also boosts its

transcriptional activity (Calnan et al. 2012). On the other hand, it was illustrated that FoxO3 methylation can negatively regulate its dependent transcription and apoptosis in neurons (Xie et al. 2012). An overview of the most important enzymes implicated in PTMs of FoxOs is provided in Table 1.

Table 1: Summary of the main PTMs of FoxOs and the responsible enzymes.

FoxO modification	Positive regulator	Negative regulator
Phosphorylation	AMPK; JNK; MST1	ERK1/2; PKB; SGK
Ubiquitination	MDM2 (Monoubiquitination)	SKP2 (Polyubiquitination)
Deubiquitination		USP7
Acetylation		CBP/p300
Deacetylation	SIRT1; SIRT2	SIRT1; SIRT2
Methylation	PRMT1; SETD7	SETD7

The table summarises the main enzymes which influence FoxO stability and activity by addition or removal of functional groups (Boccitto and Kalb 2011; Calnan and Brunet 2008; Eijkelenboom and Burgering 2013). Enzymes are organized in two groups: the ones which promote FoxO activity (Positive regulator), and the ones that inhibit FoxO proteins (Negative regulator). The proteins, whose impact on FoxO regulation is unclear, are mentioned in both groups.

The function of the FoxO TFs can also be affected by the interaction with other proteins. In this respect it is worth mentioning the binding between FoxOs and β-Catenin, which enhances FoxO transcriptional activity, especially upon oxidative stress (Essers et al. 2005). An inhibitory interaction partner of FoxOs is the Poly(ADP-ribose) polymerase 1 (PARP1), which poly(ADP-ribosyl)ates FoxO1 and suppresses FoxO1 transcriptional activity (Sakamaki et al. 2009). It was also shown that c-Myc interacts with FoxO3, and this inhibits FoxO3-dependent transcription of the *Cyclin-dependent kinase inhibitor 1B* (*CDKN1B*, named as well $p27^{kip1}$) gene (Chandramohan et al. 2008). Alternatively, FoxO proteins act together with other factors to regulate downstream gene expression. One example is described in (Bouchard et al. 2004): FoxOs and c-Myc control an overlapping set of genes, which are critical for proliferation and transformation. In this context, phosphorylated FoxO factors are required to leave the promoter to enable c-Myc-dependent activation of this group of genes (Bouchard et al. 2004). Moreover, it is known that FoxO3 clusters with the Hypoxia-inducible factor 1 (HIF1) and p300 to control the transcription HIF1 target genes (Emerling et al. 2008). Similarly, Runx1 cooperates with FoxO3 to regulate the gene expression of *BCL2-like protein 11* (*BCL2L11*, better known as *BIM*) (Wildey and Howe 2009). Upon oxidative stress, FoxO3 and the Fanconi anaemia complementation group D2 (FANCD2) form a complex that controls gene expression and contributes to the cellular antioxidative response (Li et al. 2010).

Finally, micro-RNAs precisely targeting *FoxO* mRNA have been shown to have an emerging role in regulating FoxO-dependent transcription, and hence they can directly influence FoxO protein expression (Urbanek and Klotz 2017).

The role of FoxO proteins in the endothelium

Once the equilibrium among all the regulation mechanisms directs FoxOs into the nucleus, transcriptional activity of specific gene sets is triggered. This in turn drives the cells into cell cycle arrest or apoptosis, in a cell type-specific manner. For instance, in endothelial cells (ECs) FoxO activation initiates the apoptotic machinery (Daly et al. 2004; Skurk et al. 2004). Interestingly, in this context the transcription of some key pro-apoptotic target genes happens via a poorly characterised process, which does not imply the binding with the FREs, and it is named "alternative" gene regulation (Czymai et al. 2010; Ramaswamy et al. 2002). One of the most important genes controlled via this mechanism is BIM, a pro-apoptotic Bcl-2 family member that steers the tumour-suppressing functions of FoxO proteins (Czymai et al. 2010). However, FoxO factors typically induce gene transcription by directly binding to the FREs located at the promoter and this mechanism is also known as "direct" or "classical" gene regulation (Czymai et al. 2010; Ramaswamy et al. 2002). Among the genes presenting FRE sequences there is the pro-apoptotic *Phorbol-12-myristate-13-acetate-induced protein 1* (*PAIMP*, also named *NOXA*). Other important genes controlled by the classical mechanism in ECs are established FoxO-targets such as the cell cycle regulator $p27^{kip1}$ (Czymai et al. 2010; Dijkers et al. 2000; Medema et al. 2000), and the *IGF binding protein 1* (*IGFBP1*) (Czymai et al. 2010; Ramaswamy et al. 2002). In addition, some EC-specific genes, including *Angiopoietin 2* (*ANGPT2*), are directly regulated by FoxOs (Czymai et al. 2010; Daly et al. 2004; Potente et al. 2005).

An additional function of FoxO transcription factors in the endothelium is the regulation of vascularization and angiogenesis. One of the FoxO regulated targets affecting this process is the above-mentioned ANGPT2, which is a protein involved in vascular destabilization and remodelling (Daly et al. 2004). Furthermore, FoxO activity is required for the expression of a subset of genes induced by the Vascular endothelial growth factor (VEGF) (Abid et al. 2006). If these data support the idea that FoxOs behave as promoters of angiogenesis, evidence that shows the opposite function is available as well. In an older work, Abid and colleagues demonstrated that VEGF fosters the PKB-dependent phosphorylation of FoxO3, leading to the suppression of a subgroup of its targets. Among these genes there is $p27^{kip1}$, whose reduced expression allows ECs to proliferate and angiogenesis to proceed (Abid et al. 2004). Furthermore, the activation of FoxO1 or FoxO3 blocks endothelial sprout formation and migration, and their silencing reduces ANGPT2 levels and restores the angiogenic activity in ECs (Potente et al. 2005). Accordingly, Wilhelm and colleagues showed that deletion of FoxO1 in ECs causes an uncoordinated vessel sprouting due to an intense proliferation, while its overexpression restricts ECs growth (Wilhelm et al. 2016).

Moreover, the FoxO capability of controlling the fate of ECs enables them to have an essential role in the formation, development, and growth of the endothelium *in vivo*. It was shown that early failures in angiogenesis and vessel development initiated by germline FoxO1 mutations in mice cause premature death (Furuyama et al. 2004; Hosaka et al. 2004). In accordance, data from adult mice underline the importance of FoxOs in angiogenesis and vascularisation, as they decrease migration of ECs (Potente et al. 2005). Further studies linked the capability of ECs to proliferate in proangiogenic contexts with the ability to adapt their metabolism and this depends on the presence of FoxO proteins (Andrade et al. 2021; Wilhelm et al. 2016). Lastly, other data demonstrated that FoxOs are essential TFs for the homeostasis of the vessels and the endothelium. Their deletion initiates heavy dysfunctions and makes the mice prone to develop tissue-specific tumours, like thymic lymphomas and haemangiomas (Dharaneeswaran et al. 2014; Paik et al. 2007).

Furthermore, the FoxO factors also involved in the control of the inflammatory status of the endothelium. Lee and colleagues linked FoxO3 with the Tumour necrosis factor (TNF) receptor signalling pathway. They demonstrated that the activation of FoxO3 shifts the outcome of TNF receptor pathway toward apoptosis, via the FoxO-dependent suppression of the inflammatory transcription factor Nuclear factor kappa B (NF-κB) (Lee et al. 2008). Accordingly, the FoxO1 phosphorylation caused by the PI3K/PKB cascade induces the NF-κB transcriptional activity, promoting the gene expression of age-related inflammatory genes (Kim et al. 2008). Lastly, the analysis of FoxO target genes by microarray technology revealed that FoxOs control the expression of genes involved in inflammation and blood vessel morphogenesis, such as IL-8 and Vascular cell adhesion molecule 1 (VCAM1) (Czymai et al. 2010; Potente et al. 2005).

The FoxO transcription factors in pathological conditions

The discovery of FoxO proteins was an important step for the understanding of the insulin pathway and diabetes, due to the fundamental function of FoxOs in this disease and its cardiovascular complications (Menghini et al. 2020; Pajvani and Accili 2015). An impaired PI3K/PKB pathway is associated with a lower phosphorylation of FoxO1 and a lower activity of the Endothelial nitric oxide synthase (eNOS), suggesting that FoxO1 might have a role in endothelial dysfunction and cardiovascular disease (Federici et al. 2004). In accordance, FoxO1 nuclear localization and activity are linked to atherosclerotic plaques instability and progression (Menghini et al. 2015). Furthermore, the function of FoxO1 in human adipose tissue correlates with endothelial insulin resistance in obese people and it is linked with obesity-related endothelial dysfunction (Karki et al. 2015). The increase of endothelial FoxO1 protein is sustained by a prolonged high fat diet and leads to the establishment of antiangiogenic and proinflammatory conditions. As consequence of FoxO1 accumulation, the angiogenic process is disrupted and a prediabetic phenotype arises. The depletion of FoxOs might then mitigate the inflammatory conditions, the insulin resistance, and the microvascular dysfunction typical of the type 2 diabetes (Nwadozi et al. 2016).

It was proven that in some tumour cells FoxO TFs block the progression of the cell cycle (Eijkelenboom and Burgering 2013; Nakamura et al. 2000). For instance, in several cancer cell lines some of the main genes regulated by FoxOs are involved in G1-S progression, such as $p27^{kip1}$ (Medema et al. 2000) and D-type cyclins (Ramaswamy et al. 2002; Schmidt et al. 2002). In renal cell carcinoma FoxO3 activation fosters cell cycle arrest and apoptosis and suppresses migration and invasion. In agreement with its tumour-suppressor function, high levels of FoxO3 reflect better metastasis-free survival rates among patients with renal cell carcinoma (Ni et al. 2014). Likewise, the invasion potential of several prostate cancer cell lines inversely correlates with FoxO4 protein expression. Metastasis-free survival of patients with prostate cancer also decreases when FoxO4 is downregulated, linking the loss of FoxO with the invasiveness properties of the metastases (Su et al. 2014). Therefore, considering their antiproliferative functions in many cancer types, it has been long time believed that FoxO proteins purely operate as tumour suppressors.

In contrast, recent data revealed that in some tumoral contexts FoxO presence was beneficial. The nuclear accumulation of FoxO3 as a consequence of the serum starvation results in augmented tumour cell invasion, promoted by the degradation of the extracellular matrix (Storz et al. 2009). Furthermore, the overexpression of FoxOs or their nuclear localization is linked to cancer progression and poor patient prognosis in several tumour types (Chen et al. 2010; Qian et al. 2017; Santamaria et al. 2009). Consistently, expression of phosphorylated, thus not active, FoxO1 is frequently detected at early stages in gastric carcinoma tumorigenesis, and it indicates a better prognosis (Kim et al. 2007). In neuroblastoma the FoxO3 localization in the nucleus is not only associated with bad clinical status, but it also sustains the tumoral angiogenesis and the cell growth (Hagenbuchner et al. 2016).

Altogether these data support the leading theory that FoxOs act as onco-suppressors, but they also raise the possibility that they can occasionally have oncogenic functions. The crucial aspect that shifts the role of FoxO proteins towards the one or the other direction is the context-dependent fine-tuning of their activity (Hornsveld et al. 2018; Jiramongkol and Lam 2020).

The FoxOs as transcription factors: tissue-specific gene controllers?

The FoxO factors are known to have critical and specific roles not only in ECs and in the related diseases, but also in several other tissues. For instance, in peripheral lymphoid organs FoxO3 influences activation and tolerance of T cells, contributing to T cell homeostasis (Lin, Hron, and Peng 2004). Bone formation is a process that involves FoxOs as well: FoxO1 is an early director of osteoblast differentiation, due to its function as repressor of proliferation (Siqueira et al. 2011; Teixeira et al. 2010). FoxO TFs show important functions in skeletal muscle, including regulation of muscle energy metabolism, protein homeostasis, myotube formation and adaptation to exercise (Sanchez, Candau, and Bernardi 2014). Cell metabolism is regulated by FoxO1 in cardiac muscle. Here FoxO1 maintains the balance between cell survival and cardiomyocyte damage, which is

critical for the heart functionality (Chistiakov, Orekhov, and Bobryshev 2017). Moreover, full FoxO3 knockout female mice exhibit disorders in the reproductive system and fertility (Castrillon et al. 2003; Hosaka et al. 2004).

Overall, it can be said that the FoxOs are fundamental for the cell survival, and for the maintenance of tissue homeostasis and functions. The FoxO proteins integrate growth, nutrient, and environmental stimuli, and they achieve this by coordinating metabolic processes, stress responses, cell cycle progression, cell death and pathways implicated in tumorigenesis. However, the context- and cell type-specific mechanisms that guide the different outcomes of FoxO activation are not yet fully understood.

The FoxO system in the practical laboratory routine

Considering the involvement of the FoxOs in apoptosis and cell cycle arrest, the simple activation of these transcription factors makes it difficult to investigate their functions in any relevant cell type. Therefore, it is necessary to develop an inducible system by providing FoxO proteins with a tag that allows conditional activation. This was achieved by attaching a mutated form of the murine hormone-binding domain of the Oestrogen receptor (ER) to the C-terminus of the protein, so that the nuclear localization can be prompted by stimulation with the oestrogen analogue 4-hydroxytamoxifen (4-OHT) (Czymai et al. 2010; Dijkers et al. 2000). In addition, this mutant was made insensitive to the PKB inhibition by the mutation to alanine of the three PKB-sensitive amino acids. It was also provided with a Human influenza hemagglutinin (HA) tag for purification and detection purposes (HA.FoxO.A3.ER) (Figure 3) (Biggs et al. 1999; Brunet et al. 1999; Calnan and Brunet 2008; Medema et al. 2000).

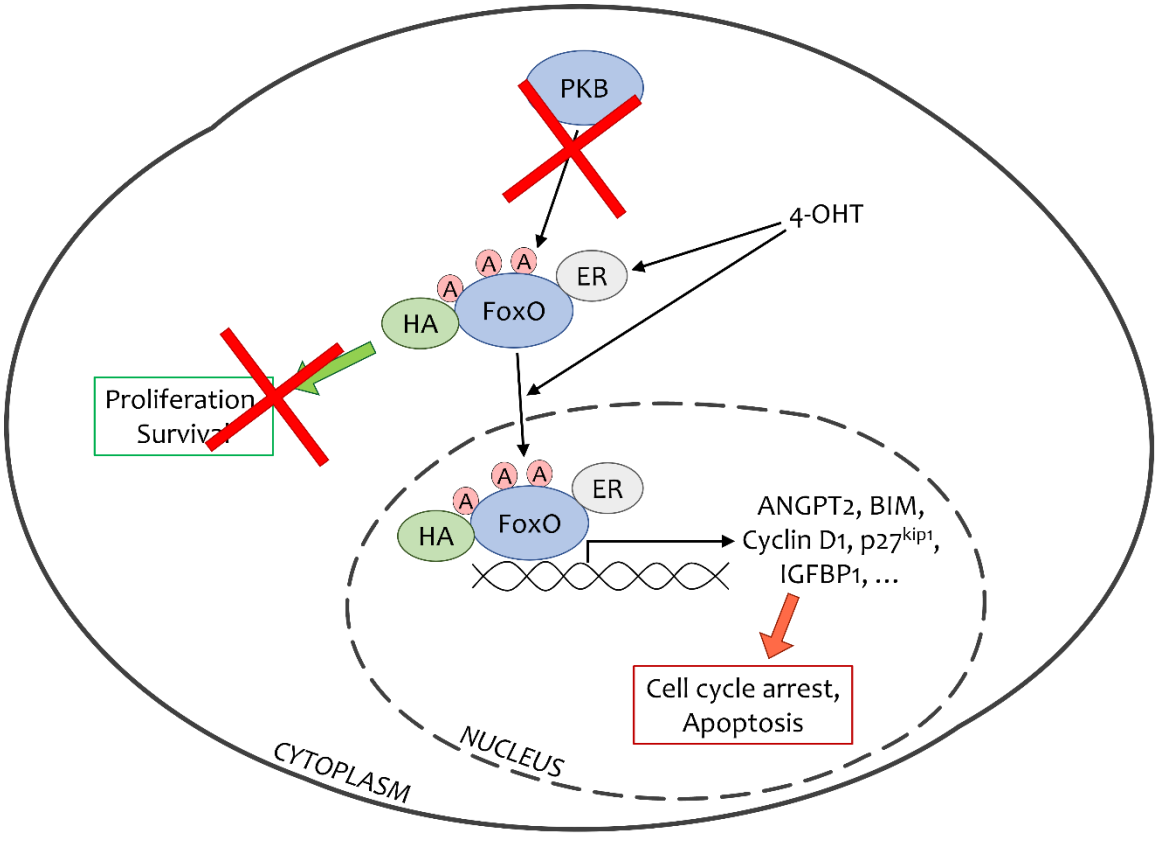

Figure 3: Cartoon explaining the inducible system established to study FoxO functions.

Schematic illustration of the engineered FoxO proteins, which give the possibility to conditionally activate the FoxOs and the consequent gene transcription processes. The "HA" represents the single or the triple HA-tag (for clarification of the latter see paragraph "A new FoxO3 construct suitable for interaction studies and its functional validation"); "ER" defines the modified murine-derived Oestrogen receptor; the three PKB-sensitive amino acids mutated into Ala are depicted as "A"; 4-OHT stands for 4-hydroxytamoxifen, the compound which binds to the ER-tag and causes nuclear localization of the tagged-FoxOs; the red crosses highlight the circumvented regulation mechanism once 4-OHT is added to the system.

The MEK5/ERK5 cascade

The ERK5 and its upstream kinase called MAPK/ERK kinase 5 (MEK5) are proteins known to direct key functions in ECs (Paudel, Fusi, and Schmidt 2021). Considering its role in sustaining endothelial integrity by hampering apoptosis, inflammation, and motility, the MEK5/ERK5 MAPK pathway is a good candidate as antagonist of the FoxO transcription factors. Here some of the most important features of ERK5 and MEK5 are described.

The Mitogen-activated protein kinase family

An evolutionary conserved mechanism of cellular signal transduction is based on a chain of Ser-Thr kinases which leads to the final activation of a Mitogen-activated protein kinase (MAPK) (Cargnello and Roux 2011). In response to specific extracellular stimuli, for example mitogens or stresses, the first group of kinases called MAPK kinase kinases (MAPKKKs) initiates the phosphorylation cascade and activates a second set of kinases named MAPK kinases (MAPKKs). These trigger the MAPKs, which in fact regulate several target proteins and control numerous physiological functions, like mitosis, inflammation, proliferation, or motility (Kyriakis and Avruch 2012). To the conventional MAPKs belong ERK1/2, p38 isoforms (p38α, β, γ and δ), JNK1, 2 and 3, and ERK5, on which the focus is set in this work (Cargnello and Roux 2011).

The unicity of MEK5/ERK5 cascade

The first evidence about the existence of ERK5 and the upstream MEK5 sets back to almost 30 years ago (Lee, Ulevitch, and Han 1995; Zhou, Bao, and Dixon 1995). ERK5 is also called Big MAP kinase 1 (BMK1) and differs from the other MAPKs in its unique large C-terminal domain, which shows additional transcriptional properties (Kasler et al. 2000). Similarly, MEK5 contains the Phox and Bem1 (PB1) domain, an exclusive domain, not present in the other MAPKKs, and needed for the interaction with ERK5 (Glatz et al. 2013). The PB1 domain is also necessary for the interaction with the MAPKKKs upstream of MEK5, namely MEKK2 and 3 (Drew, Burow, and Beckman 2012). This very specific structures confer uniqueness to this pathway. Once MEK5 is active, it phosphorylates ERK5 at two crucial amino acids in the kinase domain. As a result, ERK5 undergoes a conformational change, that unfolds the protein and prompts its kinase activity (Glatz et al. 2013; Nithianandarajah-Jones et al. 2012). In this new conformation, ERK5 discloses the NLS sequence and can shuttle to the nucleus to phosphorylate its targets (Figure 4). Furthermore, p-ERK5 sustains its enzymatic activity by auto-phosphorylation of its C-terminus, and this can be detected as a higher protein band in immunoblot analysis, after probing with specific α-ERK5 antibodies (Morimoto et al. 2007; Paudel, Fusi, and Schmidt 2021).

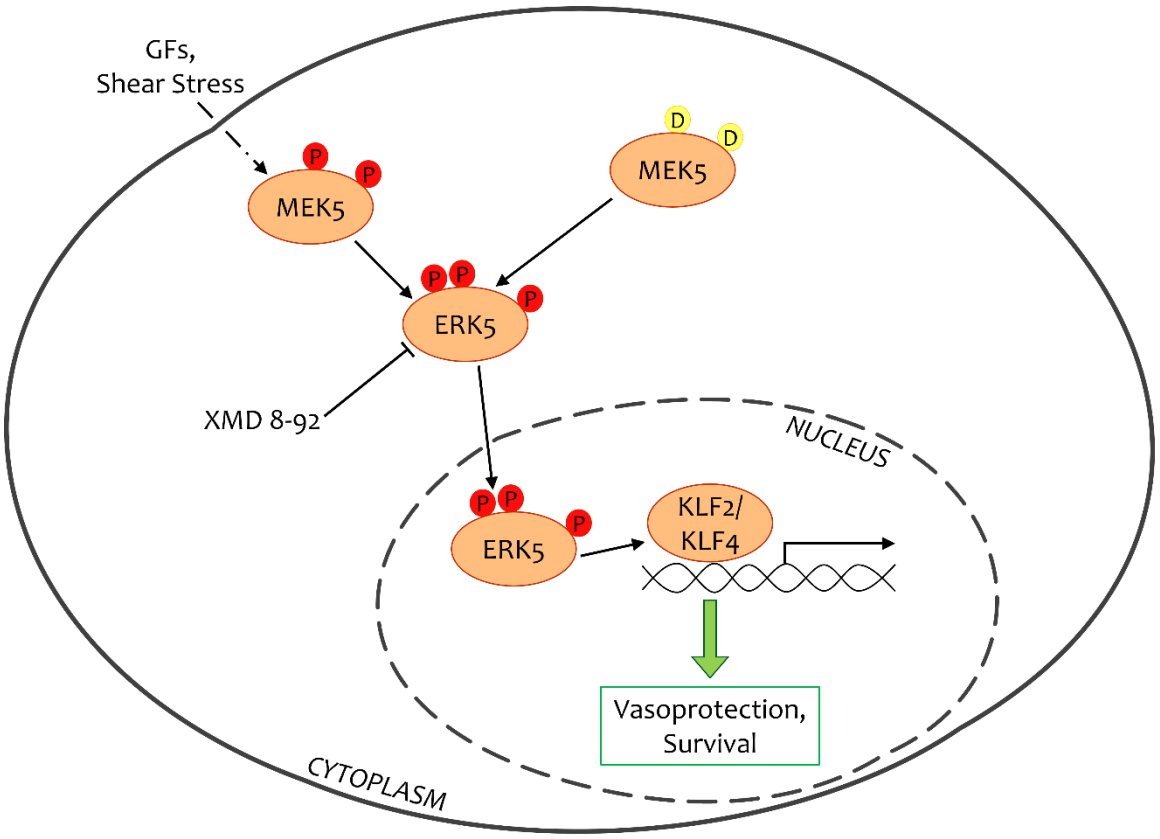

Figure 4: Schematic representation of the MEK5/ERK5 pathway.

This figure represents the MEK5/ERK5 cascade, including upstream stimuli, downstream targets (KLF2 and 4) and functional effects of the pathway (green transparent box). Other important factors are underlined: a constitutively active mutant of MEK5 (MEK5D) that present two mutated residues shown as yellow (D) and a pharmacological inhibitor of ERK5 (XMD 8-92) which is often used to investigate ERK5 properties. The critical phosphorylation sites of MEK5 and ERK5 are indicated by red (P).

The role of the MEK5/ERK5 cascade in cells and tissues

The MEK5/ERK5 cascade was believed to be only a proliferation pathway, similar to its closest relative ERK1/2. First studies revealed that MEK5/ERK5 is activated in presence of mitogenic stimuli, such as GFs (Kato et al. 1997; Kato et al. 1998). This idea was strengthened by successive findings, which showed that ERK5 influences cell cycle by regulating Cyclin D1 expression and c-Myc (English et al. 1998; Mulloy et al. 2003). In contrast, some evidence indicated that MEK5/ERK5 pathway can be initiated by several stresses, for instance by oxidative stress (Abe et al. 1996). Moreover, newer studies with focus on ERK5 role in cancer, showed that tumour cells do not depend on ERK5 for proliferation, but that MEK5/ERK5 pathway is rather triggered upon therapy stress, as an escape mechanism (Adam et al. 2020; Hoang et al. 2017; Lochhead et al. 2016; Stecca and Rovida 2019). Paudel and colleagues summarised further evidences that underline the role of the MEK5/ERK5 cascade as a stress-initiated pathway in several tissues, like for example in bone and cartilage, skeletal and heart muscles, or endothelium (Paudel, Fusi, and Schmidt 2021).

The endothelium and the MEK5/ERK5 signalling way

In the context of the vascular endothelium, MEK5 and ERK5 are strongly sustained by the Laminar shear stress (LSS) that is generated by the steady blood stream (Yan et al. 1999). In turn, ERK5 activity leads to the protection from apoptosis and to the maintenance of tissue integrity (Pi, Yan, and Berk 2004), and this is mainly mediated by the downstream transcription factors Krüppel-like factors 2 and 4 (KLF2 and 4) (Ohnesorge et al. 2010; SenBanerjee et al. 2004). To enhance its protective function, the MEK5/ERK5/KLF2/4 axis is involved in the suppression of inflammation, in the prevention of the endothelial to mesenchymal transition (a process involved in atherosclerosis development), in the inhibition of cell migration, and in the regulation of focal adhesion turnover (Komaravolu et al. 2015; Moonen et al. 2015; Ohnesorge et al. 2010; Spiering et al. 2009).

The presence of the LSS, that switches on ERK5, blocks the endothelial to mesenchymal transition of the endothelium, showing in this way an atheroprotective phenotype (Moonen et al. 2015). Similarly, the LSS-dependent and the constitutive activation of ERK5 trigger the repression of migration and motility of ECs, by sustaining KLF2 functionality (Komaravolu et al. 2015). It was likewise revealed that the initiation of ERK5 impedes both the motility and the wound healing process in ECs (Spiering et al. 2009). When the MEK5/ERK5 cascade is active, the ECs undergo less frequently apoptosis, they lower the adhesion of immune cells, and they manifest a decreased VEGF-dependent angiogenic sprouting (Ohnesorge et al. 2010). Consistently, ERK5 stimulates HIF1 ubiquitination in the endothelium and this blocks HIF1 activity. As a consequence, the angiogenetic processes are also hampered (Pi et al. 2005).

Furthermore, it was demonstrated that ERK5 inhibition in ECs is the cause of increased inflammation and vascular dysfunction. VCAM1 was found to be a mediator of these effects and its expression is upregulated in absence of ERK5 (Le et al. 2013). Comparably, the activation of the MEK5/ERK5 cascade lowers the production of TNF-induced VCAM and IL-8 (Ohnesorge et al. 2010). Hamik and colleagues also proved that VCAM is blocked upon KLF4 activation leading to a "functionally healthy endothelium", although the involvement of neither ERK5 nor MEK5 was considered (Hamik et al. 2007).

The important role of the MEK5/ERK5 pathway in ECs is reflected in its fundamental functions *in vivo* (Hayashi and Lee 2004). Broad disruption of MEK5 or ERK5 in mice causes the premature death of the embryos, due to the lack of ECs organization, which is in turn the origin of the failures in vasculature formation, heart development and angiogenesis (Regan et al. 2002; Wang et al. 2005; Yan et al. 2003). When the knockout of ERK5 is restricted to the ECs, the mice embryos do not survive and show similar phenotypes (Hayashi et al. 2004). In addition, the conditional loss of ERK5 in adult mice leads to the animal death within 2-4 weeks after the inhibition of the kinase. Once more, the reasons behind this lethal phenotype are unorganized ECs that resulted in abnormally leaky blood vessels and in haemorrhagic events in several organs (Hayashi et al. 2004).

First evidence of FoxO3 negative regulation by the MEK5/ERK5 cascade

As all the presented pieces of information underline, the MEK5/ERK5 pathway promotes survival and protection from inflammation and stresses in ECs, while the FoxO factors direct opposite events, such as arrest of the cell cycle and apoptosis. Considering the strikingly antagonistic functions of both pathways, first experiments were done to investigate a potential negative regulation of FoxOs by ERK5, as shown in Figure 5.

The first indications of a compensatory mechanisms were seen in Human umbilical vein endothelial cells (HUVEC). Here the expression of a constitutively active MEK5 mutant (MEK5D) was able to prevent the cell death caused by the 4-OHT-dependent conditional activation of HA.FoxO3.A3.ER. This was shown by Propidium iodide (PI) staining of the DNA content of the cells, followed by the analysis of the apoptotic rates by flow cytometry (Figure 5A). A confirmation that MEK5D overexpression in HUVEC could block the HA.FoxO3.A3.ER-induced apoptosis can be seen in Figure 5B, where the protein expression of HA.FoxO3.A3.ER targets, such as BIM, and of the pro-apoptotic protein Caspase 3 were hampered. Similarly, the analysis of the mRNA expression of several FoxO3-regulated genes in HUVEC revealed that the constitutively stimulation of ERK5 caused by MEK5D overexpression prevented the FoxO3-dependent mRNA induction (Figure 5C).

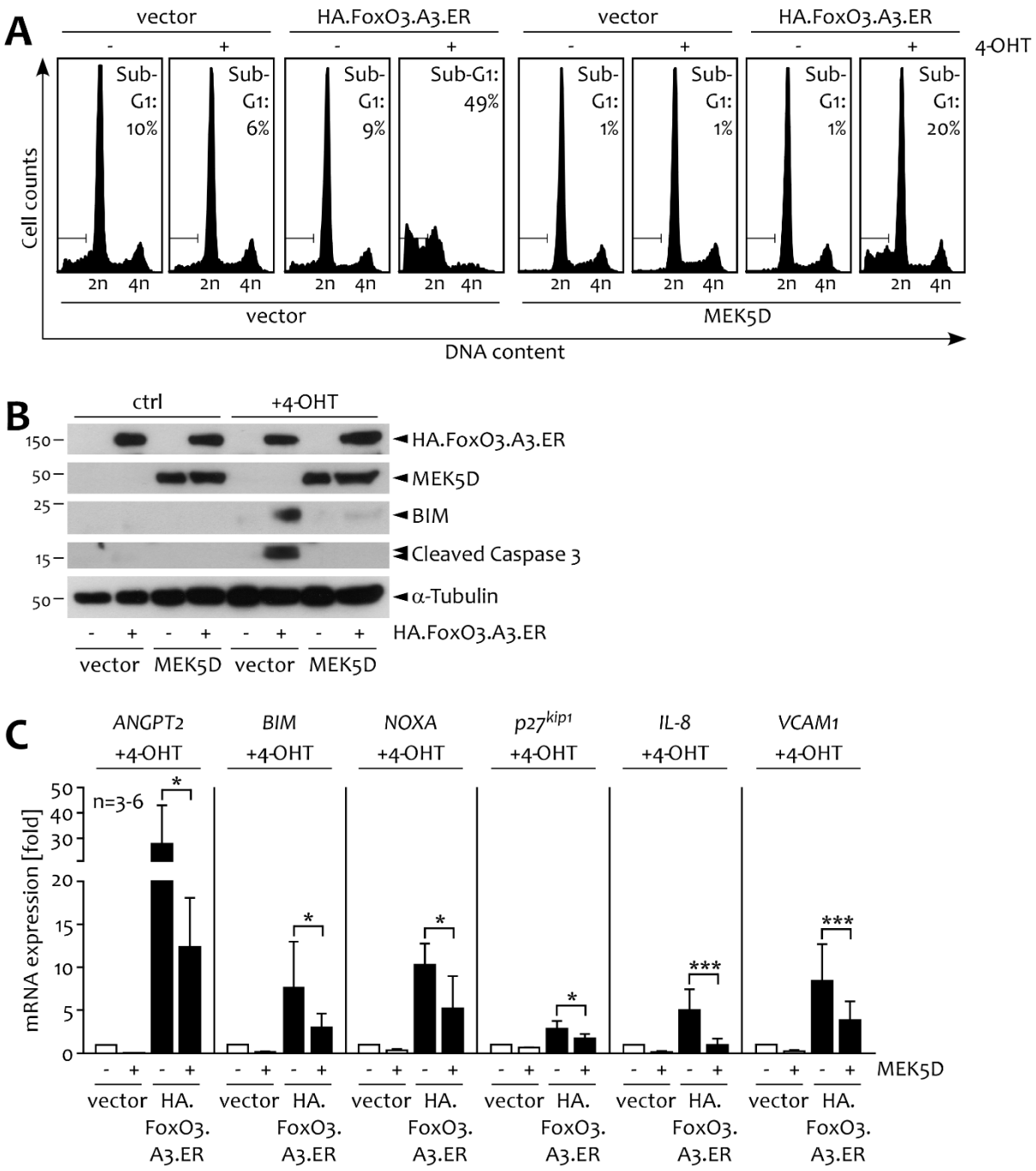

Figure 5: The effect of MEK5/ERK5 activity on FoxO3-dependent apoptosis and transcription in HUVEC.

FoxO3 induces gene transcription and apoptosis in HUVEC, while cell growth is restored, and gene expression is reduced by constitutive activation of the MEK5/ERK5 cascade. **A**-**C**) HUVEC co-infected with combinations of empty vector ("vector" or "-"), HA.FoxO3.A3.ER ("HA.FoxO3.A3.ER" or "+") and MEK5D ("MEK5D" or "+") and cultured with pure medium ("ctrl" or "-") or with the addition of 4-OHT ("+4-OHT" or "+"). **A**) Representative cell cycle profiles of n = 3 experiments revealing apoptosis rates after cell incubation with or without 4-OHT for 32 hours. Apoptotic rates are indicated as percentage of the cell population in Sub-G1 phase. **B**) Western blot displaying whole cell lysates from HUVEC handled as in *A*. α-Tubulin serves as loading control. **C**) HUVEC cells were all treated with 4-OHT for 24 hours. Histograms show the fold induction of the mRNA expression (normalised to the housekeeper GAPDH) of the indicated FoxO target genes. Means + SD from n = 3-6 independent experiments are shown. Unpaired t-tests were performed and statistical significance between the indicated samples is highlighted (*** $p \leq 0.001$; * $p \leq 0{,}05$). *Courtesy of C. Adam.*

Scope of the project

This PhD project has its roots in the uncertainty around the conditions that direct the cellular responses upon FoxO activation. Additionally, some of the mechanisms, by which the FoxOs control gene transcription, are not yet fully understood. Thus, the goals of the project were to explore the influence of potential antagonist pathways, such as the MEK5/ERK5 cascade, on the FoxO activity, and to look for new potential interacting proteins of the FoxOs that could shed some more light on FoxO-dependent classical and alternative gene regulation. The focus was mainly set on the endothelium, where the FoxO proteins have crucial functions and alternative gene expression has a fundamental role in these processes.

Starting from some existing observations in ECs (presented in the above paragraph "First evidence of FoxO3 negative regulation by the MEK5/ERK5 cascade"), the crosstalk among the MEK5/ERK5 MAPK signalling pathway and the FoxO TFs was further examined. Specifically, it was investigated how ERK5 negatively influences FoxO transcriptional activity at molecular level, with attention to FoxO localization and PTMs. In addition, the FoxO-interactome was analysed to screen for proteins that might clarify how the classical and alternative mechanisms of transcription are regulated. The examination of FoxO-binding partners aimed to shed some light on how FoxO activity can steer cellular outcomes towards stress resistance, cell cycle arrest or apoptosis, in a cell type specific manner. In this context the possibility that MEK5/ERK5 cascade could impact on the FoxO-interacting proteins, and thus on its regulation, was also considered.

RESULTS

The antagonism between FoxOs and the MEK5/ERK5 pathway

A new FoxO3 construct suitable for interaction studies and its functional validation

As a starting point of the project to better detect and purify FoxO3 in ECs, a new FoxO3 construct was cloned. The negative regulation of this construct by MEK5 and ERK5 was validated in functional and transcriptional assays.

For a more efficient purification, the N-terminal HA-tag of the existing HA.FoxO3.A3.ER in the pBP-retroviral vector system (Czymai et al. 2010) was substituted by a triple HA-tag (3xHA) to generate a new pBP-3xHA.FoxO3.A3.ER vector. A more detailed description of the cloning protocol can be found in the section "Cloning of new plasmids" of the "Methods" chapter. After the results of the Sanger sequencing that confirmed the correct sequence (data not shown), the new construct was used to generate stable Phönix retrovirus producer cells. These cells were then used for retroviral transduction of HUVEC. The 3xHA.FoxO3.A3.ER-expressing HUVEC were stimulated with 4-OHT for different times to verify the retained ability of the new FoxO3 mutant to induce apoptosis. The cells and the supernatants were pooled and fixed after 8, 16, 24, 32 and 48 hours of incubation either with pure medium or with medium with 4-OHT. The DNA of the cells was stained with PI and the apoptosis rates were analysed by flow cytometric quantification of the sub-diploid DNA content. Similar to the original construct, the data proved that the 3xHA.FoxO3.A3.ER mutant induced apoptosis in a time-dependent manner (Figure 6A), albeit with slightly less efficiency (compare with Figure 5A). The apoptosis induction with the new construct took marginally longer to achieve similar levels of cell death (48 hours instead of 32 hours). Furthermore, the experiment revealed that after 16 hours the cells exhibited no morphological signs of cell death (Figure 6A), while apoptosis was clearly evident by phase contrast microscopy after 48 hours (Figure 6B and Suppl. Figure 1). The Figure 5C illustrates the mRNA expression levels of a panel of FoxO3 targets, which were increased by expression of the original construct and strongly suppressed by the co-expression of the constitutively active MEK5D. The mRNA levels of two FoxO3 target genes selected among the validated ones were further examined. Consistently, the expression of these genes was enhanced by conditional 4-OHT-mediated activation of the newly 3xHA.FoxO3.A3.ER, while this effect was counteracted by the LSS-induced physiological activation of ERK5 (Figure 6C). Moreover, gene expression of FoxO3 targets was triggered by pharmacological inhibition of the PI3K/PKB cascade by using LY294002 in vector-infected but not MEK5D-infected cells (Figure 6D). This confirmed the negative regulation of endogenous FoxOs by ERK5 activation.

This evidence supported and expanded the initial data of the research group and supported the existence of a negative regulation of FoxO factors exerted by the MEK5/ERK5 MAPK pathway.

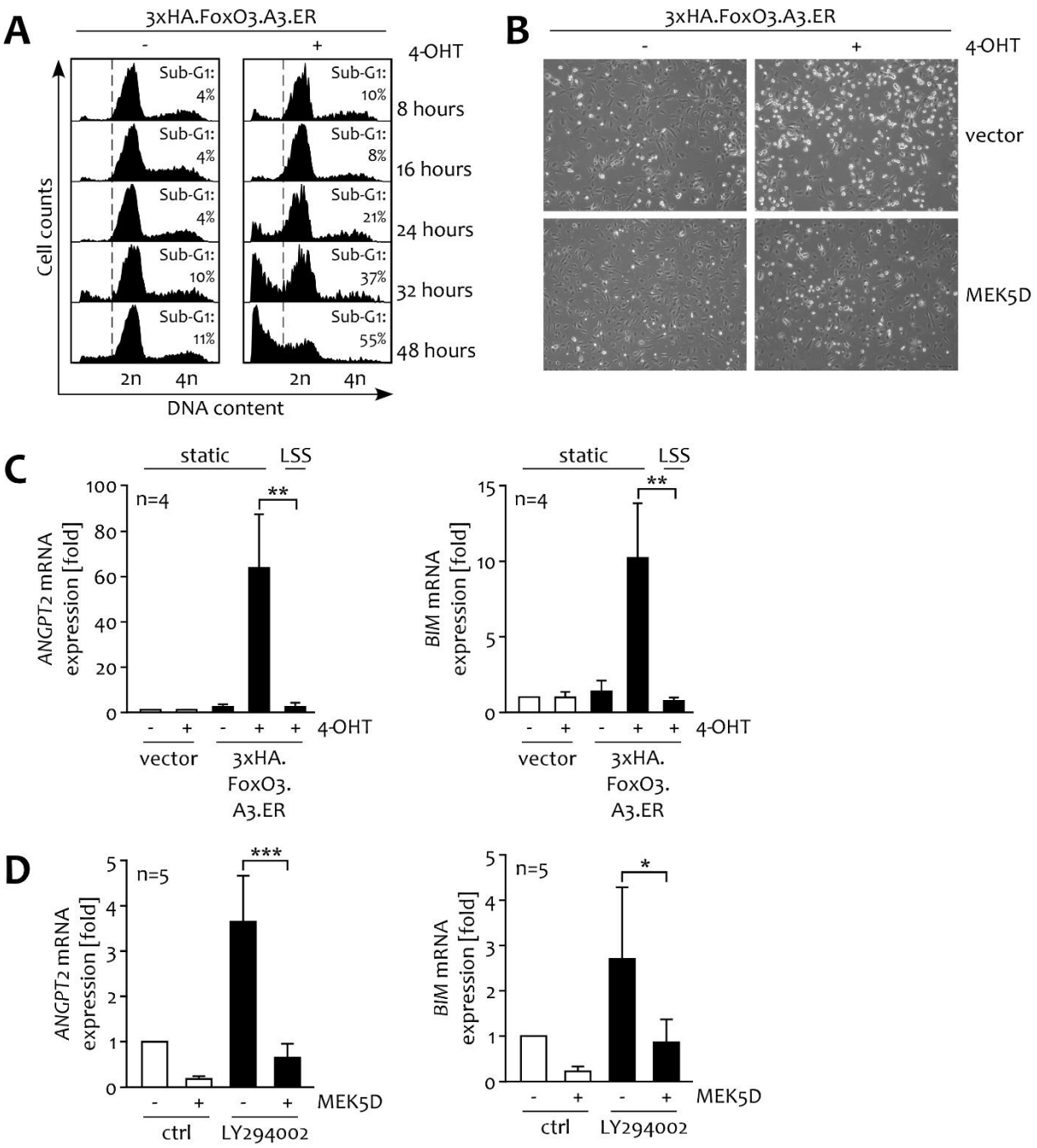

Figure 6: 3xHA.FoxO3.A3.ER activation causes apoptosis and is counteracted by the MEK5/ERK5 cascade.

The 4-OHT-mediated conditional activation of the newly cloned 3xHA.FoxO3.A3.ER in ECs causes the gradual induction of FoxO-dependent gene expression and apoptosis over time, which is suppressed by triggering the MEK5/ERK5 pathway. **A**) HUVEC were retrovirally infected with 3xHA.FoxO3.A3.ER and cultured with normal culture medium (-) or medium supplemented with 4-OHT (+) for 8, 16, 24, 32 or 48 hours. The representative cell cycle profiles display apoptotic rates as determined by flow cytometric quantification of the cells with a sub-diploid DNA content (indicated % refers to the quantified percentage of cells left of the dotted line). **B**) Phase contrast pictures of HUVEC displaying cells infected with 3xHA.FoxO3.A3.ER after 48-hours-stimulation with (+) or without (-) 4-OHT. Scale bar: 100 µm. **C**, **D**) Histograms indicating the fold induction of the mRNA expression (normalised to the housekeeper GAPDH) of *ANGPT2* and *BIM*. Means + SD from n = 4 (in *C*) or n = 5 (in *D*) independent experiments are shown. Unpaired t-tests were performed and statistical significance between the indicated samples is highlighted (*** $p \leq 0.001$; ** $p \leq 0{,}01$; * $p \leq 0{,}05$). In *C*, 3xHA.FoxO3.A3.ER- or vector-expressing HUVEC were cultured for 24 hours with (+) or without (-) 4-OHT, either under standard cell culture conditions (static) or in presence of Laminar shear stress (LSS). In *D*, HUVEC retrovirally infected with an empty vector (-) or MEK5D (+) were cultured for 16-24 hours with medium (ctrl) or LY294002-supplemented medium (LY294002).

The effect of the MEK5/ERK5 activation on FoxO3 localization

Further experiments were next performed to unravel the molecular mechanism by which EKR5 suppresses FoxO3 functions. Considering that a pivotal event in the regulation of FoxOs is their subcellular localization, it was first investigated whether the MEK5/ERK5 cascade influences FoxO nucleus-cytoplasm shuttling.

HUVEC were infected with the retroviral expression construct for HA.FoxO3.A3.ER in combination with an empty vector or MEK5D. After the addition of 4-OHT for 16 hours, Immunofluorescent stainings (IFs) of HA.FoxO3.A3.ER were carried out (Figure 7A and Suppl. Figure 2). Similarly, empty vector- or MEK5D-overexpressing HUVEC were stimulated without or with LY294002 to initiate the nuclear accumulation and the activation of the endogenous FoxO3, which was subsequently stained by immunofluorescence (Figure 7B). In both cases, the presence of MEK5D did not alter the 4-OHT- or LY294002-dependent nuclear localization of FoxO3 in comparison with the respective controls. This was also supported by nuclear/cytoplasmic fractionation experiments with HUVEC that expressed either an empty vector or MEK5D: no overt difference in the subcellular distribution of the endogenous FoxO3 in presence or absence of MEK5D was revealed (Figure 7C).

In summary, these data indicated that the interaction between the two pathways was not a consequence of the ERK5-dependent changes in FoxO3 subcellular re-localization. In addition, considering that the nuclear/cytoplasmic shuttling of FoxOs is mainly regulated by phosphorylation, these results indirectly hinted that the ERK5/MEK5 pathway may not alter FoxO3 phosphorylation at sites critical for its localization.

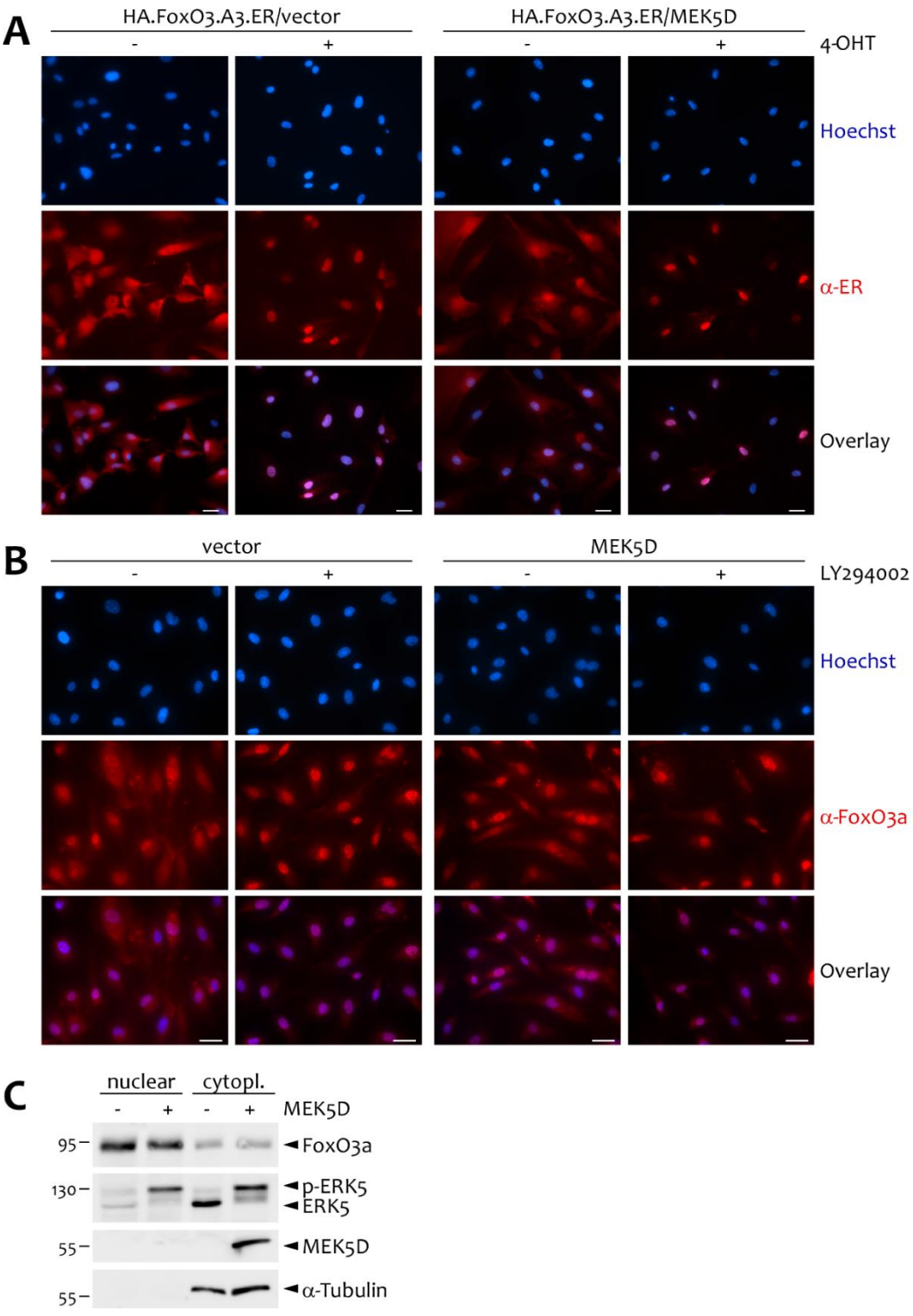

Figure 7: The MEK5/ERK5 pathway does not affect FoxO3 localization.

FoxO3 nuclear localization is not affected by the MEK5/ERK5 cascade. **A**) α-ER immunofluorescent staining of HUVEC overexpressing HA.FoxO3.A3.ER and MEK5D or the empty vector, each condition after 16 hours incubation with (+) or without (-) 4-OHT. Blue channel: Hoechst nuclear staining; red channel: α-ER staining for HA.FoxO3.A3.ER; overlay of the two channels is also displayed. Scale bar: 25 µm. **B**) α-FoxO3a immunofluorescent staining of HUVEC overexpressing MEK5D or its empty vector after incubation with (+) or without (-) LY294002 for 16 hours. Blue channel: Hoechst nuclear staining; red channel: α-FoxO3a staining for endogenous FoxO3; overlay of the two channels is also displayed. Scale bar: 25 µm. **C**) Western blots representing nuclear/cytoplasmic extracts of HUVEC overexpressing MEK5D or its empty vector. α-Tubulin represents a cytoplasmic marker and indicates clean cell fractionation.

The modulation of FoxO3-interactome by the MEK5/ERK5 pathway

Once changes in FoxO3 localization could be excluded as mechanism to explain the effect of ERK5 on FoxOs in ECs, the next aspects to be verified included the analysis of FoxO-interacting partners and of FoxO PTMs. Given that FoxO modifications are also influenced by other binding proteins, the following step was to examine the FoxO3-interactome in presence and absence of MEK5/ERK5 activation. This approach made it possible to screen for potential ERK5-influenced proteins, which could in turn control FoxO factors either by changing FoxO-PTM status or by affecting FoxO transcriptional activity by direct binding. At the same time, it was possible to look for factors that could explain FoxO-dependent direct and indirect gene regulation, independently of the presence of an active ERK5.

To achieve this, HUVEC were first retrovirally transfected with the following combinations of empty vector, 3xHA.FoxO3.A3.ER and MEK5D:

- Empty vector (vector);
- 3xHA.FoxO3.A3.ER and empty vector (3xHA.FoxO3.A3.ER/vector);
- Empty vector and MEK5D (vector/MEK5D);
- 3xHA.FoxO3.A3.ER and MEK5D (3xHA.FoxO3.A3.ER/MEK5D).

These cells were incubated for 16 hours with 4-OHT, because previous data showed that at this time point FoxO3 was already active, but did not induce massive apoptosis yet (compare Figure 6 and Figure 11). Subsequently, the protein lysates were harvested and 3xHA.FoxO3.A3.ER was immunoprecipitated using α-HA magnetic beads. The isolated FoxO3 and the bound proteins were then analysed by Nano-liquid chromatography-tandem mass spectrometry (MS) analysis (nanoLC-MS/MS) in collaboration with the research group of Prof. Dr. Andreas Schlosser[1]. Briefly, after the Immunoprecipitation (IP) of 3xHA.FoxO3.A3.ER, the eluted proteins were separated by electrophoresis, each lane was excised and digested with Trypsin. The protein fragments were extracted from the gel and analysed by nanoLC-MS/MS. The raw data were then evaluated with the MaxQuant software, considering the vector and the vector/MEK5D conditions as background for the 3xHA.FoxO3.A3.ER/ vector and the 3xHA.FoxO3.A3.ER/MEK5D samples, respectively (Figure 8A and Suppl. Table 1). The analysis revealed the Transformation/Transcription domain-associated protein (TRRAP) as a novel protein, capable to interact with FoxO3 independently of the presence or absence of MEK5D (Figure 8, A and B, left panel). In addition, the study showed that MEK5D overexpression changed the composition of the interacting partners of FoxO3, both by reducing or increasing the strength of the binding (Figure 8A and Suppl. Table 2).

[1] Professor for Mass spectrometry and proteomics at the Rudolf-Virchow-Zentrum - Center for Integrative and Translational Bioimaging at the University of Würzburg.

The Suppl. Table 2 provides a list with the proteins, whose binding strength normalized to the amount of precipitated 3xHA.FoxO3.A3.ER ("qNormalised LFQ Ratio" column) could be potentially altered by the expression of MEK5D ("Impact of MEK5D" column). The top 10 up-regulated candidates and the top 10 putative down-regulated proteins are reported, and each 5 best are indicated with a "#" in both Suppl. Table 2 and Figure 8A. Among these proteins, USP7 was particularly relevant, because it is a known negative regulator of FoxOs (van der Horst et al. 2006) and it was previously identified as a binding partner of TRRAP (Bhattacharya and Ghosh 2015). From the MS analysis it appeared that USP7 binding to FoxO3 was stronger in presence of MEK5D than in its absence (Figure 8A and Suppl. Table 2). These data suggested that the MEK5/ERK5 pathway might prevent the activity of FoxO factors by fostering FoxO-USP7 binding, which in turn could result in FoxO inhibition. Unfortunately, it was not possible to clearly confirm a differential USP7-FoxO3 interaction between the vector- and the MEK5D-coinfected conditions, since some USP7 non-specifically precipitated with the employed anti-HA beads, even in absence of 3xHA.FoxO3.A3.ER expression (Figure 8B, right panel).

In Figure 8A and in the Supplementary Tables the proteins that are already known to interact with TRRAP are highlighted with a "*". In addition to USP7, this group included E1A-binding protein p400 (EP400, (Fuchs et al. 2001)), Cullin-1 (CUL1, (Finkbeiner et al. 2008)) and DNA methyltransferase 1-associated protein 1 (DMAP1, (Doyon et al. 2004)) (Figure 8A and Suppl. Table 1). Thus, FoxO3 could obviously bind to a bigger protein complex containing TRRAP. Like TRRAP itself, the binding of several of these proteins appeared to be slightly affected by the presence of MEK5D, albeit none of the changes between the conditions non-expressing or expressing MEK5D met the threshold of 5-fold, which indicated a reliable difference (data not shown).

The raw data obtained with the nanoLC-MS/MS experiment additionally allowed to briefly evaluate PTMs of 3xHA.FoxO3.A3.ER (data not shown). Unfortunately, these first preliminary analysis indicated that MEK5D did not cause major changes in the gross acetylation- or phosphorylation-patterns of FoxO3, compared to the controls. On one hand, this result supported our conclusion from the localization studies that the PKB-independent phosphorylation of FoxO was unlikely to be the underlying mechanism of FoxO-ERK5 antagonism. On the other hand, it cannot be fully excluded that activation of the MEK5/ERK5 cascade may regulate FoxO3 at the level of PTMs since the employed readout is only suited to detect gross qualitative changes. To draw clearer conclusions regarding the quantitative changes in FoxO3 PTMs due to the MEK5D co-expression, the MS experimental protocol requires further careful adaptation and optimization.

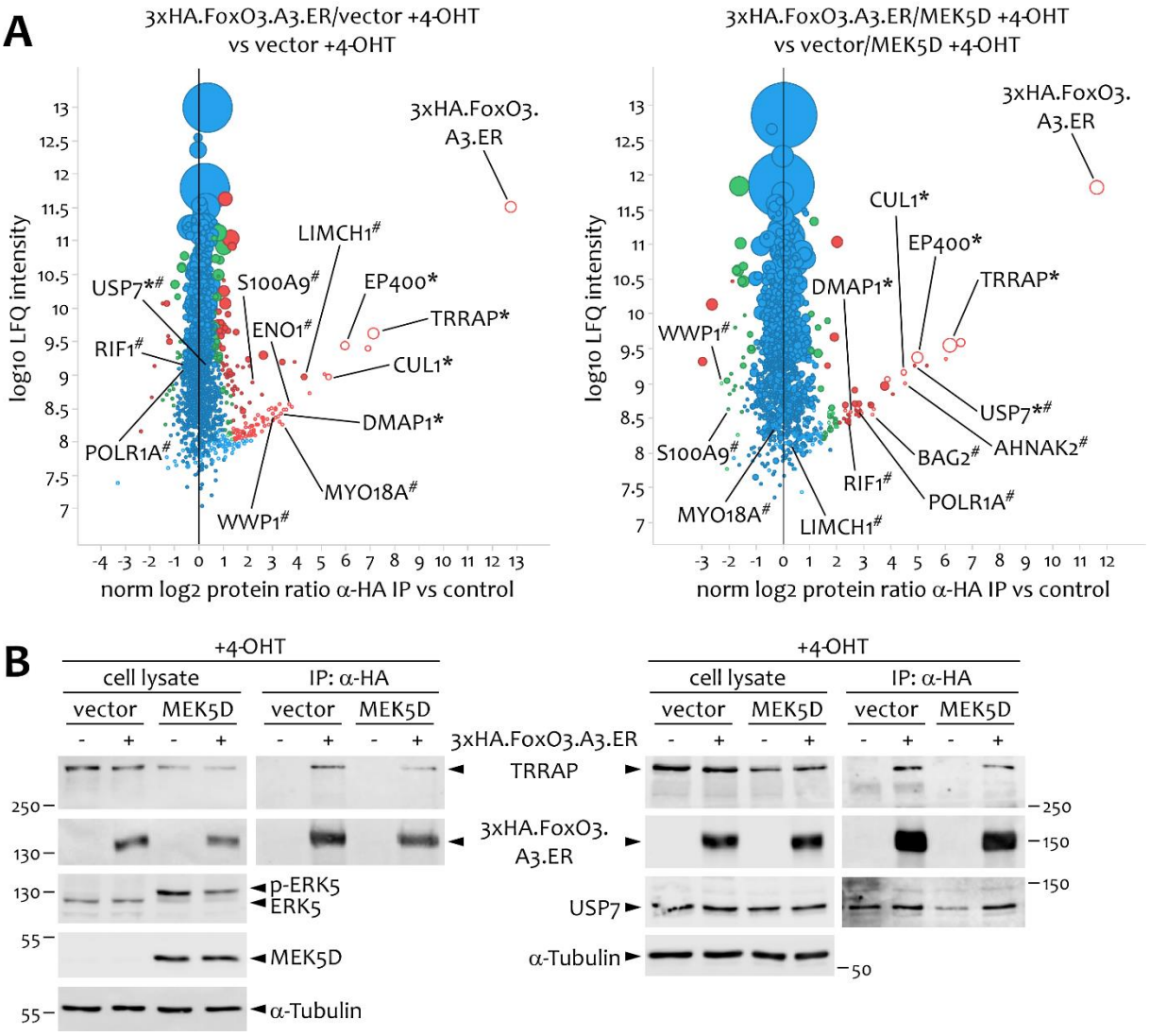

Figure 8: Analysis of FoxO3-interactome in absence and presence of MEK5D.

The FoxO3-interactome analysis revealed TRRAP and the related histone acetyltransferase complexes as new interaction partners. **A**) Scatter plot from a single mass spectrometric analysis of 3xHA.FoxO3.A3.ER-bound proteins in absence and presence of MEK5D. Elutions of HA-IPs done with HUVEC expressing vector, 3xHA.FoxO3.A3.ER/vector, vector/MEK5D or 3xHA.FoxO3.A3.ER/MEK5D after 16 hours of 4-OHT stimulation were examined by nanoLC-MS/MS. The plots display comparisons between 3xHA.FoxO3.A3.ER-expressing conditions and the respective empty vector controls, without (*left panel*) or with (*right panel*) co-expression of MEK5D. Among the best 20 FoxO3 interaction partners in both the MEK5D expressing and non-expressing conditions, the proteins previously identified to bind to TRRAP are indicated with "*" (see Suppl. Table 1 for more details). The top 5 proteins, whose intensity of the interaction with FoxO3 was substantially changed by MEK5D-overexpression are marked with "#" (see Suppl. Table 2 for better details). Red dots: proteins with significance of two; green dots: proteins with significance of one; blue dots: proteins non-specifically bound to 3xHA.FoxO3.A3.ER; dot size: number of identified razor and unique peptides; non-filled dots: quantitative value in the vector or vector/MEK5D control conditions was missing and has been arbitrarily attributed. Refer to "Analysis of FoxO3-nuclear-interactome" paragraph for detailed information about the MS parameters. **B**) Immunoblots showing total cell lysates and HA-IPs from HUVEC handled as in *A* and analysed by Western blot instead of by nanoLC-MS/MS. *Left panel*: overexpression of MEK5D and the resulting effective ERK5 phosphorylation are also presented. *Right panel*: co-IP of USP7 from an independent reproduction is additionally illustrated. α-Tubulin is shown in both panels as loading control. *MS analysis and data elaboration from A were performed in collaboration with Prof. Dr. A. Schlosser.*

The interaction of FoxO factors with TRRAP

The results presented in this chapter have been published in (Fusi et al. 2022): Fusi L, Paudel R, Meder K, Schlosser A, Schrama D, Goebeler M, Schmidt M. Interaction of transcription factor FoxO3 with histone acetyltransferase complex subunit TRRAP Modulates Gene Expression and Apoptosis. J Biol Chem. 2022 Mar;298(3):101714. doi: 10.1016/j.jbc.2022.101714. The data shown here were obtained from reproductions of the experiments included in (Fusi et al. 2022) or from the adaptation of the published figures, in agreement with the copyright policy of the journal.

As shown in the previous section, the study of the interactome of FoxO3 in ECs did not disclose any clear candidate that could regulate FoxO3 activity in a MEK5/ERK5-dependent manner. However, TRRAP was found to be a promising binding partner of FoxO3 and for this reason further investigations were conducted to confirm and evaluate this newly found interaction.

TRRAP and the histone acetyltransferase complexes

TRRAP is a very big protein (~430 kDa) and together with DNA-dependent protein kinase (DNA-PK), Ataxia-telangiectasia mutated (ATM), Ataxia- and Rad3-related (ATR), Mammalian target of rapamycin (mTOR), and Suppressor of morphogenesis in genitalia 1 (SMG1) is part of the PI3K-related kinases (PIKKs) family (Lempiainen and Halazonetis 2009). Unlike the other members of the family, TRRAP is a so called "pseudokinase", meaning that it retains the catalytic domain, but it does not show enzymatic activity due to the loss of some crucial amino acid residues (Elias-Villalobos, Fort, and Helmlinger 2019). TRRAP rather functions as a scaffold for multiprotein complexes with histone acetyltransferase (HAT) activity: in *H. sapiens*, it is the hub for enzymes of the GNAT or of the MYST HAT families, which form the so-called STAGA or Tip60 complexes, respectively (Carrozza et al. 2003). Which HAT complex binds to TRRAP is then determined by cell type- and environmental-specific stimuli (Elias-Villalobos, Fort, and Helmlinger 2019; Lempiainen and Halazonetis 2009). For instance, the TRRAP/Tip60 complex is known to be involved in DNA damage and repair processes (Murr et al. 2006). Once active, these complexes do not only guide the acetylation of the chromatin and thus the regulation of transcriptional processes, but they also coordinate the presence of several TFs around the promoter regions of the target genes (Murr et al. 2007). Intriguingly, these mechanisms might be relevant for the newly discovered FoxO3-TRRAP interaction as well: FoxO3 could be an additional TF, which associates to TRRAP to enhance its transcriptional activity.

Nuclear interaction between FoxO3 and TRRAP in HUVEC and HEK293

After having identified TRRAP as a new binding protein of FoxO3 in ECs, it was first confirmed that the interaction takes place in the nucleus.

HUVEC were retrovirally infected with either an empty vector or 3xHA.FoxO3.A3.ER and later incubated with or without 4-OHT to induce FoxO3 relocation to the nuclear compartment. Differential nuclear/cytoplasmic extracts were then harvested, and the protein expression was examined by Western blot. Figure 9A illustrates that TRRAP was exclusively present in the nucleus, while the nuclear localization of 3xHA.FoxO3.A3.ER was substantially augmented 16 hours after 4-OHT addition. Accordingly, in the same experimental setting as before, HA-IPs were carried out. As shown in Figure 9B, the co-IP of TRRAP with FoxO3 was more efficient when the cells were stimulated with 4-OHT. Additionally, HUVEC were transduced with an empty vector, with 3xHA.FoxO3.A3.ER or with 3xHA.FoxO3.A3.ER(H212R). The latter is a FoxO3 mutant which carries an Arg at position 212 instead of a His and thereby it is not able to bind the FREs in the promoter of some target genes (Czymai et al. 2010). After the stimulation with 4-OHT for all the conditions, HA-IPs were performed, and they demonstrated that 3xHA.FoxO3.A3.ER(H212R) could bind to TRRAP as well (Figure 9C). Altogether, these data confirmed that the interaction mainly occurred in the nucleus and reinforced the idea that TRRAP might be implicated in the regulation of FoxO3-dependent transcription. More precisely, TRRAP was involved in both the FoxO-dependent classical and alternative gene expression regulated by FoxO3.

In order to verify if the interaction was retained in other cell types, HEK293 were studied. Similar to HUVEC, HEK293 cells expressing the empty vector or the 3xHA.FoxO3.A3.ER construct were incubated with culture medium with or without 4-OHT. The IPs of 3xHA.FoxO3.A3.ER by means of an anti-HA antibody recapitulated the results obtained with HUVEC (Figure 9D). Furthermore, when HEK293 were transfected with the empty vectors or the combination of a wild-type HA.FoxO3 construct lacking the ER-tag and a Flag-tagged TRRAP, it was possible to co-IP both proteins (Figure 9E).

These data showed that FoxO3-TRRAP interaction was conserved in other cell types. Secondly, the results demonstrated that the binding was not an artefact of the engineered 3xHA.FoxO3.A3.ER construct, because wild type FoxO3 could also be co-precipitated with TRRAP. This could additionally exclude that neither the tags of FoxO, nor the mutation of the sites phosphorylated by PKB were necessary for the interaction.

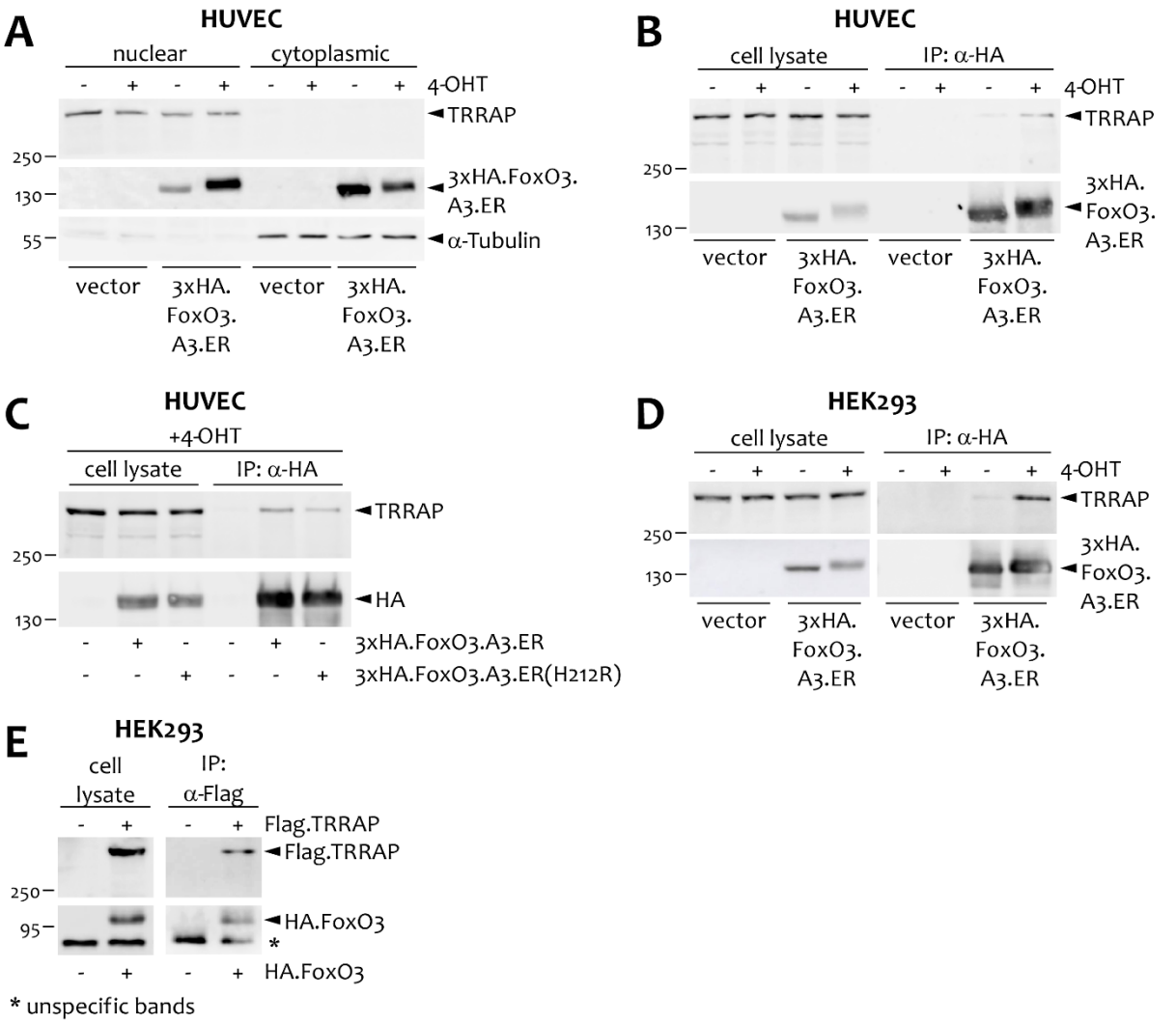

Figure 9: FoxO3 interacts with TRRAP in the nucleus in both HUVEC and in HEK293.

FoxO3-TRRAP interaction takes place in the nucleus, is maintained in other cell types, and does not depend on the direct FRE-binding capacity. **A**) Western blots indicating nuclear/cytoplasmic fractionation of HUVEC retrovirally infected with 3xHA.FoxO3.A3.ER or the corresponding empty vector after 16-hours-incubation without (-) or with (+) 4-OHT. α-Tubulin represents a cytoplasmic marker and indicates clean cell fractionation. **B**) Immunoblots displaying whole cell lysates and HA-IPs from HUVEC transduced and handled as in *A*. **C**) Western blots showing cell lysates and HA-IPs done with lysates of HUVEC expressing either an empty vector (-/-), 3xHA.FoxO3.A3.ER (+/-) or 3xHA.FoxO3.A3.ER(H2121R) (-/+) and incubated with 4-OHT for 16 hours. **D**) Immunoblots representing total lysates and the following HA-IPs from HEK293 cells stably overexpressing 3xHA.FoxO3.A3.ER or the control vector and stimulated for 16 hours with medium (-) or with medium with 4-OHT (+). **E**) Western blots illustrating cell lysates and Flag-IPs from HEK293 cells transfected with Flag.TRRAP/HA.FoxO3 (+/+) or the respective empty vectors (-/-). Bands marked with ***** were detected in all the samples by the used antibody in an unspecific way.

TRRAP binds to other FoxO family members in HEK293

The subsequent experiments were planned to prove if other FoxO factors interact as well with TRRAP, and to identify which FoxO region binds to TRRAP.

The HEK293 cells were transfected with the following constructs:

- Empty vector;
- Empty vector and Flag.TRRAP;
- HA.FoxO4.A3 and empty vector;
- HA.FoxO4.A3 and Flag.TRRAP.

The protein lysates were harvested from these cells, the HA-IPs were performed, and the following Western blots displayed in Figure 10A showed that TRRAP could bind FoxO4, too. Similar results were obtained by analysing FoxO1-TRRAP binding in HEK293 (data not shown). Once more, these data corroborated the conclusion that the interaction did not depend on the presence of the ER-tag and that TRRAP could bind multiple FoxO transcription factors.

To better define the region of FoxO4 to which TRRAP bound, two additional FoxO4 deletion mutants were analysed (represented in Figure 10B and marked in Figure 10D). The first mutant lacks the DB domain of FoxO4 and is termed HA.FoxO4.ΔDB (HA.ΔDB in Figure 10), while the second protein only encompasses the DB domain (HA.FoxO4.DB; HA.DB in Figure 10) (Medema et al. 2000). Co-transfections of HEK293 cells with the mentioned deletion mutants or HA.FoxO4.A3 in combination with Flag.TRRAP and followed by HA-IPs revealed that TRRAP preferentially associated with the full length FoxO4 or with the mutant lacking the DB domain but did not interact with the DB domain alone (Figure 10C). This result was quite surprising, considering that the DB domain is the most conserved region within the FoxOs. The alignment of the four human FoxO proteins highlighted the presence of two other significantly conserved regions, one at the N-terminus and a second one at the C-terminus, which contains the TA domain (Figure 10D).

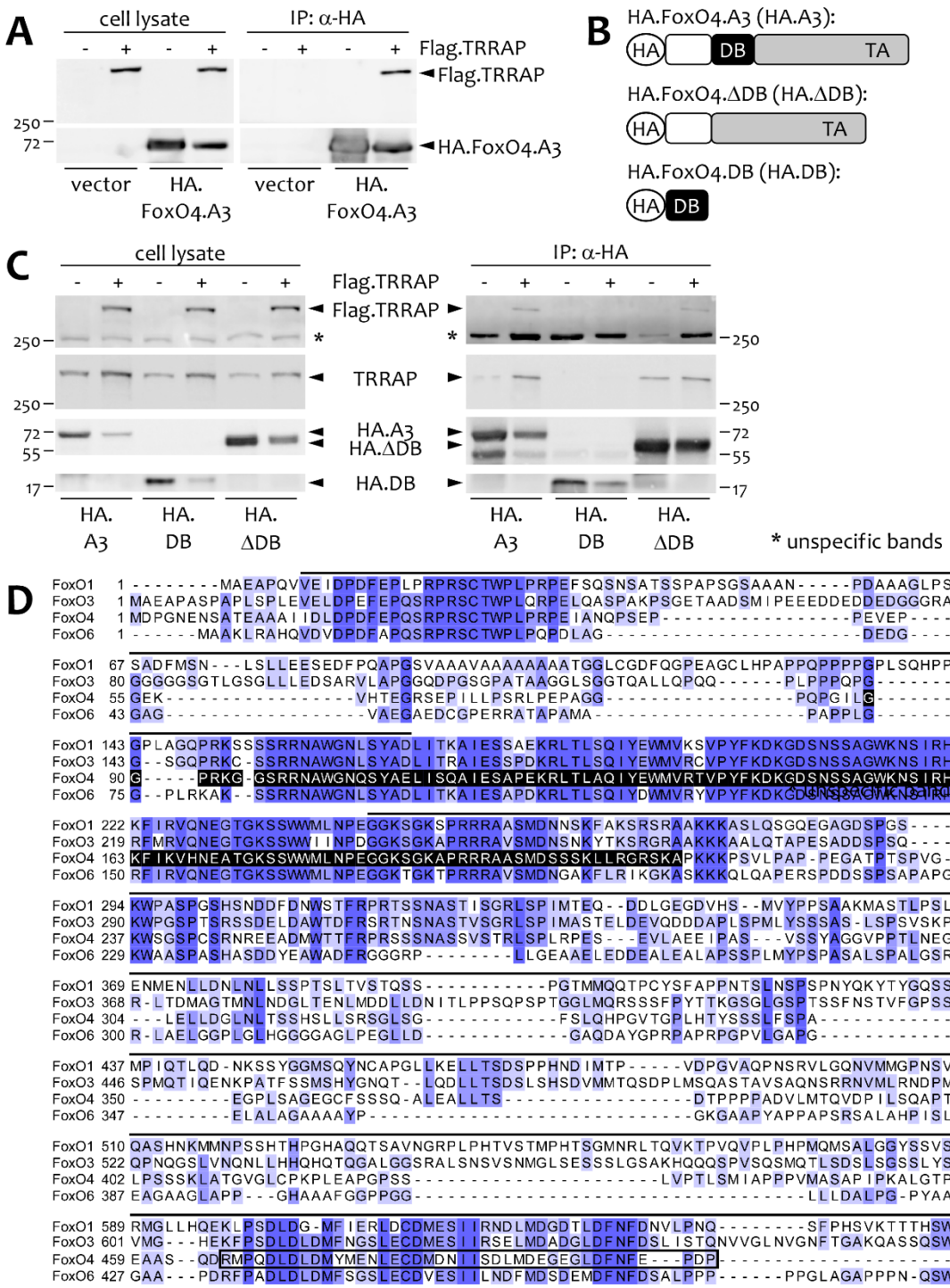

Figure 10: TRRAP interacts with FoxO4 in HEK293 and does not bind to the FoxO-DB domain.

TRRAP co-immunoprecipitates with FoxO4 but does not interact with the DB domain of FoxO4. **A**) Immunoblots representing whole lysates and HA-IPs from HEK293 cells expressing HA.FoxO4.A3 or the empty vector, each combined with Flag.TRRAP (+) or its control vector (-). **B**) Cartoon displaying the three engineered FoxO4 proteins used in this project. **C**) Western blots depicting cell lysates and HA-IPs from HEK293 cells transfected with Flag.TRRAP (+) or its empty vector (-) in combination with HA.FoxO4.A3 (HA.A3), HA.FoxO4.DB (HA.DB) or HA.FoxO4.ΔDB (HA.ΔDB). Bands marked with * were detected in all the samples by the used antibody in an unspecific way. **D**) Alignment of *H. Sapiens* FoxO protein sequences performed with Jalview program set on the Clustal alignment algorithm. Protein sequences were acquired from the UniProt database (FoxO1: #Q12778; FoxO3: #O43524; FoxO4: #P98177; FoxO6: #A8MYZ6). Blue shades: conservation degree of the amino acid residues; black shades: FoxO4.DB mutant sequence; black line on top of the sequences: FoxO4.ΔDB sequence; black transparent box: FoxO4 TA domain.

TRRAP is required for FoxO3 transcriptional activity in HUVEC

Given that a potential region of FoxOs involved in the interaction with TRRAP enclosed the TA domain, which is also necessary for FoxO-transcriptional activity, it was assessed whether the transcriptional capacity of FoxO3 in ECs is influenced by TRRAP.

First, a Luciferase reporter assay was performed to measure the induction of the 6xDBE-luc reporter, an established FoxO-responsive construct for Luciferase assays that is composed by a *Firefly* Luciferase reporter downstream of six tandem repeats of the DAF-16 DNA binding sequence (Furuyama et al. 2000). HUVEC were co-transfected with the 6xDBE-luc reporter, a *Renilla*-luc reporter for data normalisation, and FoxO3.A3.ER combined with Flag.TRRAP or its empty vector. After the incubation in culture medium with or without 4-OHT for 16 hours, the Luciferase activities were measured. As expected, the activation of FoxO3 triggered by 4-OHT turned on the 6xDBE-luc reporter. The concomitant overexpression of Flag.TRRAP amplified the activity of the FoxO-reporter, implying an involvement of TRRAP in FoxO3 transactivation (Figure 11A).

Secondly, the mRNA expression levels of relevant established endothelial FoxO-target genes were evaluated. HUVEC were first retrovirally transduced with 3xHA.FoxO3.A3.ER or its vector and then transfected with either a scrambled siRNA (siSCR) or a pool of two *TRRAP*-targeting siRNAs (siTRRAP). After incubation with 4-OHT for 16 hours, the cells were lysed, and the RNA was isolated. Initially, the efficiency of the knockdown of *TRRAP* was verified: on average an inhibition of ~50% of the *TRRAP* mRNA expression was achieved (Figure 11B). The siRNA-mediated TRRAP depletion was also likewise confirmed at the protein level (representatively shown in Figure 12C and in (Fusi et al. 2022)). In line with the previous results, the impairment of TRRAP expression resulted in the repression of FoxO3-dependent transcription of the selected target genes, such as *IGFBP1*, $p27^{kip1}$, *BIM* and *ANGPT2* (Figure 11C). Similarly, siTRRAP inhibited the expression of FoxO3-induced targets at the protein level (Fusi et al. 2022).

Taken together, these data implied that TRRAP was required to sustain the transactivation of FoxO3, and that it critically influenced FoxO3 transcriptional activity in ECs.

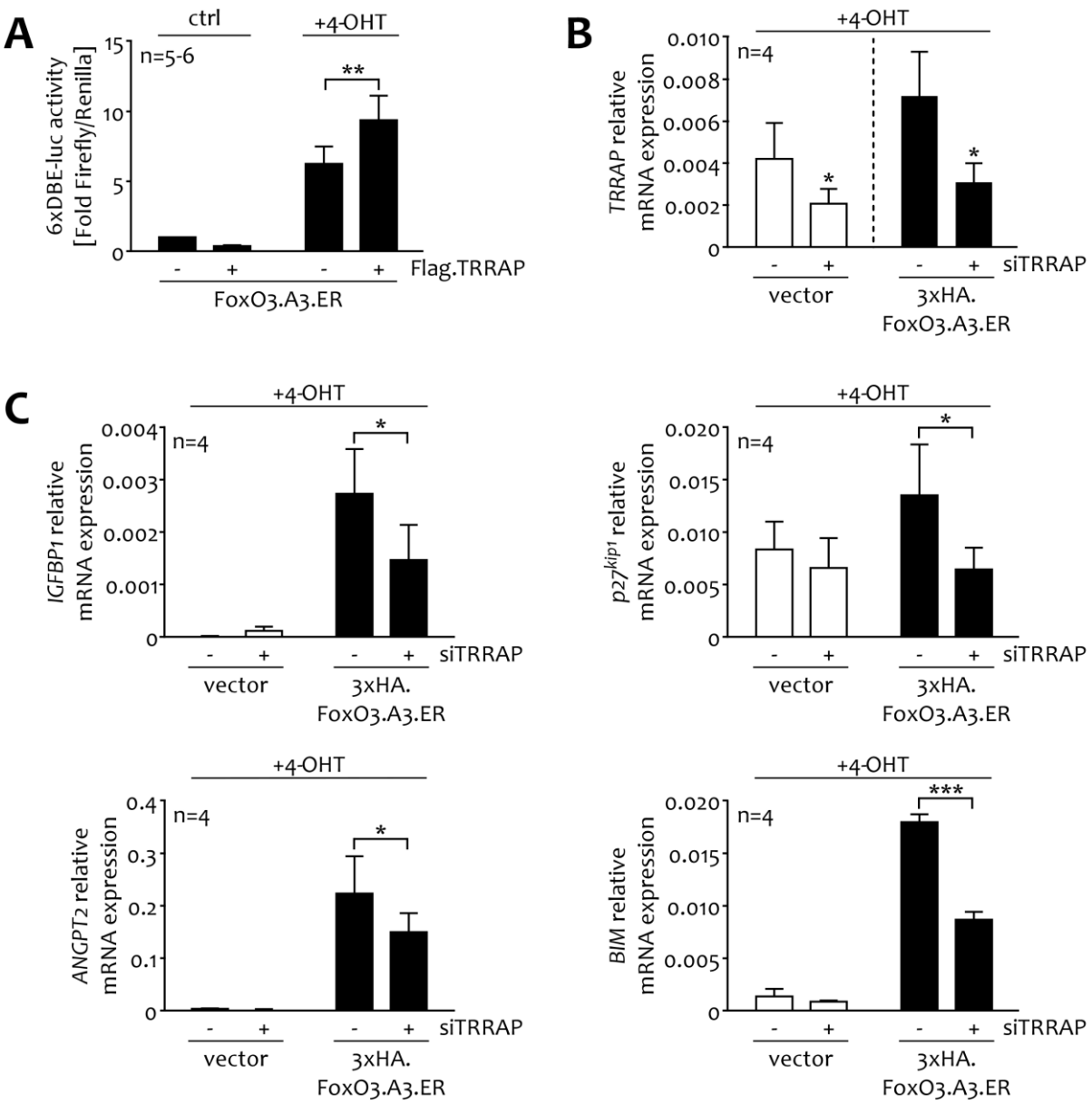

Figure 11: TRRAP augments FoxO3 transactivation.

The FoxO3-dependent transcription is supported by the presence of TRRAP in HUVEC. **A**) Bar chart depicting fold-activity of the 6xDBE-luc in HUVEC transfected with FoxO3.A3.ER in combination with Flag.TRRAP (+) or its control vector (-) after 16-hours-incubation in medium (ctrl) or medium with 4-OHT (4-OHT). FoxO-reporter activity is presented as the ratio between the light intensity emitted by the 6×DBE-luc reporter and the light intensity produced by the constitutively expressed *Renilla*-luc reporter. The diagram summarises the means + SD of n = 5–6 independent experiments. An unpaired t-test was performed and the statistical significance between the indicated samples is highlighted (** $p \leq 0{,}01$). **B**, **C**) Histograms representing the relative mRNA expression levels (normalised to GAPDH) of the specified genes. HUVEC were retrovirally transduced with an empty vector or 3xHA.FoxO3.A3.ER, successively transfected with a scrambled siRNA (-) or a pool of two siRNA against *TRRAP* (+) and stimulated for 16 hours with 4-OHT. In the bar graphs the means + SD from n = 4 independent experiments are shown. In *B*, unpaired t-tests were performed and statistical significance to the respective vector/siSCR condition is marked (* $p \leq 0{,}05$). In C, a two-way-ANOVA test with Sidak multiplicity correction was applied and significance between the specified conditions is reported by asterisks (*** $p \leq 0{,}001$; * $p \leq 0{,}05$).

FoxO3-dependent apoptosis and cell cycle arrest depend on TRRAP expression

In the endothelium, the final outcome of FoxO transactivation and of the resulting BIM expression is the enhancement of apoptosis (Czymai et al. 2010). Thereby the following planned step was to investigate if the reduction of TRRAP levels would impair the FoxO-dependent cell death as well.

HUVEC expressing 3xHA.FoxO3.A3.ER or its empty vector were transfected with siSCR or siTRRAP and subsequently incubated with or without 4-OHT for 48 hours, to allow occurrence of apoptosis (for the levels of protein overexpression or knockdown refer to Figure 12C). Figure 12A displays a representative flow cytometric analysis of cell cycle distribution after DNA staining of the cells with PI. The reported Sub-G1 percentages describe the amount of apoptotic cells. The 4-OHT treatment of 3xHA.FoxO3.A3.ER-transduced HUVEC caused an increase of apoptosis, which was blunted by the introduction of the siTRRAP (Figure 12A). Accordingly, the quantification of the apoptotic fractions measured in three independent experiments confirmed that FoxO3-induced apoptosis was dependent on the presence of TRRAP (Figure 12B). Consistently, when *TRRAP* was depleted in 3xHA.FoxO3.A3.ER-overexpressing HUVEC using a *TRRAP*-specific siRNA, the expression of the apoptosis-associated proteins BIM and Caspase 3 was reduced in relation to the respective siSCR control (Figure 12D).

To sum up, in HUVEC FoxO3 and TRRAP interacted in the nucleus and this binding served to FoxO3 to maintain its capacity to induce gene transcription via both classical and alternative mechanism, and to cause apoptosis.

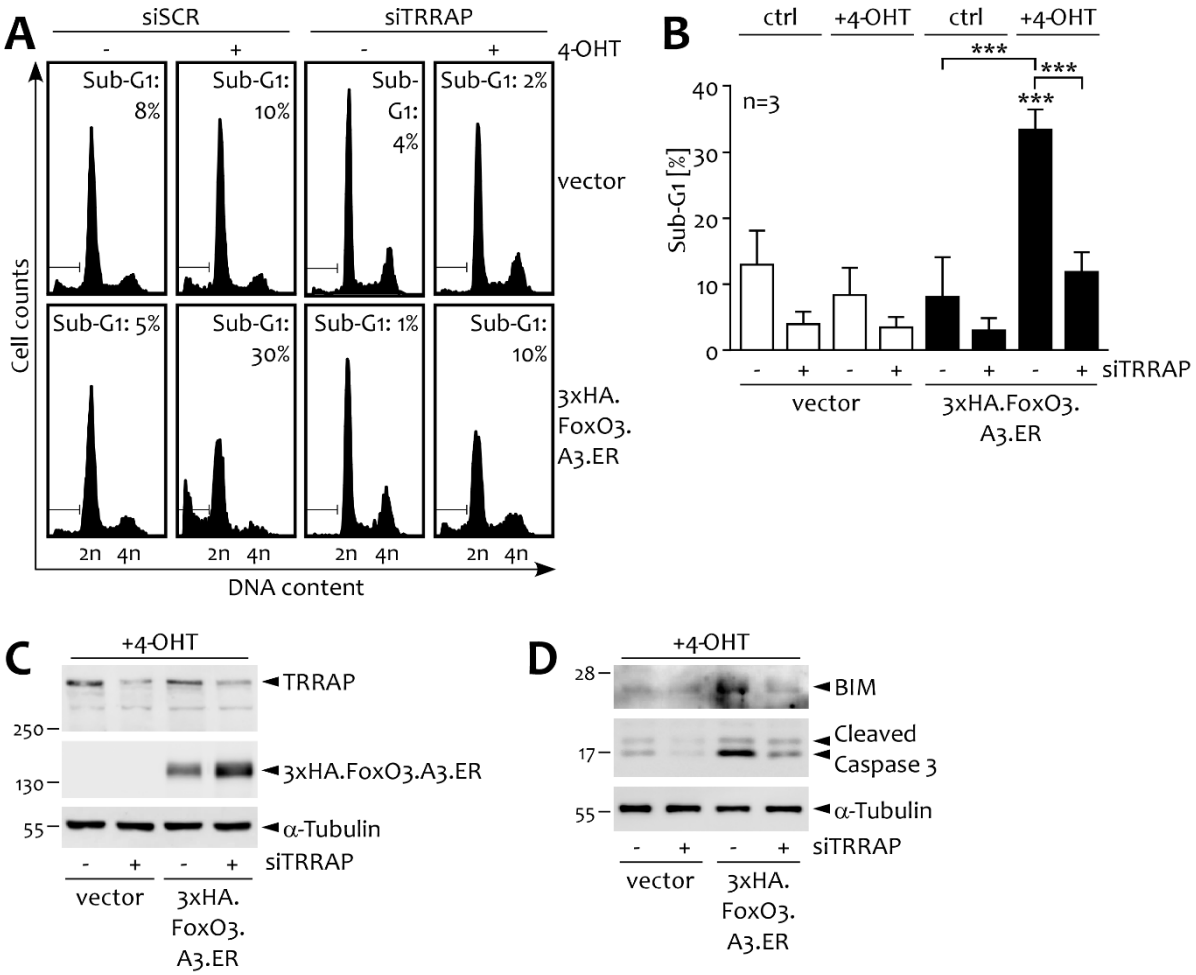

Figure 12: FoxO3-TRRAP interaction is essential for FoxO3 to trigger apoptosis.

In ECs TRRAP knockdown blocks the apoptosis induced by FoxO3. **A**) Cell cycle profiles illustrating a representative experiment, in which empty vector- or 3xHA.FoxO3.A3.ER-expressing HUVEC were transfected with siSCR or siTRRAP and cultured for 48 hours without (-) or with (+) 4-OHT. Apoptosis rates are indicated as percentage of the cell population with a sub-diploid DNA content (Sub-G1). **B**) Histogram showing the apoptosis quantification from n = 3 independent experiments done as in *A*. The means + SD of the percentage of cells in Sub-G1 phase are reported. The statistical significance was assessed by two-way-ANOVA tests with Sidak multiplicity correction (*** $p \leq 0.001$). The stars on top of the column indicate the significant regulation in comparison with the control (vector/siSCR/ctrl), while the significant differences between other samples are indicated by a horizontal bar with asterisks. **C**, **D**) Representative Western blots of HUVEC transduced with the empty vector or 3xHA.FoxO3.A3.ER, transfected with a siSCR (-) or siTRRAP (+) and stimulated with 4-OHT for 32 hours. α-Tubulin served as the loading control. *C* provides the expression controls, while *D* displays the regulation of the apoptotic proteins.

FoxO3 transcriptional activity is promoted by TRRAP in osteosarcoma cells

Considering that FoxO proteins have an important function in osteosarcoma and that the derived tumour cell lines are frequently used as models for studying FoxO impact on cell cycle progression (Medema et al. 2000; Sergi, Shen, and Liu 2019), some preliminary experiments were carried out in this context.

The UTA-6 cells, which were derived from the parental osteosarcoma U2OS cell line (Englert et al. 1995; Medema et al. 1998), were stably transfected with either an empty vector or with 3xHA.FoxO3.A3.ER. After 16 hours of incubation with 4-OHT, the HA-IPs were performed. Similar to the other investigated cell types, co-precipitation of 3xHA.FoxO3.A3.ER and TRRAP was detected, especially when cells were stimulated with 4-OHT (Figure 13A). In analogy to HUVEC, in UTA-6 cells the overexpression of Flag.TRRAP combined with FoxO3.A3.ER and 16 hours of 4-OHT treatment also boosted the 6xDBE-luc reporter activity in Luciferase assays, compared to the vector co-transfected condition (Figure 13B).

These data validated the previous findings that the interaction between FoxO3 and TRRAP was found in other cell types. Moreover, these results proved that the transactivating effect of TRRAP on FoxO3 was not only restricted to ECs.

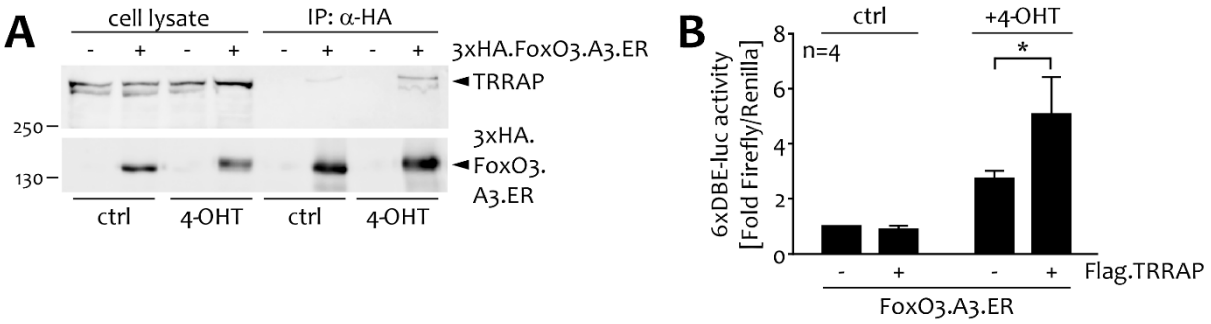

Figure 13: TRRAP binds to FoxO3 and sustains FoxO3-dependent transcription in UTA-6.

FoxO3 interacts with TRRAP in osteosarcoma cells and TRRAP presence strengthens FoxO3 activity. **A**) Western blots displaying UTA-6 cells stably expressing 3xHA.FoxO3.A3.ER (+) or its empty vector (-). The whole cell lysates were harvested after 16 hours stimulation with medium (ctrl) or with 4-OHT-supplemented medium (+4-OHT) and afterwards the HA-IPs were performed. **B**) Histogram showing fold Luciferase activity of the 6xDBE-luc reporter in UTA-6 cells expressing FoxO3.A3.ER, the FoxO3-luc-reporter and the constitutive *Renilla*-luc construct in combination with a control vector (-) or Flag.TRRAP (+). Each combination was either treated with (+4-OHT) or without (ctrl) for 16 hours. The FoxO-reporter activity is presented as the ratio of the light intensity emitted by the 6×DBE-luc reporter to the light intensity produced by the constitutively expressed *Renilla*-luc reporter. The diagram summarises the means + SD of n = 4 independent experiments. An unpaired t-test was performed and the statistical significance between the indicated samples is marked (* $p \leq 0{,}05$).

DISCUSSION AND OUTLOOK

Previous unpublished data showed that the activation of the MEK5/ERK5 pathway repressed the FoxO transcription factors and the consequent apoptosis in ECs. Therefore, the goal of this PhD project was to resolve the molecular mechanisms behind this interplay. To investigate the regulatory mechanisms that can explain the cell type specific functions of FoxOs was an additional aim of this work.

It was first possible to exclude that ERK5 suppressed FoxO activity by changing its subcellular localization, as indicated by IFs and by nuclear/cytoplasmic extraction in ECs. Moreover, the data collected by MS about FoxO3-interactome enabled an initial look at FoxO3 acetylation and phosphorylation. They revealed that MEK5D overexpression in HUVEC apparently did not affect these patterns (data not shown). This was consistent with the results of pilot investigations, where immunoblots with commercially available antibody specific for acetyl-FoxO1 or acetylated-Lysine did not suggest apparent differences in FoxO acetylation caused by MEK5D (data not shown). Certainly, these early tests need to be optimized and FoxOs and their PTMs should be inspected in a more detailed way. In this regard, a MS analysis dedicated to the detection of PTMs could be run with the focus on FoxO3 in combination with MEK5D.

To further characterise the ERK5-FoxO interaction and to investigate potential regulators of FoxO transcriptional activity, the MS analysis of the interactome of FoxO3 in ECs with and without MEK5D overexpression was carried out. To begin with, it was formally possible to exclude a direct interaction of ERK5 with FoxO3, as no peptide corresponding to ERK5 was significantly detected in any sample. Next, the MS analysis revealed USP7 as a protein that bound to FoxO3 with higher affinity in presence of MEK5D. Given that USP7 is a known inhibitor of FoxO4 (van der Horst et al. 2006), it would be consistent that the FoxO3-USP7 interaction was sustained by the MEK5/ERK5 cascade to block FoxO activity. Regrettably, the confirmation of this hypothesis was rather complicated since an amount of USP7 non-specifically bound to FoxO3 in absence of MEK5D and to the beads in the negative controls, although with less affinity. It would be desirable to validate this finding with a quantitative method, which is more accurate than a Western blot, e.g., a repetition of the MS analysis. However, van der Horst and colleagues demonstrated that USP7 inhibits FoxO transcriptional activity by changing the FoxO subcellular localization (van der Horst et al. 2006). However, since the results presented in this work suggest that the MEK5/ERK5 cascade does not affect FoxO nuclear-cytoplasmic shuttling, it is questionable whether an increased USP7-FoxO binding could explain the observed ERK5-dependent suppression of FoxO3 activity.

In contrast to USP7, the analysis of the FoxO3-interactome in ECs clearly revealed that TRRAP specifically bound to FoxO3 both in presence and absence of MEK5D. This newly found interaction between FoxO3 and TRRAP had not been characterised before and appeared to be a potential mechanism to explain the regulation of the FoxO3-dependent gene transcription.

Looking at the whole results of the MS analysis it became clear that FoxO3 did not only bind to TRRAP, but also to several other proteins known to form complexes with HAT activity around TRRAP itself (Elias-Villalobos, Fort, and Helmlinger 2019; Lempiainen and Halazonetis 2009). Most of these proteins belongs to the TRRAP/Tip60 complex, which might be the preferential HAT complex bound by FoxO3 in ECs. The Tip60 HAT complex is triggered in presence of DNA damages (Murr et al. 2006) and the FoxO transcription factors are also known to be involved in DNA repair mechanisms (Eijkelenboom and Burgering 2013; Gui and Burgering 2021). Additionally, it was demonstrated that the activation of the DNA damage response signal transduction pathway leads to the formation of a complex among FoxO3, Tip60 and ATM, another kinase belonging to the PIKK family as TRRAP (Adamowicz, Vermezovic, and d'Adda di Fagagna 2016). Consequently, TRRAP and PIKKs might be the key factors for the recruitment of FoxOs where DNA ruptures have happened.

It is known that HAT can also acetylate non-histone substrates (Lee and Workman 2007). It is therefore reasonable to believe that TRRAP might control acetylation of other proteins in the complex, which in turn may affect FoxO activity. In accord with the preliminary analysis of FoxO acetylation status (data not shown) it is rather unlikely that TRRAP directly leads to acetylation of FoxOs, but this aspect needs more detailed investigations.

Additional data unveiled that TRRAP was bound by FoxOs in the nucleus, and that the interaction was conserved in several cell types. More precisely, the IPs conducted in HEK293 cells with the FoxO4 deletion mutants demonstrated that TRRAP interacted with FoxO4 in a way that did not require the DB domain of FoxOs. This implied that the interaction took place even if FoxO could not bind the DNA. Consistently, the data obtained in ECs indicated that TRRAP still interacted with 3xHA.FoxO3.A3.ER(H212R), the FoxO3 mutant that lost the ability to directly bind its target DNA-FRE sequences. As a result, the newly discovered interaction is a very good candidate to clarify how FoxOs can support transcription of genes by the alternative system. The next step that should be done to validate this hypothesis is to characterise more in detail which domains of FoxOs and TRRAP are really needed for the interaction, either using deletion mutants or µSPOT technology.

Moreover, starting from the point that the interaction between the FoxO factors and TRRAP might involve the conserved TA domain of FoxOs, the role of TRRAP with respect to FoxO transcriptional activity in ECs was explored. The analyses of the expression of a FoxO-reporter system in Luciferase assays and of mRNA levels of FoxO3 target genes demonstrated that FoxO3-TRRAP interaction sustained the full transcriptional capacity of FoxO3. In accordance, TRRAP expression was necessary to maintain the apoptosis caused by the activation of FoxO3 in HUVEC. Interestingly, earlier papers described a similar mechanism: TRRAP lead to the recruitment at the DNA of several other TFs, such as c-Myc, p53, and E2F, turning them on (Barlev et al. 2001; McMahon et al. 1998). With this information, it can be speculated that TRRAP might work as big chromatin hub for many TFs, facilitating the transcriptional activity of precise TF subsets in response to specific cellular stimuli.

The previously described system might also be important in other cells, as FoxO3-TRRAP interaction was confirmed in additional cancer cell lines, as HEK293 and UTA-6. In the latter cell type, where FoxO was shown to cause cell cycle arrest (Medema et al. 2000), overexpression of Flag.TRRAP could upregulate the activity of the FoxO3 reporter in Luciferase assays, in agreement with the results obtained in HUVEC. On one hand, further experiments with UTA-6 should be performed to validate the effect of TRRAP overexpression or knockdown on FoxO-dependent transcription and cell cycle arrest. On the other hand, the already available data encourage the idea that TRRAP binding to FoxO factors is a conserved regulatory mechanism of FoxO-dependent gene transcription, cell cycle arrest and apoptosis. The fact that in the endothelial context TRRAP mediated the cell cycle arrest, which was triggered as first step by the activation of FoxO3 (Fusi et al. 2022), reinforces this view.

It could be speculated that TRRAP and FoxOs bind together to the FRE sequences of the target genes, thereby recruiting HAT complexes and other factors needed for the activation of the transcription of classically regulated genes. The regulation of the FRE-independent genes might be determined by the association of FoxO to TRRAP, when TRRAP is already localized at the DNA by the interaction with other TFs. Thus, the outcome of the activation of this system would depend on the balance, the combination, or the competition of the factors, which can bind to TRRAP (Figure 14).

The published data demonstrated that TRRAP and FoxO interact to strengthen FoxO activity in the endothelium (Fusi et al. 2022). However, a careful look at the Western blots in Figure 8B hinted that MEK5D overexpression might weaken the interaction between FoxO3 and TRRAP. Additionally, the analysis of the MS raw data allowed to quantify the impact of MEK5D on the intensities of the FoxO3-TRRAP interaction as well as of the interaction between FoxO3 and other known TRRAP interactants (Suppl. Table 1 and Suppl. Figure 2). The overexpression of MEK5D apparently reduced the strength of these interactions, in particular FoxO3-TRRAP binding was roughly 3 times weaker (data not shown). Since the threshold to confidently identify potential MEK5D-dependent interactions was arbitrarily set at +/- 5-fold to compensate for expected variations among the experiments, these data should be carefully interpreted. However, if the results of ongoing preliminary investigations of the research group in HEK293 cells are also considered, the hypothesis that ERK5 activation might modulate FoxO-TRRAP interaction or the composition of the protein complex involved in FoxO-dependent transcription is not too far-fetched (Figure 14). To corroborate the data obtained with HEK293 cells and to gain significant quantification data from the mass spectrometric analysis, it would be important to repeat the MS experiment at least one-to-two additional times. Moreover, this hypothesis should further be tested in additional co-immunoprecipitation experiments.

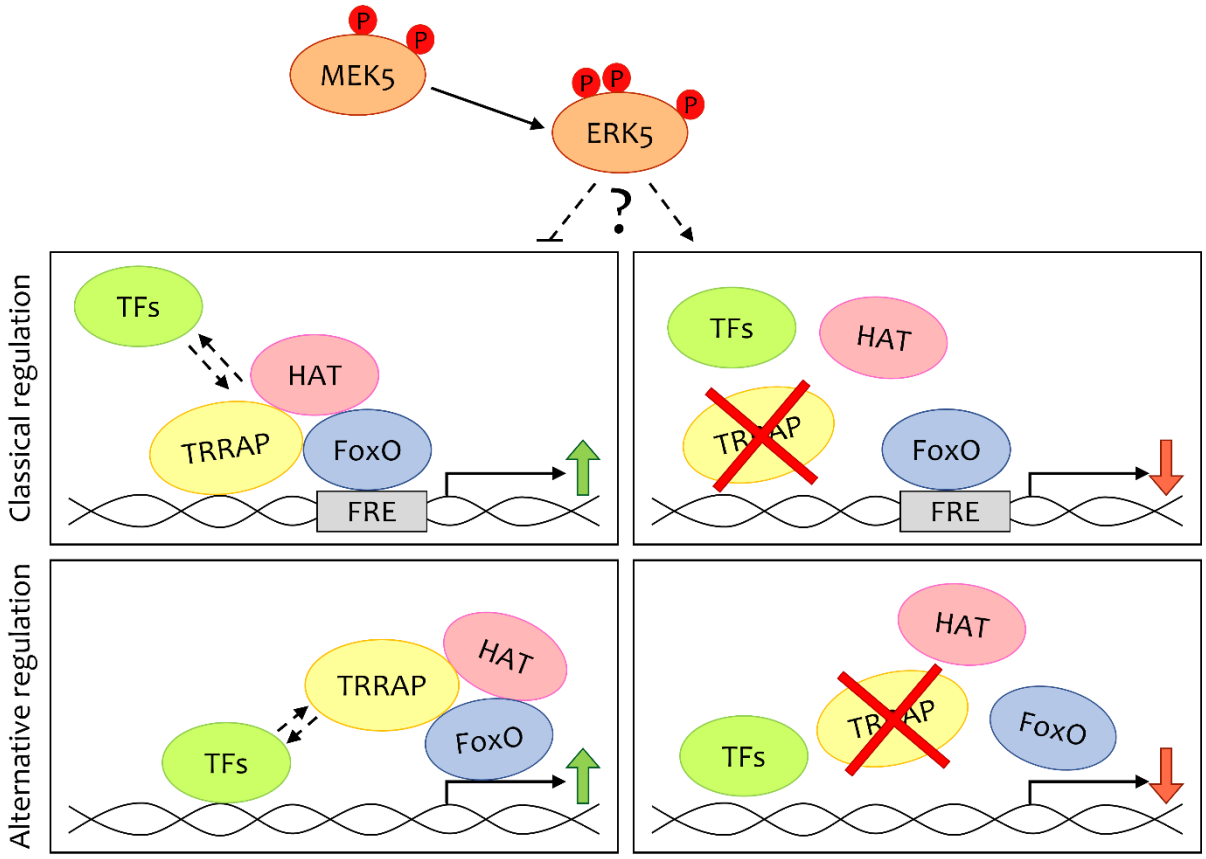

Figure 14: Illustration of the new potential regulatory mechanism of FoxO proteins.

The cartoon exemplifies the role of the novel discovered interaction between FoxOs and TRRAP with respect to the regulation of FoxO-dependent gene transcription. The potential involvement of the MEK5/ERK5 pathway is also depicted. "Classical regulation" indicates the FRE-dependent transcriptional activity of FoxOs, while "Alternative regulation" stands for the FRE-independent one. The green arrows symbolise the induction of the FoxO-dependent transcription, whilst the red arrows express a reduction of the transcription of FoxO targets. HAT: Histone acetyltransferase complex; TFs: transcription factors; FRE: FoxO responsive element.

It can be speculated that the MEK5/ERK5 pathway may interfere with FoxO activity not only in the endothelium, but also in tumoral contexts. It would be interesting to know if the FoxO-TRRAP interaction also exists in tumour cells where ERK5 is required for cell survival. The melanoma-derived cell lines might be good candidates for further experiments, as it was demonstrated that the MEK5/ERK5 activation is needed by these cancer cells to overcome the therapy-induced growth inhibition (Adam et al. 2020; Benito-Jardon et al. 2019).

Furthermore, it was published that a hot spot mutation of TRRAP at amino acid 722 (S722F) in melanoma is essential for cell survival (Wei et al. 2011). Therefore, experiments conducted in melanoma cells with a mutated TRRAP should elucidate if TRRAP mutation interferes with the interaction with FoxOs. However, very recent unpublished data from the research group of Prof. Dr. Marc Schmidt showed that in HEK293 cells the S722F mutation of TRRAP did not affect the binding between FoxOs and TRRAP.

In several melanoma cell lines, the TRRAP genomic DNA (gDNA) sequence around the hot spot mutation was characterised (Figure 15, A and B). These cell lines might be useful to conduct studies about the function of FoxOs, their synergism with TRRAP, and the role that the interaction plays in the control of the apoptosis, particularly in the context of the therapy resistance promoted by the activation of ERK5.

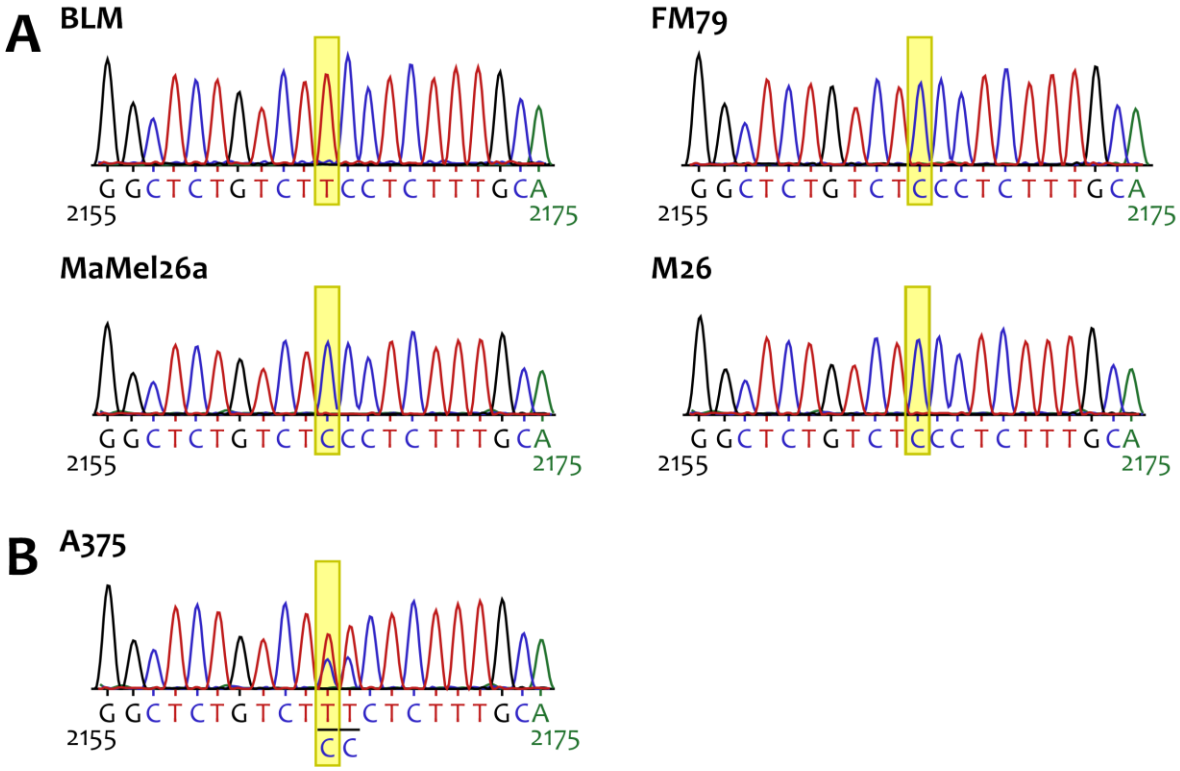

Figure 15: Determination of TRRAP status in melanoma cell lines.

Identification of the TRRAP gDNA sequence for the hotspot nucleotide position 2165. **A**, **B**) Electropherograms representing the gDNA sequence of the nucleotides 2155-2175 of the TRRAP gene in four NRAS-mutated melanoma cell line (in *A*) and in one BRAF V600E cell line (in *B*). The yellow boxes highlight the gDNA position 2165, the hotspot missense mutation (C>T) of TRRAP found in melanoma, which causes an aminoacidic change (S722F) (Wei et al. 2011).

In conclusion, the results of this PhD project described TRRAP as a new binding partner of FoxO, which sustained FoxO activity in ECs and in other cancer cells. In addition, the data support the hypothesis that the MEK5/ERK5 pathway may antagonise FoxO functions by influencing TRRAP-FoxO interaction. The activation of ERK5 might affect the binding to TRRAP of a specific group of TFs, shifting the equilibrium towards less bound FoxOs in favour of other TFs, as for instance c-Myc or p53. This would then change the transcription level of certain gene subsets that could be important not only for the ERK5-dependent apoptosis protection in ECs, but also for tumour cells exposed to therapeutic stress. Lastly, the system would be flexible and capable to steer the expression of certain groups of factors in response to specific cellular or extracellular stimuli, and this would make it possible to influence the fate of the cells in a very precise way.

MATERIALS

Materials and buffers

Common laboratory reagents and chemicals not explicitly mentioned in this work were purchased from Applichem, Carl Roth, InvivoGen, Merck, Th. Geyer or Thermo Fisher Scientific.

Cloning

Primers for pBP-HA.FoxO3.A3.ER linearization (Sigma):

- Forward: 5'-GCCGGCGCCTAGAGAAGG-3'
- Reverse: 5'-GCAGAGGCACCGGCTTCC-3'

Enzymes:

- Alkaline phosphatase, calf intestinal (CIP; New England Biolabs, #M0290)
- BamHI restriction enzyme (Thermo Fisher Scientific, #ER0051)
- BglII restriction enzyme (Thermo Fisher Scientific, #ER0081)
- T4 Ligase (Thermo Fisher Scientific, #EL0016)

Bacteria for plasmid transfection:

- Homemade competent DH5-α *E. coli* were obtained from the stock collection of the Department of the Dermatology, University Hospital Würzburg.

Bacteria culture media:

- Lennox Lysogeny broth (LB) Base (Invitrogen, #12780052)
- LB Agar (Invitrogen, #22700025)

Agarose gel electrophoresis

5x Tris-Borate-EDTA (TBE) buffer

450 mM Boric acid (Applichem)
450 mM Tris
10 mM EDTA

Running gel

0,7% to 1 % Agarose NEEO Ultra-Quality (Carl Roth, #2267.2)
5% HDGreen® Plus Safe DNA Dye (Intas, #ISII-HDGreen Plus)
1x TBE buffer

5x Sample loading buffer

60% Sucrose

1 mM Cresol Red (Alfa Aesar, #A17243)

Cell culture

With the exception of HUVEC, all the following cell lines were obtained from the stock collections of the Department of Dermatology, University Hospital Würzburg.

Cell lines:

- A375, cancer cell line isolated from the skin of a female patient with a malignant melanoma (Giard et al. 1973). The cells carry a BRAF V600E mutation.
- Phoenix-Ampho helper-free producer lines: highly transfectable HEK293T-derived cell line, that produces amphotropic retroviruses and is used for retroviral transduction (http://web.stanford.edu/group/nolan/_OldWebsite/retroviral_systems/phx.html).
- BLM, tumour cell line obtained from a lung metastasis of a mouse injected with melanoma cells from a male patient (van Muijen et al. 1991). Cells show a mutation in the NRAS protein.
- FM79, cancer cell line derived from the cutaneous malignant melanoma of a female patient (Bartkova et al. 1996). This cell line has a NRAS mutation.
- HEK293, transformed cell line originated from the kidney of a female patient (Graham et al. 1977).
- HUVEC, primary endothelial cells taken from the umbilical vein. Cells were purchased from PromoCell and came from female donors (charge number: #8031901) or male donors (charge numbers: #7022701, #1082201.1, #3102402, #449Z008 and #439Z021.1).
- M26, melanoma-derived cell line, showing a mutated NRAS (Schrama et al. 2008).
- MaMel26a, tumour cell line originated from a melanoma metastasis located in the lymph node of a male patient. These cells carry a NRAS mutation (Schrama et al. 2008).
- UTA-6, osteosarcoma cell line obtained from U2OS cells (Englert et al. 1995; Medema et al. 1998), which were isolated from the bone tumour of a female patient.

Cell culture media:

- DMEM++: Dulbecco's modified eagle medium (DMEM; Gibco, #61965-026) with 10% Foetal bovine serum (FBS) superior (Sigma) and 30 µg/ml Gentamicin (Sigma).
- HUVEC MIX: consisting of one part of EBM™ basal medium (Lonza, #CC-3121) with the EGM™ endothelial cell growth medium SingleQuots™ supplements (hEGF, Hydrocortisone, GA-1000, BBE and FBS, but no Ascorbic acid; Lonza, #CC-4133) and of two parts of M199++++ (Schmidt, Goebeler, and Martin 2016).

- M199++++: Medium 199 supplemented with 10% FBS superior (Sigma), 30 µg/ml Gentamicin (Sigma), 15 ng/ml Amphotericin B (Sigma) and 0,02 µl/ml Liquemin® N5000 (Hoffmann-La Roche).
- Medium 199 (Gibco, #41150-020).
- OptiMEM™ (Gibco, #31985-047).
- RPMI+: Roswell Park Memorial Institute 1640 medium (RPMI; Gibco, #61870-010) with 10% FBS superior (Sigma).

Freezing medium:

10% DMSO

10% FBS

Medium required by the specific cell line (as described above)

Cell culture reagents and stimuli:

- 5 µg/ml Hexadimethrine bromide (Polybrene; Sigma, #H9268)
- 100 nM 4-hydroxytamoxifen (4-OHT; Calbiochem, #579002)
- 10 µM LY-294,002 hydrochloride (LY294002; Sigma, #L9908)
- 2 µg/ml Puromycin (InvivoGen, #ant-pr-1)
- 0,4% Trypan Blue solution (Sigma, #T8154)
- 0,05% Trypsin/EDTA in 1x PBS (Gibco, #15400-054)

Cell manipulation

Plasmids:

- pBP-empty vector (Morgenstern and Land 1990)
- pBP-MEK5D (Ohnesorge et al. 2010)
- pBP-HA.FoxO3.A3.ER (Czymai et al. 2010)
- pBP-3xHA.FoxO3.A3.ER (see methods section and (Fusi et al. 2022))
- pBP-3xHA.FoxO3.A3.ER(H212R) (unpublished, see methods section)
- pCDNA3-FoxO3.A3.ER (Dijkers et al. 2000)
- pECE-HA.FoxO3 (Brunet et al. 1999)
- pMT2-HA.FoxO4.A3 (Medema et al. 2000)
- pMT2-HA.FoxO4.DB (Medema et al. 2000)
- pMT2-HA.FoxO4.ΔDB (Medema et al. 2000)
- pCbS-Flag -empty vector (Addgene, #32104) (McMahon et al. 1998)
- pCbS-Flag-TRRAP (Addgene, #32103) (McMahon et al. 1998)
- 6xDBE-luc reporter (Furuyama et al. 2000)
- Renilla-luc reporter (Promega)

- **siRNAs:**
  - siSCR, customised sequence: 5'-UUCUCCGAACGUGUCACGUdTdT-3' (Eurofins)
  - siTRRAP#1, targeting the mRNA sequence: 5'-CTACGATTCTGGTGGAATA-3' (Thermo Fisher Scientific, catalogue #4427038, siRNA #s15796)
  - siTRRAP#2, targeting the mRNA sequence: 5'-GGACTTAACTGGAGAGGTT-3' (Horizon Discovery, #D-005394-01)

Calcium-Phosphate transfection

- **Calcium Chloride solution**

  2,5 M $CaCl_2$

  DNase/RNase free water

- **2x HBS buffer pH 7,05**

  280 mM Na-Chloride

  50 mM HEPES pH 7,05

  12 mM Glucose

  10 mM KCl

  1,5 mM Na_2HPO_4

DEAD-Dextran transfection

- **HEPES solution**

  1 mM HEPES pH 7,3

  1x PBS

- **Chloroquine solution**

  150 µM Chloroquine diphosphate salt (Sigma, #C6628)

  Medium M199++++

DNA analysis

- **Propidium Iodide (PI) buffer**

  250 µg/ml RNase (Applichem)

  10 µg/ml Propidium Iodide (Sigma-Aldrich)

  1x PBS

RNA analysis

Master mix for qPCR

50% TaqMan® gene expression master mix (Applied Biosystems, #4369016) or PowerUp™ SYBR™ Green master mix (Applied Biosystems, #4369016)

35% DNase/RNase free water

10% Sample cDNA (1:10 dilution after cDNA synthesis)

5% Assay mix or Primer solution (see below)

20x Probes for TaqMan qPCR (Assay mix; Applied Biosystems):

- ANGPT2 (#Hs01048041_m1)
- BIM (#Hs01076940_m1)
- GAPDH (#Hs99999905_m1)
- IL-8 (#Hs00174103_m1)
- NOXA (#Hs00560402_m1)
- $p27^{kip1}$ (#Hs01597588_m1)
- TRRAP (#Hs00268883_m1)
- VCAM1 (#Hs01003372_m1)

5 µM Primer pairs for SYBR™ Green qPCR (Primer solution; Sigma):

- GAPDH (fwd: 5'-CCACCCATGGCAAATTCC-3'; rv: 5'-GATGGGATTTCCATTGATGACA-3')
- IGFBP1 (fwd: 5'-GGGACGCCATCAGTACC-3'; rv: 5'-CCATTTTTTGATGTTGGTGAC-3')

Immunofluorescence

Fixation solution

3,7% Formaldehyde

1x PBS

Permeabilization solution

0,5% Triton X-100

1x PBS

Buffer A

1% BSA (Sigma-Aldrich)

1x PBS

- **Buffer B**

  1% Normal Goat Serum (Jackson ImmunoResearch; #005-000-121)

  1% BSA (Sigma-Aldrich)

  1x PBS

- **Washing buffer**

  0,1% BSA (Sigma-Aldrich)

  1x PBS

- **Primary antibodies:**
  - FoxO3a, monoclonal (75D8), rabbit, 1:200 in Buffer B (Cell Signaling, #2497)
  - ER, rabbit, 1 µg/ml in Buffer B (1:2000; Santa Cruz, #sc-542 X)
  - Hoechst 33342, 1:1000 in Buffer A (Sigma)

- **Secondary antibody:**
  - Goat anti-rabbit IgG, Alexa Fluor™ 568, 10 µg/ml in Buffer A (1:200; ThermoFisher, #A-11036)

Protein analysis

- **E1A lysis buffer (ELB+++)**

  150 mM NaCl

  50 mM HEPES pH 7,5

  20 mM β-glycerophosphate (freshly added)

  5 mM EDTA

  500 µM Na-orthovanadate (freshly added)

  0,1 % NP-40

  1x cOmplete Protease Inhibitor Cocktail (Roche, freshly added)

- **Buffer C (cytosolic fraction)**

  10 mM HEPES pH 7,9

  10 mM KCl

  1 mM DTT (freshly added)

  500 µM PMSF (freshly added)

  100 µM EDTA

  100 µM EGTA

- **Buffer N (nuclear fraction)**

  400 mM NaCl

  20 mM HEPES pH 7,9

  1 mM DTT (freshly added)

  1 mM EDTA

  1 mM EGTA

  1 mM PMSF (freshly added)

- **4x Lämmli sample buffer**

  250 mM Tris/HCl pH 6,8

  40% Glycerol

  10% β-Mercaptoethanol

  8% SDS

  0,01 % Bromophenol blue

Western Blot

- **Running gel buffer**

  375 mM Tris/HCl pH 8,8

  6-12% Acrylamide 4K solution (Applichem)

  0,1% APS (Sigma)

  0,1% SDS

  0,04% SureCast™ TEMED (Invitrogen)

- **Stacking gel buffer**

  125 mM Tris/HCl pH 6,8

  3% Acrylamide 4K solution (Applichem)

  0,15% APS (Sigma)

  0,1% SDS

  0,1% SureCast™ TEMED (Invitrogen)

- **10x Electrophoresis buffer**

  1,92 M Glycine

  250 mM Tris

  1% SDS

- **10x Blotting buffer**

  1,92 M Glycine

  250 mM Tris

- **Ponceau buffer**

  5% Acetic Acid

  0,1% Ponceau S (Serva)

- **10x Tris buffered saline (TBS) pH 7,6**

  1,37 M NaCl

  200 mM Tris

- **1x TBS with Tween20 (TBST)**

  0,05% Tween20 (Merck)

  1x TBS pH 7,6

- **Blocking buffer**

  5% Non-fat dry milk powder (Millipore) or 5% Bovine serum albumin (BSA; Sigma-Aldrich)

  1x TBST

- **Enhanced chemiluminescence (ECL) buffer**

Solution 1	+	Solution 2
0,1 M Tris solution pH 8,5		0,1 M Tris solution pH 8,5
2,5 mM Luminol (freshly added)		0,02% H_2O_2 (freshly added)
400 µM P-coumaric acid (freshly added)		

- **Stripping buffer**

  100 mM β-Mercaptoethanol

  62,5 mM Tris/HCl pH 6,7

  2% SDS

- **Primary antibodies:**
  - BIM, rabbit, 1 µg/ml in 5% Milk/TBST (1:1000; Sigma, #B7929)
  - Cleaved Caspase 3, monoclonal (5A1E), rabbit, 1:1000 in 5% Milk/TBST (Cell Signaling, #9664)
  - ERK5/p-ERK5, rabbit, 1,8 µg/ml in 5% Milk/TBST (1:8000; Sigma, #E1523)
  - Flag, rabbit, 250-300 ng/ml in 5% Milk/TBST (1:2500; Rockland, #600-401-383)
  - Flag, monoclonal (M2), mouse, 8 µg/ml in 5% Milk/TBST (1:500; Sigma, #F3165)

- FoxO3a, monoclonal (75D8), rabbit, 1: 1000 in 5% Milk/TBST (Cell Signaling, #2497)
- HA, monoclonal (3F10), rat, 200 ng/ml in 5% Milk/TBST (1:500; Roche, #1867423)
- MEK5, rabbit, 1 µg/ml in 5% Milk/TBST (1: 1000; Millipore, #AB3184)
- TRRAP, rabbit, 1: 1000 in 5% BSA/TBST (Cell Signaling, #3966)
- α-tubulin, monoclonal (B-5-1-2), mouse, 2-2,5 µg/ml in 5% Milk/TBST (1:10 000; Sigma, #T5168)
- USP7, rabbit, 1 µg/ml in 5% Milk/TBST (1:10 000; Bethyl Laboratories, #A300-033A)

Secondary antibodies:

- ECL™ anti-mouse HRP, 1:2000 in 1,7% Milk/TBST (GE Healthcare, #NA9310V)
- ECL™ anti-rabbit HRP, 1: 2000 in 1,7% Milk/TBST (GE Healthcare, #NA9340V)
- Goat anti-rat IgG (HRP), 200 ng/ml in 1,7% Milk/TBST (1:5000; Abcam, #ab97057)

Immunoprecipitation

Washing buffer

300 mM Potassium acetate
20 mM HEPES pH 7,5
0,01% NP-40

High salt washing buffer

500 mM NaCl
50 mM HEPES pH 7,5
20 mM β-glycerophosphate (freshly added)
5 mM EDTA
500 µM Na-orthovanadate (freshly added)
0,1 % NP-40
1x cOmplete Protease Inhibitor Cocktail (Roche, freshly added)

Antibodies and beads for immunoprecipitation:

- Pierce™ anti-HA magnetic beads (ThermoFisher, #88837)
- Anti-Flag® M2 magnetic beads (Sigma, #M8823)

Mass spectrometry

Destaining buffer

30% Acetonitrile
100 mM NH_4HCO_3 pH 8

- **Digestion Buffer**

  0,1 µg Trypsin for each gel band

  100 mM NH_4HCO_3 pH 8

TRRAP status definition

- **Primers for TRRAP amplification (Wei et al. 2011) (Sigma):**
  - Forward: 5'-GTAAAACGACGGCCAGTTTGCTACGATTCTGGTGGAA-3'
  - Reverse: 5'-CGTGAGGCCCTGTCTCTAAC-3'

- **Primer for TRRAP sequencing (Wei et al. 2011) (Sigma):**
  - 5'-GTAAAACGACGGCCAGT-3'

Commercial kits and consumables

- 4–15% Mini-PROTEAN® TGX™ Precast Protein Gels, 15-well, 15 µl (Bio-Rad, #4561086)
- 4x NuPAGE™ LDS sample buffer (Invitrogen, #NP0008)
- 4x TruePAGE, LSD sample buffer (Sigma, #PCG3009)
- 20x NuPAGE™ MOPS SDS Running Buffer (Invitrogen, #NP0001)
- BD FACSClean™ (BD Biosciences, #340345)
- BD FACSFlow™ (BD Biosciences, #342003)
- BD FACS™ Shutdown solution (BD Biosciences, #334224)
- Countess™ cell counting chamber slides (Invitrogen, #C10228)
- Dual-Glo® Luciferase Assay System (Promega, #E2940)
- Genopure Plasmid Maxi Kit (Roche, #3143422001)
- Genopure Plasmid Midi Kit (Roche, #3143414001)
- Ibidi Mounting Medium (Ibidi, #50001)
- Lipofectamine® 2000 transfection reagent (Invitrogen, #11668-027)
- Monarch Genomic DNA Purification Kit (New England Biolabs, #T3010)
- NEBuilder® HiFi DNA assembly master mix (New England Biolabs, #M5520A)
- NuPAGE™ 4 to 12%, Bis-Tris, 1,0-1,5 mm, Mini protein gels (Invitrogen, #NP0321BOX)
- Oligofectamine™ transfection reagent (Invitrogen, #12252-011)
- Perfusion set (yellow/green, length: 50 cm, ID: 1,6 mm, 10 ml reservoirs; Ibidi, #10964)
- PicoFrit capillary column, 30 cm × 150 µm ID (New Objective, #PF360-150-15-N-5)
- Protein assay dye reagent concentrate (Bio-Rad, #5000006) diluted 1:5 in ddH_2O.
- QIAGEN Plasmid Maxi Kit (Qiagen, #12162)
- QIAGEN Plasmid Midi Kit (Qiagen, #12143)
- QuantiTect® reverse transcription kit (Qiagen, #205313)
- Quick start BSA standard (Bio-Rad, #5000206)
- ReproSil-Pur 120 C18-AQ, 1,9 µm (Dr Maisch, #r119.aq)
- RNase-Free DNase Set (Qiagen, #79256)
- RNeasy® mini kit (Qiagen, #74106)
- SimplyBlue™ SafeStain (Invitrogen, #LC6060)
- Wizard® SV gel and PCR clean-up system (Promega, #A9282)
- µ-slides I Luer, 0,4 mm, tissue culture treated (Ibidi, #80176)

Technical equipment

- Amersham™ Imager 600 (GE Healthcare Life Sciences)
- BD FACS Canto™ flow cytometry system (BD Biosciences)
- Centrifuge 5424 (Eppendorf)
- Centrifuge 5427 R (Eppendorf)
- Concentrator 5301 (Eppendorf)
- Countess™ II FL automated cell counter (Life Technologies)
- Digital PicoView® 450 nanospray ion source (New Objective)
- EASY-nLC 1000 liquid chromatograph
- Eclipse Ti fluorescence microscope (Nikon) equipped with a SOLA solid-state light source (Lumencor®) and a Nikon Digital Sight DS-Qi1Mc monochrome camera (Nikon)
- Flow system consisting of one pump and two fluidic units with perfusion sets and µ-slides (Ibidi), matched with a New Brunswick™ Galaxy® 14 S CO_2 incubator (Eppendorf)
- Incubator Hood TH 30 (Edmund Bühler)
- Infinite® M200 Pro plate reader (Tecan)
- Julabo® TW 12 water bath (Merck)
- MEGA STAR 3.0R centrifuge (VWR)
- Mini-PROTEAN Tetra cell for gel electrophoresis (Bio-Rad)
- NanoQuant Plate™ (Tecan)
- New Brunswick™ Galaxy® 170 R CO_2 incubator (Eppendorf)
- New Brunswick™ Galaxy® 170 S CO_2 incubator (Eppendorf)
- Orbitrap Fusion™ Tribrid™ mass spectrometer (ThermoFisher)
- peqSTAR thermocycler with 2x48 blocks (VWR Peqlab)
- ROTINA 420R (Hettich)
- RM 10W-30V rotating mixer (CAT)
- Safe 2020 Class II Biological Safety Cabinets (ThermoFisher)
- StepOnePlus™ real-time PCR system (Applied Biosystems)
- Thermomixer 5436 (Eppendorf)
- Water bath WNB (Memmert)
- ZEISS Axio Vert.A1 inverted microscope (ZEISS) supplied with an Axio CAM MRm monochrome digital camera (ZEISS)

Software

- Amersham Imager 600 software v1.2.0 (GE Healthcare Life Sciences)
- BD FACSDiva Software v5.0.3 (BD Biosciences)
- Canvas X.0.1
- EndNote X9.2
- Fiji ImageJ 2.1.0
- FlowJo 7.6.5 (Tree Star/BD Biosciences)
- GraphPad Prism 6.07
- iControl 1.10 (Tecan)
- Jalview 2.11.0
- Magellan 7.1 SP1 (Tecan)
- MaxQuant software, version 1.5.7.4 (freely available at https://maxquant.org)
- Nikon NIS-Elements AR 4.20.00 (Nikon)
- Office 2016 (Microsoft)
- PumpControl v1.5.2 (Ibidi)
- SnapGene 3.3.1
- StepOnePlus™ v2.3 (Applied Biosystems)
- ZEN 2012 (ZEISS)

METHODS

The data illustrated in this work correspond to experiments, which were replicated independently at least three times, unless differently stated.

If not otherwise specified, protocols were conducted at room temperature.

Cloning of new plasmids

Cloning of 3xHA.FoxO3.A3.ER and 3xHA.FoxO3.A3.ER(H212R)

The majority of the plasmids used in this work were already stocked in the lab of Prof. Dr. Marc Schmidt (Department of the Dermatology, University Hospital Würzburg) and their characterization was previously published (see the above "Cloning" section). To optimise the IP of FoxO3, the HA-tag of the already available retroviral construct pBP-HA.FoxO3.A3.ER (Czymai et al. 2010) was substituted with the sequence of three HA-tags (Fusi et al. 2022). As illustrated in Figure 16, the original plasmid was linearized by PCR using two primers (the sequence can be found in the paragraph "Cloning"), which excluded the amplification of the existing HA-tag and offered 3' and 5' sequences complementary to the endings of the extremities of a new insert. The PCR result was then loaded on an agarose gel and the band corresponding to the open plasmid was purified. The new insert was designed to have the 3' and 5' sequences complementary to the linearized plasmid. Besides, it included the Localization and purification tag (LAP-tag), which covered the sequences for a 3xHA-tag, an Enhanced green fluorescent protein (EGFP), a Tobacco etch virus (TEV) protease cutting site, and an S-tag, and it was in frame with the FoxO3.A3.ER sequence. This new tag was meant to be used for live fluorescent FoxO3 imaging and for an alternative method of FoxO3 isolation. The custom DNA oligo corresponding to this new insert was then ordered from Integrated DNA Technologies. The HiFi DNA assembly master mix (containing the required buffers and enzymes, i.e., the exonuclease, the DNA polymerase, and the ligase) was pipetted together with 0,0035 pmol of the linearized plasmid and 0,007 pmol of the new insert to assemble a new circular plasmid. The assembling-and-ligation reaction was run according to the manufacturer's protocol. Subsequently, the EGFP sequence together with the TEV-site and the S-tag were removed by enzymatic digestion with BamHI and an open pBP-3xHA.FoxO3.A3.ER was obtained. The T4 ligase was used to close the plasmid, which was then purified and used for *E. coli* transformation and expansion. By means of commercial MIDI PREP kits the plasmid was isolated and the sequence was carefully verified by Sanger sequencing.

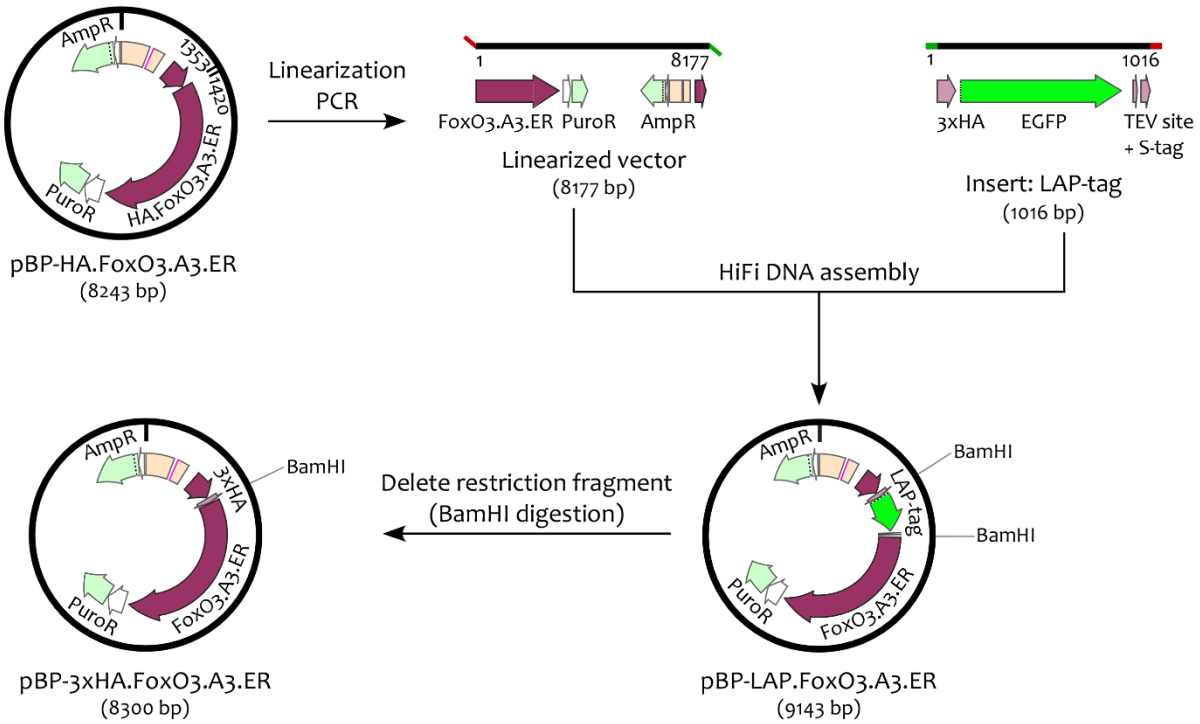

Figure 16: Cartoon describing the cloning process of pBP-3xHA.FoxO3.A3.ER.

The scheme is adapted from the cloning history of pBP-3xHA.FoxO3.A3.ER generated with the SnapGene software. Fragments coloured in red and green indicate the complementary endings of the linearized vector and of the new insert, which are necessary for the HiFi DNA assembly protocol. The positions of BamHI cutting sites are indicated. AmpR: Ampicillin resistance gene necessary for selection of successfully transformed *E. coli* colonies; PuroR: Puromycin resistance gene required for selection of correctly infected cells after transduction with retroviruses.

Once the validation of the functionality of the new pBP-3xHA.FoxO3.A3.ER in ECs was positively completed (see Figure 6 and data not shown), the 3xHA tag was also implemented in the construct coding for the FoxO3(H212R), the FoxO3 mutant that does not recognize the FREs (Figure 17). Both the available pBP-HA.FoxO3.A3.ER(H212R) (Czymai et al. 2010) and the pBP-3xHA.FoxO3.A3.ER were digested using the BglII restriction enzyme. The digestion products were separated by agarose gel electrophoresis and the bands corresponding to the backbone of pBP-3xHA.FoxO3.A3.ER (marked in green in Figure 17) and to the FoxO3(H212R) sequence derived from pBP-HA.FoxO3.A3.ER(H212R) (marked in red in Figure 17) were isolated. The fragment obtained from the pBP-3xHA.FoxO3.A3.ER was treated with the CIP phosphatase and then the two fragments were ligated overnight at 16° C with the help of the T4 ligase.

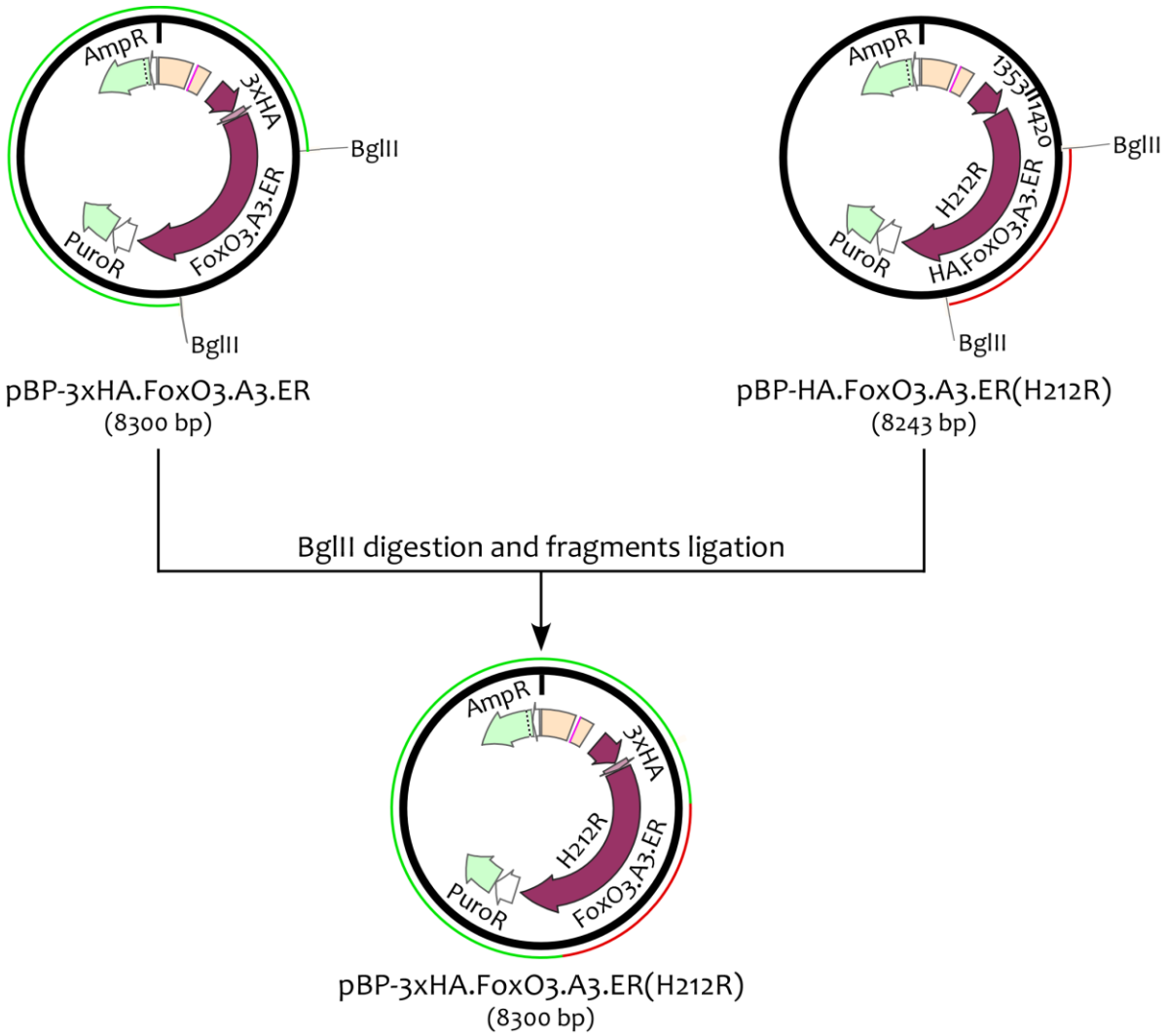

Figure 17: Representation of the cloning history of pBP-3xHA.FoxO3.A3.ER(H212R).

The sketch shows the cloning process of the pBP-3xHA.FoxO3.A3.ER(H212R) construct and it is an adaptation of the scheme provided by the SnapGene software. The positions of BglII cutting sites are indicated. AmpR: Ampicillin resistance gene necessary for selection of successfully transformed *E. coli* colonies; PuroR: Puromycin resistance gene required for selection of correctly infected cells after transduction with retroviruses; green mark: fragment taken from pBP-3xHA.FoxO3.A3.ER; red mark: fragment taken from pBP-HA.FoxO3.A3.ER(H212R).

After the DNA purification and the bacteria transformation, a few single-clone colonies of *E. coli* were picked and grown out, the plasmid DNA was purified and sequenced to check the right orientation of the FoxO3 -insert. Finally, only one clone with the correct in-frame insertion was kept as new pBP-3xHA.FoxO3.A3.ER(H212R) construct.

Both pBP-3xHA.FoxO3.A3.ER and pBP-3xHA.FoxO3.A3.ER(H212R) plasmids were ultimately used for production of new Phoenix-Ampho producer lines for retroviral infections as described below ("Generation of stable retrovirus-producing cell lines" paragraph).

Bacteria transformation and plasmidic DNA isolation

A 50 µl aliquot of self-made competent *E. coli* was carefully thawed up on ice and 1 µl or 2 µl of the desired plasmid was added. After a 30-minutes-long incubation at 4° C, a short heat shock step at 42° C for 45 seconds was performed. Bacteria were then chilled for 2 minutes on ice. For the starter culture, 450 µl of pure LB medium were added to the reaction and the transformed bacteria were grown in a shaker at 37° C, 225 rpm, for 1 hour. Afterwards, 50-to-200 µl of the bacteria were streaked on LB agar plates with the correct selection antibiotic and the bacteria grew overnight at 37° C. The following day 3-to-5 single-clone colonies were picked and let grow for 2-to-4 hours in 3-to-5 ml LB medium with the selection antibiotic. Subsequently the best growing clone was chosen for DNA isolation: its pre-culture was properly diluted in a bigger amount of LB medium with the selection antibiotic and incubated overnight in a shaker at 37° C at 225 rpm. Bacteria were then pelleted and further handled for DNA purification with the chosen MIDI or MAXI kit, following the manufacturer's instructions.

Once the DNA was isolated, 2 µl of the solution or 2 µl of DNase/RNase free water for the blank were used for measurement of the DNA concentration using the NanoQuant Plate™ and the Infinite® M200 Pro plate reader from Tecan. The instrument measured the absorbance (Optical density, OD) [OD = log (initial light intensity/final light intensity)] at 260 nm and at 280 nm to determine the concentration and the purity of the solution. The DNA concentration was calculated according to the following formula: [(OD_{260} sample – OD_{260} blank) · 50 µg/ml · 20]. Here 50 µg/ml is a conventional factor indicating the concentration of a sample which gives an OD_{260} of 1 after a 1-cm-long path, and 20 is the correction factor for the shorter length of the path of the NanoQuant Plate™. The purity of the solution is indicated by the ratio between the OD_{260} and the OD_{280} and for a double strand DNA (dsDNA) solution it must be around 1,8.

Cell culture

Thawing of cells

Before thawing the cells, an appropriate Petri dish or a flask with the required culture medium was pre-incubated at 37° C. The frozen cell aliquots were carefully picked from the liquid nitrogen tank and quickly thawed up at 37° C in the water bath. The cells were gently resuspended into to an appropriate amount of pre-warmed medium and distributed into the respective culture vessels according to the experimental requirements.

Passaging, counting, and reseeding of cells

Once in culture, the adherent cells that had to be kept in culture as stocks, were routinely passaged every 3-to-4 days as follows: the culture medium was removed, the cells were washed twice with 1x PBS, and the pre-warmed 0,05% Trypsin/EDTA/PBS was distributed on the cells. After

a short incubation step at 37° C (for maximum 5 minutes), the Trypsin activity was blocked by adding at least the double amount of either culture medium or 10% FBS/PBS. This solution was first resuspended to fully detach the cells from the surface, and it was then collected in a Falcon-tube. The cells were pelleted using a benchtop centrifuge at 1100 rpm for 5 minutes. The supernatants were then discarded, and the cells resuspended in a suitable amount of fresh culture medium. For passaging, an appropriate amount of the cell suspension was homogenously distributed in a new Petri dish or in a flask prefilled with warm culture medium and the cells were then kept in the incubator. If the cells had to be seeded for experiment, a 10 µl aliquot of the cell suspension was mixed with 10 µl of 0,4% Trypan Blue to estimate the concentration of the suspension. The mixture was loaded on a Neubauer improved counting chamber or on a Countess™ cell counting chamber slide for manual or automated live cell count, respectively. In case of manual count, the concentration in cells/ml was calculated as follows: [(counted live cells · 10 000 · 2) / (n° of big squares in which cells were counted)]. The factor 10 000 represents the volume of the solution applied to the chamber and the number 2 is the dilution factor used. Starting from the cell suspension concentration, it was possible to reseed equal number of cells for each condition required by the experimental settings.

Freezing of cells

To freeze the cell lines for long-term preservation, the cells were detached from the surface by means of trypsinization as just described. After the centrifuge step, the cell pellets were resuspended in a proper amount of ice-cold Freezing medium and distributed into cryo-vials, each with 1 ml of cell suspension. The cryo-vials were then rapidly transferred to -80° C in Styrofoam racks and 24 hours later stocked in the liquid nitrogen tank.

Culturing conditions

The purchased primary cell stocks were first expanded and frozen in small aliquots (Schmidt, Goebeler, and Martin 2016), which were then freshly brought in culture for each experiment and not passaged for more than 4-to-5 times. The cancer cells and the Phoenix producers were passaged for a maximum of 20 times and afterwards a new stock aliquot was thawed up.

HUVEC were cultured in the described HUVEC MIX, the melanoma cell lines were grown in RPMI+ medium, while the Phoenix-Ampho producer, HEK293, and UTA-6 cells were cultured in DMEM++ medium. All the cells were kept at 37° C, with 5% CO_2, and routinely tested to detect potential Mycoplasma contamination. Unfortunately, A375, M26 and MaMel26a cell lines resulted to be positive for Mycoplasma and therefore they were kept in a separate incubator and handled with care.

Cell transduction and transfection

Generation of stable retrovirus-producing cell lines

The Amphotropic Phoenix producer cells were reseeded at a density of 50 000 cells/cm² in medium without antibiotics. The following day the cells were transfected with 16 µg GAG-pol, 5 µg VSV-G and 7 µg of the plasmid of interest using the Lipofectamine® 2000 transfection reagent as indicated by the manufacturer. The transfection medium was replaced by the standard culture medium 16-to-24 hours after manipulation. At day 4, the cells were passaged and distributed in three flasks for expansion and selection (splitting ratio 1:3). Two-to-three days later, the producer cells were selected with the required antibiotic and kept under selection pressure for at least two weeks to obtain stable retrovirus-producing cell lines.

Retroviral transduction

For the retroviral transduction of HUVEC, the Phoenix-Ampho producer cells which stably integrated the desired plasmid were seeded at a density of 50 000 cells/cm². A day later, 5 µg/ml polybrene were added to the producers to boost the transduction efficiency and HUVEC were brought in culture at a density of 4200-to-4500 cells/cm². The day before transduction, the producer cells were supplied with the medium required by the target cells (e.g., HUVEC MIX when HUVEC were to be infected). At day 4 for the first two infection rounds, culture supernatants from the producer cells were collected and filtered with a sterile 0,8 µm filter and 5 µg/ml polybrene were added. If the infections with two constructs were planned, the filtered supernatants with the wished single-constructs-producing viruses were mixed in a 1:1 ratio. Afterwards the retroviruses-enriched culture media were added to the HUVEC as replacement of their standard medium, while the fresh medium needed by the target cells was given to the producers. The two infection steps were performed with a 6-hours-interval in between. A third infection was additionally done on day 5 after an overnight incubation step. Six hours after the third transduction round, the target cells were provided with fresh standard culture medium. Roughly 48 hours after the last medium change, HUVEC were pulsed overnight (16-to-18 hours) with 2 µg/ml puromycin to select for the transduced cells. Subsequently, the cells were cultured without selection antibiotics, and after one day of recovery they were reseeded for further experiments.

DEAD-dextran transfection

To prepare HUVEC for the Luciferase assay, the cells were transfected according to an established DEAD-dextran transfection protocol (Czymai et al. 2010; Viemann et al. 2007). Freshly thawed up HUVEC were seeded at a density of 4000 cells/cm² in 10-cm-Petri dishes and were grown for 72 hours. Afterwards the cells were washed once with the HEPES solution and incubated for 30 minutes at 37° C with the Plasmid solution (250 µg/ml DEAE-Dextran hydrochloride (Sigma, #D9885), 4 µg 6xDBE-luc reporter, 1 µg each overexpression plasmid, 266 ng *Renilla*-luc reporter

(1/15 of the luciferase reporter) in the HEPES solution). Subsequently, the Chloroquine solution was gently added dropwise. A 3-hours-incubation step at 37° C followed and then the transfection mix was removed. The warm pure Medium M199 was pipetted on top of the cells, DMSO was freshly added to a final concentration of 10% to generate a heat shock to improve the plasmid uptake, and the cells were shaken on a 3D-tumbler at room temperature for exactly 2 minutes and 30 seconds. The medium was promptly removed, the fresh standard HUVEC MIX was added, and the cells rested overnight at 37° C before further handling.

Calcium-Phosphate transfection

The transient transfection of HEK293 cells for IPs or of UTA-6 cells for IPs and Luciferase assay were executed following traditional Calcium-Phosphate transfection procedures. Briefly, the target cells were plated without any antibiotic at a density of 50 000 cells/cm^2 for HEK293 and of 13 000 cells/cm^2 for UTA-6. The following day a solution with 450 µl of DNase/RNase free water, 50 µl Calcium chloride solution (250 mM final concentration) and 12 µg plasmidic DNA (for co-transfections, 6 µg of each plasmid) was prepared for each wished condition. After a quick vortex and spin down step, 500 µl of the 2x HBS buffer (1x final concentration) were added to complete the transfection mix, which was gently mixed and carefully distributed dropwise to the cells. After 16 hours of incubation, fresh culture medium was added to the cells and the experiments were carried out starting from 24 hours later. For Luciferase assay with UTA-6 cells, 8-to-10 µg of the overexpression plasmid combined with 2-to-4 µg of 6xDBE-luc reporter and 133-to-266 ng of *Renilla*-luc were used for each transfection.

Transfection of siRNA

The siRNA transfections of HUVEC were completed using the Oligofectamine transfection reagent and on the basis of the manufacturer's guidelines. Shortly, the cells were plated at a density of 12 000 cells/cm^2 either in 6-cm-Petri dishes or in 6-well-plates. The following day a microcentrifuge tube with Solution A (90 µl OptiMEM™ medium and 10 µl siRNA mixture (200 nM final concentration)) and a second microcentrifuge tube with Solution B (90 µl OptiMEM™ medium and 10 µl Oligofectamine™ transfection reagent) were prepared and incubated for 10 minutes. Solution B was pipetted into Solution A prior to a second incubation step for 30 minutes. In the meantime, the cells were washed twice with pure OptiMEM™ medium and 800 µl of fresh OptiMEM™ medium were distributed on the cells. At the end of the second incubation time, the mixture of Solution A and B was gently distributed dropwise on the cells, and the cells were incubated for 4-to-5 hours at 37° C. Finally, the transfection medium was replaced with fresh HUVEC MIX and the cells were kept for 16-to-24 hours at 37° C before further handling for the experiments. The two siRNAs targeting TRRAP were used as pool for all the shown experiments, maintaining the final total concentration of siRNA equal to 200 nM.

Cell cycle and apoptosis analysis

Following the required manipulation steps, HUVEC were incubated for the indicated times with culture medium with or without 100 nM 4-OHT. The culture supernatants were harvested into a Falcon-tube, the cells were washed and detached using Trypsin (protocol described above in the paragraph "Passaging, counting, and reseeding of cells") and the buffers used in each step were collected and pooled in the Falcon-tube together with the corresponding culture supernatants. A 5-minutes-centrifuge step at 1100 rpm in a table centrifuge served to pellet the collected dead and alive cells. The cell pellets were washed twice with 1x PBS, centrifuging as before. Lastly, the pelleted cells were resuspended in 100-to-200 µl of 1x PBS, fixed with 1 ml of ice-cold 70% ethanol and transferred into a microcentrifuge tube. The fixed cells were kept at 4° C for at least 16 hours.

Before the analysis with the flow cytometer, the fixed cells were pelleted using in a microcentrifuge for 5 minutes at 5000 rpm and then the pellets were washed twice with 1x PBS, centrifuging as just described. Afterwards 250-to-500 µl of PI buffer were used to resuspend the cells and within few hours the samples were analysed with the BD FACS Canto™ flow cytometry system. The fluorescent emission of PI generated by the single-cell-solution flowing through the instrument was triggered by the 488 nm laser and detected in the PE channel (the excitation maximus of PI bound to the DNA is at 535 nm, while the emission maximum is at 617 nm). Given that the PI intercalates the DNA double helix, the measurement of the fluorescent intensity in a linear scale allowed to quantitatively determine the DNA amount present in each cell. Accordingly, fluorescent peaks corresponding to 2n and 4n DNA content could be discriminated to quantify the amount of cells in G1 phase (2n), S phase (DNA content among 2n and 4n) and G2/M phase (4n). Additionally, the apoptotic cells could be identified as the cells with a sub-diploid DNA content (less than 2n), due to the Caspase-dependent degradation of the DNA occurring during apoptosis.

For the PE channel a threshold for the signal intensity was set at 5 to remove the signal coming from dust, debris, or electronic noise. Furthermore, the analysis was restricted to the single-cell population: the cell clumps and the cell doublets obscuring the cells with true 4n DNA content were excluded by gating the right population in the PE-width vs the PE-area plot. Afterwards the plot displaying the histogram vs PE-area was used to define the cell cycle phase distribution. These settings were first fixed for the experimental control and then kept without modifications for the analysis of all the samples. After the data collection, the raw files were re-analysed with the FlowJo software to finer determine the sub-diploidy rates.

mRNA expression analysis: two-step real-time PCR

First step: mRNA extraction and cDNA synthesis

The commercial RNeasy MINI kit was employed to isolate the RNA from HUVEC after manipulation and treatment. The cells were washed twice with 1x PBS and typically 350 µl of the provided RLT buffer (freshly supplemented with 10% β-Mercaptoethanol) were used to lyse the cells. The samples were stored at -20° C until the column RNA isolation was performed as indicated by the manufacturer's protocol, including the suggested optional steps for gDNA removal and high RNA quality.

After the isolation of the RNA, the concentration of the solution was measured as done for the DNA solutions (see paragraph "Bacteria transformation and plasmidic DNA isolation"). Here, the formula for finding the RNA concentration was: $[(OD_{260}$ sample $- OD_{260}$ blank$) \cdot 40$ µg/ml $\cdot 20]$. The concentration of a sample which gives an OD_{260} of 1 after a 1-cm-long path for RNA is 40 µg/ml, and 20 is the correction factor for the pathlength of the NanoQuant Plate™. The RNA solution is considered pure from contaminants when the ratio OD_{260}/OD_{280} is around 2.

The complementary DNA (cDNA) synthesis was carried out with freshly isolated RNA, starting with the same amount of purified RNA for all the samples (typically 0,5 to 1 µg depending on the experimental conditions). The QuantiTect Reverse Transcription Kit was used in compliance with the manufacturer's suggestions. The solutions containing the final cDNA were then further diluted 1:10 in DNase/RNase free water to reduce potential interference with the following quantitative real-time PCR (qPCR) reactions.

Second step: quantitative real-time PCR

The diluted single strand cDNA products of the synthesis were then used as templates for the qPCRs. The settings of the reactions followed the classic PCR rules: after a first high temperature step to activate the hot start polymerase, 40 cycles composed of a denaturation, an annealing and an extension phase were run. During the first cycle the polymerase synthetised the complementary strand of the cDNA and afterwards the amplification of the target gene took place. The real time PCR machine allowed to follow the exponential production of the fragment of the gene of interest (called amplicon) by measuring the intensity of the fluorescent signal at the end of each PCR cycle. This signal was generated by the gene-specific fluorescent reporters used in the reaction, such as SYBR™ Green, a dye which binds to the dsDNA, or TaqMan® fluorescent-labelled and mRNA-specific probes. When the TaqMan® technology was used, the reaction master mix included not only a gene-specific primer pair, but also a gene-specific probe equipped with a fluorophore and a quencher. The Taq polymerase had an additional 5' nuclease activity, which allowed the enzyme to degrade the DNA bound to the PCR template downstream of DNA synthesis. During the extension phase of each cycle, the TaqMan® probe bound to the target

sequence in the amplicon was cleaved by the Taq polymerase. This led to the separation of the fluorophore from the quencher and to the release of the fluorescence. This method allowed to achieve a very high specificity, reinforced by the fact that the TaqMan® probes were chosen among the ones tested and evaluated by Applied Biosystems. When the SYBR™ Green technology was used, a primer pair specific for the target gene led to the generation of a double strand amplicon. The binding between the SYBR™ Green fluorescent dye and the dsDNA caused then the release of a fluorescent signal. Upon these setting the presence of unspecific dsDNA (primer pairs or unspecific gDNA) generated a false positive signal. For this reason, the elimination of the contaminating dsDNA during the cDNA synthesis process was very important. Furthermore, the presence of a single product of the qPCR was verified by the production of homogeneous amplicon melting curves. Another measure taken to increase the specificity of the SYBR™ Green qPCRs was the choice of a primer pair, which spanned the exon-exon boundary of two successive exons in the mRNA template.

At the end of each qPCR cycle the fluorescence intensity mirrored the amount of the amplicon, which grew exponentially until it overcame the baseline signal at a certain qPCR cycle. This cycle was defined as Threshold cycle (C_t) and it was dependent on the initial load of the specific cDNA sequence (the more abundant was the mRNA, the earlier the C_t was reached). The C_t values were then used for the determination of the mRNA expression levels by means of two approaches. The so called ΔC_t was calculated as the difference between the C_t values of the gene of interest and the C_t values of the housekeeping gene GAPDH. The first method considered a second step of comparison by calculating the $\Delta\Delta C_t$, that is the difference between the ΔC_t of the chosen sample and the ΔC_t of the experimental control sample. The fold mRNA expression was estimated as $2^{(-\Delta\Delta Ct)}$. The second procedure allowed the determination of the mRNA levels in each sample, without the correlation to the controls. Relative mRNA expression was assessed according to the formula $2^{(-\Delta Ct)}$.

In this work, the amounts of mRNA of the selected FoxO3 targets in HUVEC were detected by single-plex qPCR, by using either TaqMan®- or SYBR™ Green-based technology and by pipetting triplicates for each sample. The gene-specific FAM™-labelled assay mixes and the master mix for TaqMan® qPCRs together with the SYBR™ Green master mix were purchased from Applied Biosystems. The custom primer pairs for SYBR™ Green qPCRs were ordered from Sigma.

Application of LSS

A cell suspension with 110 000 HUVEC in 110 µl of HUVEC MIX was seeded without generating air bubbles in the special µ-slide for laminar shear stress application. Once the cells were adherent, the flow procedures were started or alternatively a medium change was carried out, the reservoirs of the µ-slide were filled up with medium and the cells were kept overnight in the incubator.

Prior to the start of the flow, the system was equilibrated to remove all the air bubbles. To achieve this, 15 ml of medium without or with the desired stimuli were homogeneously distributed in the columns of each perfusion set, already mounted on the flow units. With the help of the PumpControl software the system was set up to run for 15-to-30 minutes, without any µ-slide attached. After having stopped the system, the µ-slides were connected to the perfusion set tubes, paying attention to avoid the formation of air bubbles. The units were then placed back in the proper incubator and were ready for the start of the LSS. The flow rate was set to reach the final strength of 20 dyne/cm^2 after a few steps with increasing power. A typical configuration was: 5 minutes at 5 dyne/cm^2, followed by 5 minutes at 10 dyne/cm^2 and by another 5 minutes at 15 dyne/cm^2 before fixing 20 dyne/cm^2 for the desired time. Immediately after the end of the run, the RNA samples were harvested as described above (see paragraph "mRNA expression analysis").

Immunofluorescent staining

The transduced HUVEC were seeded at a density of 13 000 cells/cm^2 on cover slips and treated the following day with 100 nM 4-OHT or 10 µM LY294002. After two washing steps with 1x PBS, the cells for the ER staining were fixed and permeabilized with ice-cold methanol for 20 minutes. The cells for the FoxO3a staining were first fixed for 10 minutes with the Fixation solution and, after washing twice with 1x PBS for 5 minutes, were permeabilized for 10 minutes with the Permeabilization solution. The protocol proceeded in the same way for both the IFs, starting with two washing steps with 1x PBS. When the blocking with the Buffer B for 30-to-60 minutes was over, the cells were incubated for 45-to-60 minutes with the primary antibody. The Washing buffer was used three times for 5-minutes-washing rounds before the cover slips were incubated in the darkness for 1 hour with the secondary antibody. The nuclei were then stained with Hoechst 33342 for 5 minutes in the darkness. Another three washing steps with 1x PBS, each 5 minutes long, were executed and finally the cover slips were mounted on the supporting slides with the help of the Ibidi mounting medium. The slides were sealed with commercial nail polish, dried, and stored at 4° C in the darkness until visualization by fluorescence microscopy. Pictures were obtained with the Eclipse Ti fluorescence microscope and analysed with the Nikon NIS-Elements software.

Protein extraction

Total cell lysis

After stimulation, the cells were washed twice with ice-cold 1x PBS, then 100 µl to 1 ml of ELB+++ lysis buffer was thoroughly distributed on the plate surface (the amount of buffer was chosen according to the size of the Petri dish and to the experimental goal) and 1-hour-incubation at 4° C followed. The whole cell lysates were scraped together and transferred in a microcentrifuge tube for a 10-minutes-centrifugation step at 10 000 rpm, at 4° C. The supernatants containing the lysates were stored at -20° C until next use or directly incubated with the magnetic beads for IPs.

Extraction of nuclear and cytoplasmic fractions

For the nuclear and cytoplasmic extracts, the trypsinization of the cells to detach them from the dishes was performed as described (see paragraph "Cell culture"). The cell pellets were washed two times with ice-cold 1x PBS (the benchtop centrifuge was set at 1100 rpm for 5 minutes at 4° C) and then gently resuspended in 500 µl of ice-cold Buffer C. After incubation at 4° C for 15 minutes, the lysates were pressed for 20 times through a 1 ml syringe with a 26G 3/8 (0,45 × 10) needle to disrupt the cellular membranes while keeping the nuclei intact. To separate the two fractions, the lysates were centrifuged in a microcentrifuge at 4° C for 5 minutes, 5000 rpm. The cytoplasmic extracts in the supernatants were collected and stored on ice, while the pellets with the nuclear fraction were gently washed twice with 500 µl of buffer C, centrifuging as before. The nuclear fraction pellets were resuspended in 50 µl of buffer N and shaken for 15 minutes at 4° C on a Thermomixer to finally break them and release the nuclear proteins. The debris from both nuclear and cytoplasmic extracts were removed by centrifugation at 4° C for 10 minutes, 14 000 rpm in a microcentrifuge and the final clean supernatants were stored at –20° C until use.

Determination of protein concentration

The protein concentration was measured by Bradford assay, a conventional method based on the capacity of the protein to bind to the Coomassie dye and to induce a colour change. Briefly, under acidic conditions, some amino acid residues (in particular Arg, Lys and His) reacted with the red-brown dye and caused a colour shift towards blue: the higher was the protein concentration, the stronger was the intensity of the resulting blue dye. This colour change allowed photometric determination of the protein content by measuring the light absorbance at 595 nm. To know the concentration of the experimental probes, a small aliquot of the samples was mixed with the Bradford protein assay dye reagent in an appropriate ratio that depended on the expected protein concentration. In parallel, some serial dilutions of BSA with a known concentration were prepared and mixed with the dye reagent, too. Typical concentrations for the BSA standard curve were: 0 mg/ml, 2 mg/ml, 5 mg/ml, 10 mg/ml, and 20 mg/ml. After measuring the absorbance, a standard curve was created with the data from the BSA dilutions and was used to determine the concentration of each sample.

Western blot

Equal amounts of protein were prepared for Western blot detection by mixing the lysates in a 1:4 ratio with 4× Lämmli buffer. The samples were boiled for 5 minutes at 95° C to denature the proteins and then loaded on self-made SDS-polyacrylamide gels for electrophoretic separation according to the protein size. Only for the simultaneous detection of TRRAP and the HA.FoxO4 deletion mutants, pre-cast gradient gels were employed. The SDS-PAGE was run using the Mini-PROTEAN Tetra cell and with 1x Electrophoresis buffer, keeping the current intensity constant

(25 mA/gel were typically calculated) until the running front reached the end of the gel. The proteins were then blotted onto nitrocellulose or polyvinylidene fluoride (PVDF) membranes at 4° C, 400 mA constant and using the 1x Blotting buffer. The blotting times were set between 15 and 80 minutes for each gel/membrane sandwich according to the size of the proteins of interest. To verify the homogeneous and regular transfer, the membranes were transiently stained with Ponceau S buffer. Prior to the overnight incubation at 4° C with the desired first antibodies, the membranes, or the pieces of them, were washed with 1x TBST buffer and were incubated with the proper Blocking buffer for at least 1 hour. The following day the primary antibody was removed, and the blots were washed 4 times with 1x TBST buffer. The secondary antibodies were added for at least 1 hour and then the membranes were washed again, 3 times with 1x TBST buffer and once with 1x TBS buffer. For the signal detection, a self-made ECL solution was freshly prepared, the membranes were dipped in it for 1-to-2 minutes and placed in the specific support of the Amersham Imager device. The images of the protein bands emerging by the generation of chemiluminescence by the bound horseradish peroxidase-coupled secondary antibody were acquired. Several exposition times were selected to achieve optimal pictures, according to the intensity of the signal generated by the secondary antibody.

For stripping, a short washing step with 1x TBS buffer was performed, and the membranes were successively incubated for 30 minutes at 50° C with the pre-warmed Stripping buffer, to remove the bound antibodies. Two washing steps with 1x TBST buffer were performed and then the above-mentioned procedure was repeated from the blocking step onwards.

Immunoprecipitations

The HEK293 and UTA-6 cells were transiently transfected via the Calcium-Phosphate protocol and whole cell lysates were harvested 40 hours after transfection as already described above. The retrovirally transduced and selected HUVEC were harvested for protein lysis and IPs 16 hours after 100 nM 4-OHT addition.

The HA-tagged proteins were immunoprecipitated using the anti-HA magnetic beads and all the steps were carried out at 4° C. For the collection of the beads, a rack equipped with a magnet was used. The protein lysates were prepared in a way that the same total amount of protein (the minimum amount used was 600 µg) in the same volume could be used for each reaction. For the simple detection via immunoblot, the ideal condition was to start the IP with ca. 2 mg of protein in ca. 1,5 ml of lysis buffer, while for the MS analysis 6,4 mg of HUVEC lysate in 14,4 ml buffer were used. In this last experiment, and generally when the lysate protein concentration was so low that a big volume was needed, the samples were equally distributed into two 15 ml Falcon-tubes to obtain a better volume-to-beads ratio and two separate IPs per condition were performed. Following the manufacturer's guidelines, for each reaction 25 µl of beads (corresponding to 0,25 mg) were equilibrated by washing with 0,05% TBST buffer (the same buffer used for the

Western blots). The prepared samples and the equilibrated beads were mixed and incubated for 2 hours at 4° C on an upside/down shaker. Three washing rounds were performed each with 300 µl of the Washing buffer or of the High salt washing buffer (the latter was used when more stringent conditions were desired) for 5 minutes on the upside/down shaker at 4° C. The immunoprecipitated proteins were eluted at 70° C for 15 minutes on a rocker with 70-to-100 µl of 1× TruPAGE LDS sample buffer, if the samples were intended for the MS analysis, or with 25-to-100 µl of 2× Lämmli buffer, when the proteins were analysed by Western blot.

The Flag-IPs were carried out with the anti-FLAG M2 magnetic beads, according to the manufacturer's guidelines, and with the help of a magnetic rack for the collection of the beads. In brief, the samples were equilibrated to obtain a final amount of 2-to-2,6 mg in 1 ml and 25 µl of the beads per sample were equilibrated as suggested in the company protocol. As for the HA-IP, Flag-IPs were done at 4° C for 2 hours in an upside/down shaker. After removal of the supernatant, the beads were quickly washed for three times with the same buffers as for the HA-magnetic ones. The elution of the immunoprecipitated proteins consisted in resuspending the beads in 25-to-70 µl of the 2× Lämmli buffer and in boiling them for 3 minutes on a rocker.

For both the IP types, at the end of the protocol the beads were discarded, while the samples were preserved at -20° C until the next analysis.

Analysis of FoxO3-nuclear-interactome

The co-infected HUVEC with combinations of pBP-3xHA.FoxO3.A3.ER, pBP-MEK5D and pBP-empty vector were incubated for 16 hours with 100 nM 4-OHT. The HA-IPs were then performed as described above (see the previous section "Immunoprecipitations"). The samples were typically analysed by Western blot, except for one experiment, whose samples were handed over to the research group of Prof. Dr. Andreas Schlosser for the nanoLC-MS/MS analysis, done as describe here below.

For the MS analysis, a fourfold amount of acetone was added to the eluted proteins overnight at -20° C for the precipitation. The pellets were washed at -20° C with acetone, resuspended in 1x NuPAGE LDS sample buffer, treated first for 10 minutes with 50 mM DTT at 70° C, and then for 20 minutes with 120 mM iodoacetamide at room temperature. The samples were loaded on the NuPAGE Bis-Tris pre-cast polyacrylamide gels and the electrophoresis was run with 1x MOPS buffer following the manufacturer's protocol. Three washing steps with water, each for 5 minutes, were carried out. The gels were then stained with the SimplyBlue™ SafeStain reagent for 1 hour and, after another 1-hour-washing step, the lanes were cut each into 15 pieces. The staining was removed by means of the Destaining buffer, the slices were shrunk with pure acetonitrile and finally dried using the vacuum concentrator. Each piece underwent tryptic digestion, which took place overnight at 37° C in the Digestion Buffer. The supernatants were

removed and stored, while the peptides were first extracted from the slices with 5% formic acid and then pooled with the respective supernatants. The samples were then ready to be examined.

The analysis was done using the Orbitrap Fusion Mass Spectrometer supplied with a PicoView Ion Source and paired to an EASY-nLC 1000 liquid chromatograph. Capillary columns self-filled with ReproSil-Pur 120 C18-AQ were employed. The peptides were separated at a flow rate of 500 nl/min with a 30-minute-linear gradient from 3% to 30% acetonitrile and 0,1% formic acid. The Orbitrap analyser was set with a resolution of 60 000 for the MS scans and of 15 000 for the MS/MS scans, and the higher energy collisional dissociation fragmentation with 35% normalised collision energy was implemented. Furthermore, a top speed data-dependent MS/MS method with a fixed 3-seconds-cycle was used. A dynamic exclusion with a repeat count of one and exclusion duration of 30 seconds was applied. The single charged precursors were dismissed and the threshold for minimum signal for precursor selection was fixed to 50 000. The predictive automatic gain control was utilised, and the automatic gain control was given a target value of 2e5 for MS scans and of 5e4 for MS/MS scans. An internal calibration was performed with EASY-IC.

The evaluation of the raw data was executed with the MaxQuant software (Cox and Mann 2008). The search in the database was performed with the integrated Andromeda search engine, comparing the obtained data against the UniProt human database, with the sequence of 3xHA.FoxO3.A3.ER in addition. Another database containing common contaminants was also included. Further analysis parameters encompassed the specificity of tryptic cleavage (set to three allowed miscleavages), while the identification of the proteins was regulated by the false discovery rate (FDR; <1% FDR on protein and peptide-to-spectrum match levels). The MaxQuant default settings included a main search peptide tolerance of 4,5 ppm and a MS/MS match tolerance of 20 ppm. Additionally, the software made an investigation looking for some variable PTMs, like protein N-terminal acetylation, Gln to pyro-Glu formation (N-term. Gln), and oxidation (Met), whereas carbamidomethyl (Cys) was considered as a fixed modification. The quantification of the protein amounts derived from the Label-free quantification (LFQ) intensities and proteins, for which less than two razor/unique peptides were identified, were excluded (Cox et al. 2014). Finally, additional analysis of the data was accomplished with R scripts, which were created in the department of Prof. Dr. Andreas Schlosser.

When the LFQ intensities for a protein could not be detected in the control samples, the LFQ values were arbitrarily fixed close to the baseline. The data attribution was carried out using values corresponding to a standard normal distribution with a mean of the 5% quantile of the combined log10-transformed LFQ intensities and a standard deviation of 0,1. To consider an imputed protein as a real call, a minimum of three razor/unique peptides had to be present. For the confirmation of significantly enriched proteins, intensity bins of at least 300 proteins determined boxplot outliers. The protein ratios of the 3xHA.FoxO3.A3.ER-containing samples versus the controls without 3xHA.FoxO3.A3.ER were calculated as a log2. These values which were outside a

1.5× or 3× interquartile range, were marked as enriched with a significance of 1 (green dots in Figure 8A) or of 2 (red dots in Figure 8A), respectively.

Luciferase assay

The Calcium-Phosphate transfections of UTA-6 and the DEAD-Dextran transfections of HUVEC were executed as described above (see section "Cell transduction and transfection"). One day later the cells were reseeded in triplicates into a 96-well plate at a density of 18 000 cells/well for HUVEC and of 15 000 cells/well for UTA-6. After attachment to the surface, cells were incubated for 16 hours with or without 100 nM 4-OHT. The detection of the luminescence was accomplished using the Dual-Glo luciferase assay system according to the manufacturer's protocol. Briefly, after removing the culture supernatant, the cells were provided with 30 µl of pure DMEM medium and 30 µl of the supplied lyses buffer, and then incubated for 10 minutes in the darkness. 60 µl of the solution with the lysed cells were then transferred in a white non-transparent plate with flat bottom (Costar) for the measurement of the *Firefly* Luciferase-dependent luminescence. The activity of the 6xDBE-luc reporter of each well was detected with the Infinite® M200 Pro plate reader by recording the signal for 7 seconds. A second solution freshly prepared with the reagents provided by the kit was added (30 µl/well), and it served to stop the *Firefly* Luciferase reaction and to trigger the *Renilla* Luciferase emission. After a 10-minutes-incubation step in the darkness, the samples were again ready for luminescence detection as before. This time the activity of the constitutively expressed *Renilla*-luc reporter was recorded. A blank condition without cells but anyway handled as the samples was taken along for background adjustment.

For the calculation of the 6xDBE-luc reporter activity, the mean of the blank values was calculated and subtracted from each sample-generated raw value, for both *Firefly* and *Renilla* luminescence data. For each well the new *Firefly* luminescence intensity was divided by the corresponding *Renilla* blank-subtracted measurement, to normalise the data for the transfection efficiency. The mean among the values of the triplicates represented then the 6xDBE-luc reporter activity. Furthermore, the induction of the reporter was calculated as fold of the experimental control (FoxO3.A3.ER/vector/ctrl), which was arbitrarily set as 1.

gDNA extraction and TRRAP status determination

For the gDNA isolation, 4 x 10^6 cells of each melanoma cell line were used. The cells were pelleted by centrifuging for 5 minutes at 300 g in a benchtop centrifuge. After careful removal of the supernatants, the pellets were resuspended in ice-cold 1x PBS and the gDNA was extracted with the Monarch Genomic DNA Purification Kit following the manufacturer's instructions.

The extracted gDNA was used as a template for the PCR amplification of a DNA fragment around the hot spot nucleotide at position 2165 (C>T). The PCR cycler was set as follows:

- 94° C for 2 minutes;
- 30 cycles: 94° C for 30 seconds, 57° C for 30 seconds, 72° C for 30 seconds;
- 72° C for 5 minutes.

The dimension of the PCR product was verified by running the samples on a 1% agarose gel and the correct band was then isolated from the gel. After the DNA purification, the sequence of TRRAP was finally characterised by Sanger sequencing. The primers for the fragment amplification and for the sequencing were published in (Wei et al. 2011) and are reported in the section "TRRAP status definition" of the "Materials" chapter.

Statistical evaluation

For the statistical analysis, the GraphPad Prism software was used. The histograms are representative of at least three independent experiments, and they display the average of the obtained results, while the error bars indicate the Standard deviation (SD). The significant p values ($p \leq 0,05$) were calculated by running unpaired t-tests or two-way ANOVA tests followed by Sidak's multiplicity correction, accordingly to the experimental conditions.

SUPPLEMENTARY MATERIAL

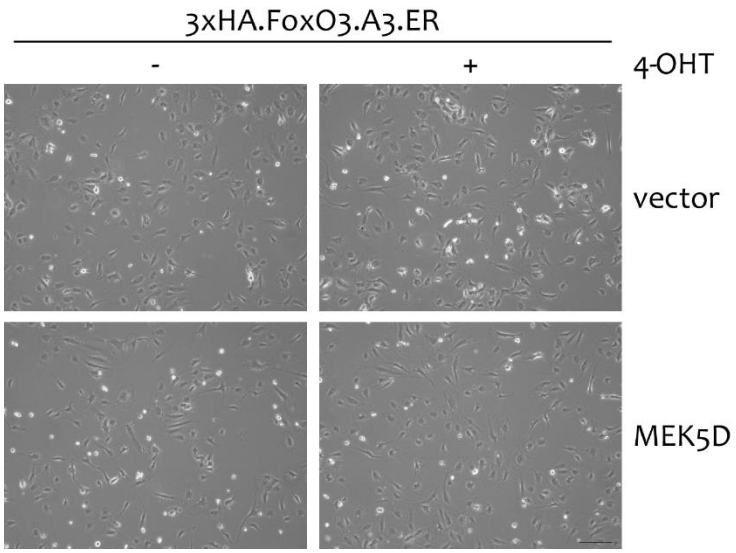

Suppl. Figure 1: Density controls for the phase contrast pictures in Figure 6B.

Controls for cell density at the stimulation time for the pictures proving FoxO3-dependent apoptosis after 48-hours-incubation with 4-OHT. Phase contrast pictures of HUVEC displaying the cells infected with 3xHA.FoxO3.A3.ER shortly after the stimulation with (+) or without (-) 4-OHT. Scale bar: 100 µm.

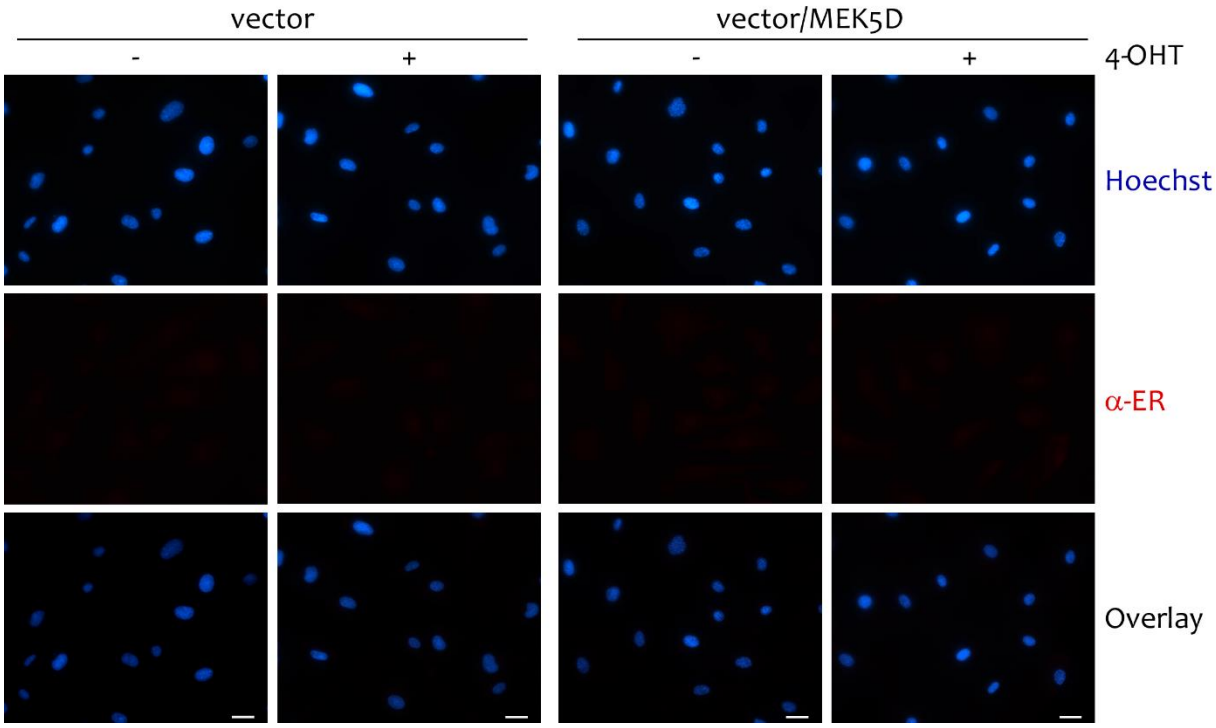

Suppl. Figure 2: Negative controls for the IF in Figure 7A.

Negative controls for the immunofluorescent staining of the ER-tag. HUVEC overexpressing an empty vector or the combination of MEK5D and the empty vector were incubated for 16 hours with (+) or without (-) 4-OHT. Blue channel: Hoechst nuclear staining; red channel: α-ER staining for HA.FoxO3.A3.ER; overlay of the two channels is also displayed. Scale bar: 25 µm.

Suppl. Table 1: Enriched nuclear FoxO3-binding proteins without and with MEK5D.

The table shows a merged list of the 20 most enriched nuclear interaction partners of FoxO3 identified in each 3xHA.FoxO3.A3.ER/vector vs vector and 3xHA.FoxO3.A3.ER/MEK5D vs vector/MEK5D conditions after one nanoLC-MS/MS analysis. The proteins that were identified in both analyses are noted only once. Both the protein and the respective gene names are reported, together with the "qNormalised LFQ ratio" values, which show the strength of the enrichment of the protein in the condition with 3xHA.FoxO3.A3.ER/vector or with 3xHA.FoxO3.A3.ER/MEK5D in comparison with vector or vector/MEK5D, respectively. The "qNormalised LFQ ratio" is calculated as the normalised log 2 of the ratio between the LFQ intensity values in the samples with 3xHA.FoxO3.A3.ER and the LFQ intensity values in the respective controls and after a second quantile normalisation to adjust for intra-experiment differences (n.d.: non determined). The proteins which were already characterised as binding partners of TRRAP are indicated by "*" and the respective references are added in brackets. The established FoxO3 targets found as bound proteins were handled as false positive results and were omitted form the list.

PROTEIN	GENE	qNORMALISED LFQ RATIO (FoxO3/vector vs vector)	qNORMALISED LFQ RATIO (FoxO3/MEK5D vs vector/MEK5D)
3xHA.FoxO3.A3.ER		12.17	12.17
Transformation/Transcription domain-associated protein*	*TRRAP*	7.79	6.33
F-box only protein 11	*FBXO11*	6.53	7.47
E1A-binding protein p400 (Fuchs et al. 2001)*	*EP400*	6.05	4.78
Cullin-1 (Finkbeiner et al. 2008)*	*CUL1*	5.56	4.06
Kelch-like protein 21	*KLHL21*	5.18	3.67
LIM and calponin homology domains-containing protein 1	*LIMCH1*	4.55	0.27
Tissue factor pathway inhibitor 2	*TFPI2*	4.29	5.25
Cullin-3	*CUL3*	4.14	1.78
Alpha-enolase	*ENO1*	4.00	n.d.
Unconventional myosin-XVIIIa	*MYO18A*	3.44	-0.13
DNA methyltransferase 1-associated protein 1 (Doyon et al. 2004)*	*DMAP1*	3.34	2.52
Proteasome subunit beta type-6	*PSMB6*	3.29	3.04
Proteasome subunit alpha type-2	*PSMA2*	3.26	2.24
Tissue factor pathway inhibitor	*TFPI*	3.19	n.d.
Clusterin	*CLU*	3.06	3.39
Proteasome subunit beta type-1	*PSMB1*	2.98	0.14
Rho-related GTP-binding protein RhoJ	*RHOJ*	2.96	n.d.
Transmembrane emp24 domain-containing protein 7	*TMED7*	2.94	n.d.
Proteasome subunit beta type-4	*PSMB4*	2.90	1.87
NEDD4-like E3 ubiquitin-protein ligase WWP1	*WWP1*	2.87	-2.12

Nesprin-2	*SYNE2*	2.65	3.56
26S protease regulatory subunit 10B	*PSMC6*	1.99	2.85
Protein disulphide-isomerase A3	*PDIA3*	1.96	2.95
Heat shock protein 105 kDa	*HSPH1*	1.70	3.19
Staphylococcal nuclease domain-containing protein 1	*SND1*	1.26	2.97
26S proteasome non-ATPase regulatory subunit 1	*PSMD1*	1.21	3.26
Glutathione peroxidase 8	*GPX8*	0.59	2.88
Ubiquitin carboxyl-terminal hydrolase 7 (Bhattacharya and Ghosh 2015)*	*USP7*	0.13	4.50
Melanoma-associated antigen D2	*MAGED2*	-0.05	2.91
Ubiquitin-like modifier-activating enzyme 1	*UBA1*	-0.29	2.80
Protein AHNAK2	*AHNAK2*	n.d.	4.19
BAG family molecular chaperone regulator 2	*BAG2*	n.d.	3.31

Suppl. Table 2: Potential FoxO3-interacting proteins differentially regulated by MEK5D.

In this table the top 10 FoxO3-bound proteins putatively upregulated by MEK5D together with the top 10 downregulated ones are reported. As for Suppl. Table 1, the protein names, the gene names and the "qNormalised LFQ ratio" values are indicated. The "qNormalised LFQ ratio" is calculated as the normalised log 2 of the ratio between the LFQ intensity values in the samples with 3xHA.FoxO3.A3.ER and the LFQ intensity values in the respective controls and after a second quantile normalisation to adjust for intra-experiment differences (n.d.: non determined). The "Impact of MEK5D" column indicates the fold-induction, or the fold-repression, of the interaction strength and it is determined as 2 to the power of [the positive difference between the "qNormalised LFQ ratio" of the two indicated conditions]. The interactions were considered as putatively regulated by MEK5D when the "Impact of MEK5D" value was smaller than -5-fold or higher than +5-folf. The best 5 up- and the best 5 down-regulated proteins are marked with "#", while the proteins which were already characterised as binding partners of TRRAP are indicated by "*". The established FoxO3 targets found as bound proteins were handled as false positive results and were omitted form the list.

PROTEIN	GENE	qNORMALISED LFQ RATIO (FoxO3/vector vs vector)	qNORMALISED LFQ RATIO (FoxO3/MEK5D vs vector/MEK5D)	IMPACT OF MEK5D (Fold)
NEDD4-like E3 ubiquitin-protein ligase WWP1#	*WWP1*	2.87	-2.12	-31.95
LIM and calponin homology domains-containing protein 1#	*LIMCH1*	4.55	0.27	-19.41
Alpha-enolase#	*ENO1*	4.00	n.d.	-15.95
Protein S100-A9#	*S100A9*	2.23	-1.70	-15.25
Unconventional myosin-XVIIIa#	*MYO18A*	3.44	-0.13	-11.89
Tissue factor pathway inhibitor	*TFPI*	3.19	n.d.	-9.12
Mitochondrial calcium uniporter protein	*MCU*	1.74	-1.37	-8.65
Rho-related GTP-binding protein RhoJ	*RHOJ*	2.96	n.d.	-7.78
Transmembrane emp24 domain-containing protein 7	*TMED7*	2.94	n.d.	-7.69
Proteasome subunit beta type-1	*PSMB1*	2.98	0.14	-7.16
Ubiquitin carboxyl-terminal hydrolase 7*#	*USP7*	0.13	4.50	+20.73
Protein AHNAK2#	*AHNAK2*	n.d.	4.19	+18.25
DNA-directed RNA polymerase I subunit A#	*POLR1A*	-0.75	2.66	+10.63
BAG family molecular chaperone regulator 2#	*BAG2*	n.d.	3.31	+9.91
Telomere-associated protein RIF1#	*RIF1*	-0.86	2.31	+9.03
Ubiquitin-like modifier-activating enzyme 1	*UBA1*	-0.29	2.80	+8.51
Coatomer subunit alpha	*COPA*	-0.35	2.71	+8.36
Melanoma-associated antigen D2	*MAGED2*	-0.05	2.91	+7.75
Regulator of nonsense transcripts 1	*UPF1*	-0.48	2.41	+ 7.39
Small subunit processome component 20 homolog	*UTP20*	-1.50	1.17	+6.34

REFERENCES

Abe, J., M. Kusuhara, R. J. Ulevitch, B. C. Berk, and J. D. Lee. 1996. 'Big mitogen-activated protein kinase 1 (BMK1) is a redox-sensitive kinase', *J Biol Chem*, 271: 16586-90.

Abid, M. R., S. Guo, T. Minami, K. C. Spokes, K. Ueki, C. Skurk, K. Walsh, and W. C. Aird. 2004. 'Vascular endothelial growth factor activates PI3K/Akt/forkhead signaling in endothelial cells', *Arterioscler Thromb Vasc Biol*, 24: 294-300.

Abid, M. R., S. C. Shih, H. H. Otu, K. C. Spokes, Y. Okada, D. T. Curiel, T. Minami, and W. C. Aird. 2006. 'A novel class of vascular endothelial growth factor-responsive genes that require forkhead activity for expression', *J Biol Chem*, 281: 35544-53.

Adam, C., L. Fusi, N. Weiss, S. G. Goller, K. Meder, V. G. Frings, H. Kneitz, M. Goebeler, R. Houben, D. Schrama, and M. Schmidt. 2020. 'Efficient Suppression of NRAS-Driven Melanoma by Co-Inhibition of ERK1/2 and ERK5 MAPK Pathways', *J Invest Dermatol*, 140: 2455-65 e10.

Adamowicz, M., J. Vermezovic, and F. d'Adda di Fagagna. 2016. 'NOTCH1 Inhibits Activation of ATM by Impairing the Formation of an ATM-FOXO3a-KAT5/Tip60 Complex', *Cell Rep*, 16: 2068-76.

Andrade, J., C. Shi, A. S. H. Costa, J. Choi, J. Kim, A. Doddaballapur, T. Sugino, Y. T. Ong, M. Castro, B. Zimmermann, M. Kaulich, S. Guenther, K. Wilhelm, Y. Kubota, T. Braun, G. Y. Koh, A. R. Grosso, C. Frezza, and M. Potente. 2021. 'Control of endothelial quiescence by FOXO-regulated metabolites', *Nat Cell Biol*, 23: 413-23.

Barlev, N. A., L. Liu, N. H. Chehab, K. Mansfield, K. G. Harris, T. D. Halazonetis, and S. L. Berger. 2001. 'Acetylation of p53 activates transcription through recruitment of coactivators/histone acetyltransferases', *Mol Cell*, 8: 1243-54.

Bartkova, J., J. Lukas, P. Guldberg, J. Alsner, A. F. Kirkin, J. Zeuthen, and J. Bartek. 1996. 'The p16-cyclin D/Cdk4-pRb pathway as a functional unit frequently altered in melanoma pathogenesis', *Cancer Res*, 56: 5475-83.

Benito-Jardon, L., M. Diaz-Martinez, N. Arellano-Sanchez, P. Vaquero-Morales, A. Esparis-Ogando, and J. Teixido. 2019. 'Resistance to MAPK Inhibitors in Melanoma Involves Activation of the IGF1R-MEK5-Erk5 Pathway', *Cancer Res*, 79: 2244-56.

Bhattacharya, S., and M. K. Ghosh. 2015. 'HAUSP regulates c-MYC expression via de-ubiquitination of TRRAP', *Cell Oncol (Dordr)*, 38: 265-77.

Biggs, W. H., 3rd, J. Meisenhelder, T. Hunter, W. K. Cavenee, and K. C. Arden. 1999. 'Protein kinase B/Akt-mediated phosphorylation promotes nuclear exclusion of the winged helix transcription factor FKHR1', *Proc Natl Acad Sci U S A*, 96: 7421-6.

Boccitto, M., and R. G. Kalb. 2011. 'Regulation of Foxo-dependent transcription by post-translational modifications', *Curr Drug Targets*, 12: 1303-10.

Bouchard, C., J. Marquardt, A. Bras, R. H. Medema, and M. Eilers. 2004. 'Myc-induced proliferation and transformation require Akt-mediated phosphorylation of FoxO proteins', *EMBO J*, 23: 2830-40.

Brenkman, A. B., P. L. de Keizer, N. J. van den Broek, A. G. Jochemsen, and B. M. Burgering. 2008. 'Mdm2 induces mono-ubiquitination of FOXO4', *PLoS One*, 3: e2819.

Brunet, A., A. Bonni, M. J. Zigmond, M. Z. Lin, P. Juo, L. S. Hu, M. J. Anderson, K. C. Arden, J. Blenis, and M. E. Greenberg. 1999. 'Akt promotes cell survival by phosphorylating and inhibiting a Forkhead transcription factor', *Cell*, 96: 857-68.

Brunet, A., J. Park, H. Tran, L. S. Hu, B. A. Hemmings, and M. E. Greenberg. 2001. 'Protein kinase SGK mediates survival signals by phosphorylating the forkhead transcription factor FKHRL1 (FOXO3a)', *Mol Cell Biol*, 21: 952-65.

Calissi, G., E. W. Lam, and W. Link. 2021. 'Therapeutic strategies targeting FOXO transcription factors', *Nat Rev Drug Discov*, 20: 21-38.

Calnan, D. R., and A. Brunet. 2008. 'The FoxO code', *Oncogene*, 27: 2276-88.

Calnan, D. R., A. E. Webb, J. L. White, T. R. Stowe, T. Goswami, X. Shi, A. Espejo, M. T. Bedford, O. Gozani, S. P. Gygi, and A. Brunet. 2012. 'Methylation by Set9 modulates FoxO3 stability and transcriptional activity', *Aging (Albany NY)*, 4: 462-79.

Cargnello, M., and P. P. Roux. 2011. 'Activation and function of the MAPKs and their substrates, the MAPK-activated protein kinases', *Microbiol Mol Biol Rev*, 75: 50-83.

Carrozza, M. J., R. T. Utley, J. L. Workman, and J. Cote. 2003. 'The diverse functions of histone acetyltransferase complexes', *Trends Genet*, 19: 321-9.

Castrillon, D. H., L. Miao, R. Kollipara, J. W. Horner, and R. A. DePinho. 2003. 'Suppression of ovarian follicle activation in mice by the transcription factor Foxo3a', *Science*, 301: 215-8.

Chandramohan, V., N. D. Mineva, B. Burke, S. Jeay, M. Wu, J. Shen, W. Yang, S. R. Hann, and G. E. Sonenshein. 2008. 'c-Myc represses FOXO3a-mediated transcription of the gene encoding the p27(Kip1) cyclin dependent kinase inhibitor', *J Cell Biochem*, 104: 2091-106.

Chen, J., A. R. Gomes, L. J. Monteiro, S. Y. Wong, L. H. Wu, T. T. Ng, C. T. Karadedou, J. Millour, Y. C. Ip, Y. N. Cheung, A. Sunters, K. Y. Chan, E. W. Lam, and U. S. Khoo. 2010. 'Constitutively nuclear FOXO3a localization predicts poor survival and promotes Akt phosphorylation in breast cancer', *PLoS One*, 5: e12293.

Chistiakov, D. A., A. N. Orekhov, and Y. V. Bobryshev. 2017. 'The impact of FOXO-1 to cardiac pathology in diabetes mellitus and diabetes-related metabolic abnormalities', *Int J Cardiol*, 245: 236-44.

Cox, J., M. Y. Hein, C. A. Luber, I. Paron, N. Nagaraj, and M. Mann. 2014. 'Accurate proteome-wide label-free quantification by delayed normalization and maximal peptide ratio extraction, termed MaxLFQ', *Mol Cell Proteomics*, 13: 2513-26.

Cox, J., and M. Mann. 2008. 'MaxQuant enables high peptide identification rates, individualized p.p.b.-range mass accuracies and proteome-wide protein quantification', *Nat Biotechnol*, 26: 1367-72.

Czymai, T., D. Viemann, C. Sticht, G. Molema, M. Goebeler, and M. Schmidt. 2010. 'FOXO3 modulates endothelial gene expression and function by classical and alternative mechanisms', *J Biol Chem*, 285: 10163-78.

Daly, C., V. Wong, E. Burova, Y. Wei, S. Zabski, J. Griffiths, K. M. Lai, H. C. Lin, E. Ioffe, G. D. Yancopoulos, and J. S. Rudge. 2004. 'Angiopoietin-1 modulates endothelial cell function and gene expression via the transcription factor FKHR (FOXO1)', *Genes Dev*, 18: 1060-71.

Dharaneeswaran, H., M. R. Abid, L. Yuan, D. Dupuis, D. Beeler, K. C. Spokes, L. Janes, T. Sciuto, P. M. Kang, S. S. Jaminet, A. Dvorak, M. A. Grant, E. R. Regan, and W. C. Aird. 2014. 'FOXO1-mediated activation of Akt plays a critical role in vascular homeostasis', *Circ Res*, 115: 238-51.

Dijkers, P. F., R. H. Medema, J. W. Lammers, L. Koenderman, and P. J. Coffer. 2000. 'Expression of the pro-apoptotic Bcl-2 family member Bim is regulated by the forkhead transcription factor FKHR-L1', *Curr Biol*, 10: 1201-4.

Doyon, Y., W. Selleck, W. S. Lane, S. Tan, and J. Cote. 2004. 'Structural and functional conservation of the NuA4 histone acetyltransferase complex from yeast to humans', *Mol Cell Biol*, 24: 1884-96.

Drew, B. A., M. E. Burow, and B. S. Beckman. 2012. 'MEK5/ERK5 pathway: the first fifteen years', *Biochim Biophys Acta*, 1825: 37-48.

Eijkelenboom, A., and B. M. Burgering. 2013. 'FOXOs: signalling integrators for homeostasis maintenance', *Nat Rev Mol Cell Biol*, 14: 83-97.

Elias-Villalobos, A., P. Fort, and D. Helmlinger. 2019. 'New insights into the evolutionary conservation of the sole PIKK pseudokinase Tra1/TRRAP', *Biochem Soc Trans*, 47: 1597-608.

Emerling, B. M., F. Weinberg, J. L. Liu, T. W. Mak, and N. S. Chandel. 2008. 'PTEN regulates p300-dependent hypoxia-inducible factor 1 transcriptional activity through Forkhead transcription factor 3a (FOXO3a)', *Proc Natl Acad Sci U S A*, 105: 2622-7.

Englert, C., X. Hou, S. Maheswaran, P. Bennett, C. Ngwu, G. G. Re, A. J. Garvin, M. R. Rosner, and D. A. Haber. 1995. 'WT1 suppresses synthesis of the epidermal growth factor receptor and induces apoptosis', *EMBO J*, 14: 4662-75.

English, J. M., G. Pearson, R. Baer, and M. H. Cobb. 1998. 'Identification of substrates and regulators of the mitogen-activated protein kinase ERK5 using chimeric protein kinases', *J Biol Chem*, 273: 3854-60.

Essers, M. A., L. M. de Vries-Smits, N. Barker, P. E. Polderman, B. M. Burgering, and H. C. Korswagen. 2005. 'Functional interaction between beta-catenin and FOXO in oxidative stress signaling', *Science*, 308: 1181-4.

Federici, M., A. Pandolfi, E. A. De Filippis, G. Pellegrini, R. Menghini, D. Lauro, M. Cardellini, M. Romano, G. Sesti, R. Lauro, and A. Consoli. 2004. 'G972R IRS-1 variant impairs insulin regulation of endothelial nitric oxide synthase in cultured human endothelial cells', *Circulation*, 109: 399-405.

Finkbeiner, M. G., C. Sawan, M. Ouzounova, R. Murr, and Z. Herceg. 2008. 'HAT cofactor TRRAP mediates beta-catenin ubiquitination on the chromatin and the regulation of the canonical Wnt pathway', *Cell Cycle*, 7: 3908-14.

Fuchs, M., J. Gerber, R. Drapkin, S. Sif, T. Ikura, V. Ogryzko, W. S. Lane, Y. Nakatani, and D. M. Livingston. 2001. 'The p400 complex is an essential E1A transformation target', *Cell*, 106: 297-307.

Furuyama, T., K. Kitayama, Y. Shimoda, M. Ogawa, K. Sone, K. Yoshida-Araki, H. Hisatsune, S. Nishikawa, K. Nakayama, K. Nakayama, K. Ikeda, N. Motoyama, and N. Mori. 2004. 'Abnormal angiogenesis in Foxo1 (Fkhr)-deficient mice', *J Biol Chem*, 279: 34741-9.

Furuyama, T., T. Nakazawa, I. Nakano, and N. Mori. 2000. 'Identification of the differential distribution patterns of mRNAs and consensus binding sequences for mouse DAF-16 homologues', *Biochem J*, 349: 629-34.

Fusi, L., R. Paudel, K. Meder, A. Schlosser, D. Schrama, M. Goebeler, and M. Schmidt. 2022. 'Interaction of transcription factor FoxO3 with histone acetyltransferase complex subunit TRRAP Modulates Gene Expression and Apoptosis', *J Biol Chem*: 101714.

Giard, D. J., S. A. Aaronson, G. J. Todaro, P. Arnstein, J. H. Kersey, H. Dosik, and W. P. Parks. 1973. 'In vitro cultivation of human tumors: establishment of cell lines derived from a series of solid tumors', *J Natl Cancer Inst*, 51: 1417-23.

Glatz, G., G. Gogl, A. Alexa, and A. Remenyi. 2013. 'Structural mechanism for the specific assembly and activation of the extracellular signal regulated kinase 5 (ERK5) module', *J Biol Chem*, 288: 8596-609.

Golson, M. L., and K. H. Kaestner. 2016. 'Fox transcription factors: from development to disease', *Development*, 143: 4558-70.

Graham, F. L., J. Smiley, W. C. Russell, and R. Nairn. 1977. 'Characteristics of a human cell line transformed by DNA from human adenovirus type 5', *J Gen Virol*, 36: 59-74.

Gui, T., and B. M. T. Burgering. 2021. 'FOXOs: masters of the equilibrium', *FEBS J*, doi: 10.1111/febs.16221.

Hagenbuchner, J., M. Rupp, C. Salvador, B. Meister, U. Kiechl-Kohlendorfer, T. Muller, K. Geiger, C. Sergi, P. Obexer, and M. J. Ausserlechner. 2016. 'Nuclear FOXO3 predicts adverse clinical outcome and promotes tumor angiogenesis in neuroblastoma', *Oncotarget*, 7: 77591-606.

Hamik, A., Z. Lin, A. Kumar, M. Balcells, S. Sinha, J. Katz, M. W. Feinberg, R. E. Gerzsten, E. R. Edelman, and M. K. Jain. 2007. 'Kruppel-like factor 4 regulates endothelial inflammation', *J Biol Chem*, 282: 13769-79.

Hayashi, M., S. W. Kim, K. Imanaka-Yoshida, T. Yoshida, E. D. Abel, B. Eliceiri, Y. Yang, R. J. Ulevitch, and J. D. Lee. 2004. 'Targeted deletion of BMK1/ERK5 in adult mice perturbs vascular integrity and leads to endothelial failure', *J Clin Invest*, 113: 1138-48.

Hayashi, M., and J. D. Lee. 2004. 'Role of the BMK1/ERK5 signaling pathway: lessons from knockout mice', *J Mol Med (Berl)*, 82: 800-8.

Hoang, V. T., T. J. Yan, J. E. Cavanaugh, P. T. Flaherty, B. S. Beckman, and M. E. Burow. 2017. 'Oncogenic signaling of MEK5-ERK5', *Cancer Lett*, 392: 51-59.

Hornsveld, M., T. B. Dansen, P. W. Derksen, and B. M. T. Burgering. 2018. 'Re-evaluating the role of FOXOs in cancer', *Semin Cancer Biol*, 50: 90-100.

Hosaka, T., W. H. Biggs, 3rd, D. Tieu, A. D. Boyer, N. M. Varki, W. K. Cavenee, and K. C. Arden. 2004. 'Disruption of forkhead transcription factor (FOXO) family members in mice reveals their functional diversification', *Proc Natl Acad Sci U S A*, 101: 2975-80.

Huang, H., K. M. Regan, F. Wang, D. Wang, D. I. Smith, J. M. van Deursen, and D. J. Tindall. 2005. 'Skp2 inhibits FOXO1 in tumor suppression through ubiquitin-mediated degradation', *Proc Natl Acad Sci U S A*, 102: 1649-54.

Jacobs, F. M., L. P. van der Heide, P. J. Wijchers, J. P. Burbach, M. F. Hoekman, and M. P. Smidt. 2003. 'FoxO6, a novel member of the FoxO class of transcription factors with distinct shuttling dynamics', *J Biol Chem*, 278: 35959-67.

Jiramongkol, Y., and E. W. Lam. 2020. 'FOXO transcription factor family in cancer and metastasis', *Cancer Metastasis Rev*, 39: 681-709.

Karki, S., M. G. Farb, D. T. Ngo, S. Myers, V. Puri, N. M. Hamburg, B. Carmine, D. T. Hess, and N. Gokce. 2015. 'Forkhead box O-1 modulation improves endothelial insulin resistance in human obesity', *Arterioscler Thromb Vasc Biol*, 35: 1498-506.

Kasler, H. G., J. Victoria, O. Duramad, and A. Winoto. 2000. 'ERK5 is a novel type of mitogen-activated protein kinase containing a transcriptional activation domain', *Mol Cell Biol*, 20: 8382-9.

Kato, Y., V. V. Kravchenko, R. I. Tapping, J. Han, R. J. Ulevitch, and J. D. Lee. 1997. 'BMK1/ERK5 regulates serum-induced early gene expression through transcription factor MEF2C', *EMBO J*, 16: 7054-66.

Kato, Y., R. I. Tapping, S. Huang, M. H. Watson, R. J. Ulevitch, and J. D. Lee. 1998. 'Bmk1/Erk5 is required for cell proliferation induced by epidermal growth factor', *Nature*, 395: 713-6.

Kim, D. H., J. Y. Kim, B. P. Yu, and H. Y. Chung. 2008. 'The activation of NF-kappaB through Akt-induced FOXO1 phosphorylation during aging and its modulation by calorie restriction', *Biogerontology*, 9: 33-47.

Kim, J. H., M. K. Kim, H. E. Lee, S. J. Cho, Y. J. Cho, B. L. Lee, H. S. Lee, S. Y. Nam, J. S. Lee, and W. H. Kim. 2007. 'Constitutive phosphorylation of the FOXO1A transcription factor as a prognostic variable in gastric cancer', *Mod Pathol*, 20: 835-42.

Komaravolu, R. K., C. Adam, J. R. Moonen, M. C. Harmsen, M. Goebeler, and M. Schmidt. 2015. 'Erk5 inhibits endothelial migration via KLF2-dependent down-regulation of PAK1', *Cardiovasc Res*, 105: 86-95.

Kops, G. J., N. D. de Ruiter, A. M. De Vries-Smits, D. R. Powell, J. L. Bos, and B. M. Burgering. 1999. 'Direct control of the Forkhead transcription factor AFX by protein kinase B', *Nature*, 398: 630-4.

Kyriakis, J. M., and J. Avruch. 2012. 'Mammalian MAPK signal transduction pathways activated by stress and inflammation: a 10-year update', *Physiol Rev*, 92: 689-737.

Lam, E. W., J. J. Brosens, A. R. Gomes, and C. Y. Koo. 2013. 'Forkhead box proteins: tuning forks for transcriptional harmony', *Nat Rev Cancer*, 13: 482-95.

Le, N. T., K. S. Heo, Y. Takei, H. Lee, C. H. Woo, E. Chang, C. McClain, C. Hurley, X. Wang, F. Li, H. Xu, C. Morrell, M. A. Sullivan, M. S. Cohen, I. M. Serafimova, J. Taunton, K. Fujiwara, and J. Abe.

2013. 'A crucial role for p90RSK-mediated reduction of ERK5 transcriptional activity in endothelial dysfunction and atherosclerosis', *Circulation*, 127: 486-99.

Lee, H. Y., S. W. Youn, J. Y. Kim, K. W. Park, C. I. Hwang, W. Y. Park, B. H. Oh, Y. B. Park, K. Walsh, J. S. Seo, and H. S. Kim. 2008. 'FOXO3a turns the tumor necrosis factor receptor signaling towards apoptosis through reciprocal regulation of c-Jun N-terminal kinase and NF-kappaB', *Arterioscler Thromb Vasc Biol*, 28: 112-20.

Lee, J. D., R. J. Ulevitch, and J. Han. 1995. 'Primary structure of BMK1: a new mammalian map kinase', *Biochem Biophys Res Commun*, 213: 715-24.

Lee, K. K., and J. L. Workman. 2007. 'Histone acetyltransferase complexes: one size doesn't fit all', *Nat Rev Mol Cell Biol*, 8: 284-95.

Lee, S., and H. H. Dong. 2017. 'FoxO integration of insulin signaling with glucose and lipid metabolism', *J Endocrinol*, 233: R67-R79.

Lempiainen, H., and T. D. Halazonetis. 2009. 'Emerging common themes in regulation of PIKKs and PI3Ks', *EMBO J*, 28: 3067-73.

Li, J., W. Du, S. Maynard, P. R. Andreassen, and Q. Pang. 2010. 'Oxidative stress-specific interaction between FANCD2 and FOXO3a', *Blood*, 115: 1545-8.

Lin, K., J. B. Dorman, A. Rodan, and C. Kenyon. 1997. 'daf-16: An HNF-3/forkhead family member that can function to double the life-span of Caenorhabditis elegans', *Science*, 278: 1319-22.

Lin, L., J. D. Hron, and S. L. Peng. 2004. 'Regulation of NF-kappaB, Th activation, and autoinflammation by the forkhead transcription factor Foxo3a', *Immunity*, 21: 203-13.

Lochhead, P. A., J. Clark, L. Z. Wang, L. Gilmour, M. Squires, R. Gilley, C. Foxton, D. R. Newell, S. R. Wedge, and S. J. Cook. 2016. 'Tumor cells with KRAS or BRAF mutations or ERK5/MAPK7 amplification are not addicted to ERK5 activity for cell proliferation', *Cell Cycle*, 15: 506-18.

McMahon, S. B., H. A. Van Buskirk, K. A. Dugan, T. D. Copeland, and M. D. Cole. 1998. 'The novel ATM-related protein TRRAP is an essential cofactor for the c-Myc and E2F oncoproteins', *Cell*, 94: 363-74.

Medema, R. H., R. Klompmaker, V. A. Smits, and G. Rijksen. 1998. 'p21waf1 can block cells at two points in the cell cycle, but does not interfere with processive DNA-replication or stress-activated kinases', *Oncogene*, 16: 431-41.

Medema, R. H., G. J. Kops, J. L. Bos, and B. M. Burgering. 2000. 'AFX-like Forkhead transcription factors mediate cell-cycle regulation by Ras and PKB through p27kip1', *Nature*, 404: 782-7.

Menghini, R., V. Casagrande, M. Cardellini, M. Ballanti, F. Davato, I. Cardolini, R. Stoehr, M. Fabrizi, M. Morelli, L. Anemona, I. Bernges, E. Schwedhelm, A. Ippoliti, A. Mauriello, R. H. Boger, and M. Federici. 2015. 'FoxO1 regulates asymmetric dimethylarginine via downregulation of dimethylaminohydrolase 1 in human endothelial cells and subjects with atherosclerosis', *Atherosclerosis*, 242: 230-5.

Menghini, R., V. Casagrande, G. Iuliani, S. Rizza, M. Mavilio, M. Cardellini, and M. Federici. 2020. 'Metabolic aspects of cardiovascular diseases: Is FoxO1 a player or a target?', *Int J Biochem Cell Biol*, 118: 105659.

Moonen, J. R., E. S. Lee, M. Schmidt, M. Maleszewska, J. A. Koerts, L. A. Brouwer, T. G. van Kooten, M. J. van Luyn, C. J. Zeebregts, G. Krenning, and M. C. Harmsen. 2015. 'Endothelial-to-mesenchymal transition contributes to fibro-proliferative vascular disease and is modulated by fluid shear stress', *Cardiovasc Res*, 108: 377-86.

Morgenstern, J. P., and H. Land. 1990. 'Advanced mammalian gene transfer: high titre retroviral vectors with multiple drug selection markers and a complementary helper-free packaging cell line', *Nucleic Acids Res*, 18: 3587-96.

Morimoto, H., K. Kondoh, S. Nishimoto, K. Terasawa, and E. Nishida. 2007. 'Activation of a C-terminal transcriptional activation domain of ERK5 by autophosphorylation', *J Biol Chem*, 282: 35449-56.

Mulloy, R., S. Salinas, A. Philips, and R. A. Hipskind. 2003. 'Activation of cyclin D1 expression by the ERK5 cascade', *Oncogene*, 22: 5387-98.

Murr, R., J. I. Loizou, Y. G. Yang, C. Cuenin, H. Li, Z. Q. Wang, and Z. Herceg. 2006. 'Histone acetylation by Trrap-Tip60 modulates loading of repair proteins and repair of DNA double-strand breaks', *Nat Cell Biol*, 8: 91-9.

Murr, R., T. Vaissiere, C. Sawan, V. Shukla, and Z. Herceg. 2007. 'Orchestration of chromatin-based processes: mind the TRRAP', *Oncogene*, 26: 5358-72.

Myatt, S. S., and E. W. Lam. 2007. 'The emerging roles of forkhead box (Fox) proteins in cancer', *Nat Rev Cancer*, 7: 847-59.

Nakamura, N., S. Ramaswamy, F. Vazquez, S. Signoretti, M. Loda, and W. R. Sellers. 2000. 'Forkhead transcription factors are critical effectors of cell death and cell cycle arrest downstream of PTEN', *Mol Cell Biol*, 20: 8969-82.

Ni, D., X. Ma, H. Z. Li, Y. Gao, X. T. Li, Y. Zhang, Q. Ai, P. Zhang, E. L. Song, Q. B. Huang, Y. Fan, and X. Zhang. 2014. 'Downregulation of FOXO3a promotes tumor metastasis and is associated with metastasis-free survival of patients with clear cell renal cell carcinoma', *Clin Cancer Res*, 20: 1779-90.

Nithianandarajah-Jones, G. N., B. Wilm, C. E. Goldring, J. Muller, and M. J. Cross. 2012. 'ERK5: structure, regulation and function', *Cell Signal*, 24: 2187-96.

Nwadozi, E., E. Roudier, E. Rullman, S. Tharmalingam, H. Y. Liu, T. Gustafsson, and T. L. Haas. 2016. 'Endothelial FoxO proteins impair insulin sensitivity and restrain muscle angiogenesis in response to a high-fat diet', *FASEB J*, 30: 3039-52.

Obsilova, V., J. Vecer, P. Herman, A. Pabianova, M. Sulc, J. Teisinger, E. Boura, and T. Obsil. 2005. '14-3-3 Protein interacts with nuclear localization sequence of forkhead transcription factor FoxO4', *Biochemistry*, 44: 11608-17.

Ohnesorge, N., D. Viemann, N. Schmidt, T. Czymai, D. Spiering, M. Schmolke, S. Ludwig, J. Roth, M. Goebeler, and M. Schmidt. 2010. 'Erk5 activation elicits a vasoprotective endothelial phenotype via induction of Kruppel-like factor 4 (KLF4)', *J Biol Chem*, 285: 26199-210.

Paik, J. H., R. Kollipara, G. Chu, H. Ji, Y. Xiao, Z. Ding, L. Miao, Z. Tothova, J. W. Horner, D. R. Carrasco, S. Jiang, D. G. Gilliland, L. Chin, W. H. Wong, D. H. Castrillon, and R. A. DePinho. 2007. 'FoxOs are lineage-restricted redundant tumor suppressors and regulate endothelial cell homeostasis', *Cell*, 128: 309-23.

Pajvani, U. B., and D. Accili. 2015. 'The new biology of diabetes', *Diabetologia*, 58: 2459-68.

Paudel, R., L. Fusi, and M. Schmidt. 2021. 'The MEK5/ERK5 Pathway in Health and Disease', *Int J Mol Sci*, 22.

Pi, X., G. Garin, L. Xie, Q. Zheng, H. Wei, J. Abe, C. Yan, and B. C. Berk. 2005. 'BMK1/ERK5 is a novel regulator of angiogenesis by destabilizing hypoxia inducible factor 1alpha', *Circ Res*, 96: 1145-51.

Pi, X., C. Yan, and B. C. Berk. 2004. 'Big mitogen-activated protein kinase (BMK1)/ERK5 protects endothelial cells from apoptosis', *Circ Res*, 94: 362-9.

Potente, M., C. Urbich, K. Sasaki, W. K. Hofmann, C. Heeschen, A. Aicher, R. Kollipara, R. A. DePinho, A. M. Zeiher, and S. Dimmeler. 2005. 'Involvement of Foxo transcription factors in angiogenesis and postnatal neovascularization', *J Clin Invest*, 115: 2382-92.

Puig, O., and J. Mattila. 2011. 'Understanding Forkhead box class O function: lessons from Drosophila melanogaster', *Antioxid Redox Signal*, 14: 635-47.

Qian, Z., L. Ren, D. Wu, X. Yang, Z. Zhou, Q. Nie, G. Jiang, S. Xue, W. Weng, Y. Qiu, and Y. Lin. 2017. 'Overexpression of FoxO3a is associated with glioblastoma progression and predicts poor patient prognosis', *Int J Cancer*, 140: 2792-804.

Ramaswamy, S., N. Nakamura, I. Sansal, L. Bergeron, and W. R. Sellers. 2002. 'A novel mechanism of gene regulation and tumor suppression by the transcription factor FKHR', *Cancer Cell*, 2: 81-91.

Regan, C. P., W. Li, D. M. Boucher, S. Spatz, M. S. Su, and K. Kuida. 2002. 'Erk5 null mice display multiple extraembryonic vascular and embryonic cardiovascular defects', *Proc Natl Acad Sci U S A*, 99: 9248-53.

Sakamaki, J., H. Daitoku, K. Yoshimochi, M. Miwa, and A. Fukamizu. 2009. 'Regulation of FOXO1-mediated transcription and cell proliferation by PARP-1', *Biochem Biophys Res Commun*, 382: 497-502.

Sanchez, A. M., R. B. Candau, and H. Bernardi. 2014. 'FoxO transcription factors: their roles in the maintenance of skeletal muscle homeostasis', *Cell Mol Life Sci*, 71: 1657-71.

Santamaria, C. M., M. C. Chillon, R. Garcia-Sanz, C. Perez, M. D. Caballero, F. Ramos, A. G. de Coca, J. M. Alonso, P. Giraldo, T. Bernal, J. A. Queizan, J. N. Rodriguez, P. Fernandez-Abellan, A. Barez, M. J. Penarrubia, M. B. Vidriales, A. Balanzategui, M. E. Sarasquete, M. Alcoceba, J. Diaz-Mediavilla, J. F. San Miguel, and M. Gonzalez. 2009. 'High FOXO3a expression is associated with a poorer prognosis in AML with normal cytogenetics', *Leuk Res*, 33: 1706-9.

Schmidt, M., S. Fernandez de Mattos, A. van der Horst, R. Klompmaker, G. J. Kops, E. W. Lam, B. M. Burgering, and R. H. Medema. 2002. 'Cell cycle inhibition by FoxO forkhead transcription factors involves downregulation of cyclin D', *Mol Cell Biol*, 22: 7842-52.

Schmidt, M., M. Goebeler, and S. F. Martin. 2016. 'Methods to Investigate the Role of Toll-Like Receptors in Allergic Contact Dermatitis', *Methods Mol Biol*, 1390: 319-40.

Schrama, D., G. Keller, R. Houben, C. G. Ziegler, C. S. Vetter-Kauczok, S. Ugurel, and J. C. Becker. 2008. 'BRAFV600E mutations in malignant melanoma are associated with increased expressions of BAALC', *J Carcinog*, 7: 1.

SenBanerjee, S., Z. Lin, G. B. Atkins, D. M. Greif, R. M. Rao, A. Kumar, M. W. Feinberg, Z. Chen, D. I. Simon, F. W. Luscinskas, T. M. Michel, M. A. Gimbrone, Jr., G. Garcia-Cardena, and M. K. Jain. 2004. 'KLF2 Is a novel transcriptional regulator of endothelial proinflammatory activation', *J Exp Med*, 199: 1305-15.

Sergi, C., F. Shen, and S. M. Liu. 2019. 'Insulin/IGF-1R, SIRT1, and FOXOs Pathways-An Intriguing Interaction Platform for Bone and Osteosarcoma', *Front Endocrinol (Lausanne)*, 10: 93.

Siqueira, M. F., S. Flowers, R. Bhattacharya, D. Faibish, Y. Behl, D. N. Kotton, L. Gerstenfeld, E. Moran, and D. T. Graves. 2011. 'FOXO1 modulates osteoblast differentiation', *Bone*, 48: 1043-51.

Skurk, C., H. Maatz, H. S. Kim, J. Yang, M. R. Abid, W. C. Aird, and K. Walsh. 2004. 'The Akt-regulated forkhead transcription factor FOXO3a controls endothelial cell viability through modulation of the caspase-8 inhibitor FLIP', *J Biol Chem*, 279: 1513-25.

Spiering, D., M. Schmolke, N. Ohnesorge, M. Schmidt, M. Goebeler, J. Wegener, V. Wixler, and S. Ludwig. 2009. 'MEK5/ERK5 signaling modulates endothelial cell migration and focal contact turnover', *J Biol Chem*, 284: 24972-80.

Stecca, B., and E. Rovida. 2019. 'Impact of ERK5 on the Hallmarks of Cancer', *Int J Mol Sci*, 20.

Storz, P., H. Doppler, J. A. Copland, K. J. Simpson, and A. Toker. 2009. 'FOXO3a promotes tumor cell invasion through the induction of matrix metalloproteinases', *Mol Cell Biol*, 29: 4906-17.

Su, B., L. Gao, C. Baranowski, B. Gillard, J. Wang, R. Ransom, H. K. Ko, and I. H. Gelman. 2014. 'A genome-wide RNAi screen identifies FOXO4 as a metastasis-suppressor through counteracting PI3K/AKT signal pathway in prostate cancer', *PLoS One*, 9: e101411.

Teixeira, C. C., Y. Liu, L. M. Thant, J. Pang, G. Palmer, and M. Alikhani. 2010. 'Foxo1, a novel regulator of osteoblast differentiation and skeletogenesis', *J Biol Chem*, 285: 31055-65.

Tullet, J. M. 2015. 'DAF-16 target identification in C. elegans: past, present and future', *Biogerontology*, 16: 221-34.

Tzivion, G., M. Dobson, and G. Ramakrishnan. 2011. 'FoxO transcription factors; Regulation by AKT and 14-3-3 proteins', *Biochim Biophys Acta*, 1813: 1938-45.

Urbanek, P., and L. O. Klotz. 2017. 'Posttranscriptional regulation of FOXO expression: microRNAs and beyond', *Br J Pharmacol*, 174: 1514-32.

van der Horst, A., A. M. de Vries-Smits, A. B. Brenkman, M. H. van Triest, N. van den Broek, F. Colland, M. M. Maurice, and B. M. Burgering. 2006. 'FOXO4 transcriptional activity is regulated by monoubiquitination and USP7/HAUSP', *Nat Cell Biol*, 8: 1064-73.

van Muijen, G. N., K. F. Jansen, I. M. Cornelissen, D. F. Smeets, J. L. Beck, and D. J. Ruiter. 1991. 'Establishment and characterization of a human melanoma cell line (MV3) which is highly metastatic in nude mice', *Int J Cancer*, 48: 85-91.

Viemann, D., M. Schmidt, K. Tenbrock, S. Schmid, V. Muller, K. Klimmek, S. Ludwig, J. Roth, and M. Goebeler. 2007. 'The contact allergen nickel triggers a unique inflammatory and proangiogenic gene expression pattern via activation of NF-kappaB and hypoxia-inducible factor-1alpha', *J Immunol*, 178: 3198-207.

Wang, X., A. J. Merritt, J. Seyfried, C. Guo, E. S. Papadakis, K. G. Finegan, M. Kayahara, J. Dixon, R. P. Boot-Handford, E. J. Cartwright, U. Mayer, and C. Tournier. 2005. 'Targeted deletion of mek5 causes early embryonic death and defects in the extracellular signal-regulated kinase 5/myocyte enhancer factor 2 cell survival pathway', *Mol Cell Biol*, 25: 336-45.

Wang, Z., T. Yu, and P. Huang. 2016. 'Post-translational modifications of FOXO family proteins (Review)', *Mol Med Rep*, 14: 4931-41.

Wei, X., V. Walia, J. C. Lin, J. K. Teer, T. D. Prickett, J. Gartner, S. Davis, Nisc Comparative Sequencing Program, K. Stemke-Hale, M. A. Davies, J. E. Gershenwald, W. Robinson, S. Robinson, S. A. Rosenberg, and Y. Samuels. 2011. 'Exome sequencing identifies GRIN2A as frequently mutated in melanoma', *Nat Genet*, 43: 442-6.

Weigel, D., G. Jurgens, F. Kuttner, E. Seifert, and H. Jackle. 1989. 'The homeotic gene fork head encodes a nuclear protein and is expressed in the terminal regions of the Drosophila embryo', *Cell*, 57: 645-58.

Wildey, G. M., and P. H. Howe. 2009. 'Runx1 is a co-activator with FOXO3 to mediate transforming growth factor beta (TGFbeta)-induced Bim transcription in hepatic cells', *J Biol Chem*, 284: 20227-39.

Wilhelm, K., K. Happel, G. Eelen, S. Schoors, M. F. Oellerich, R. Lim, B. Zimmermann, I. M. Aspalter, C. A. Franco, T. Boettger, T. Braun, M. Fruttiger, K. Rajewsky, C. Keller, J. C. Bruning, H. Gerhardt, P. Carmeliet, and M. Potente. 2016. 'FOXO1 couples metabolic activity and growth state in the vascular endothelium', *Nature*, 529: 216-20.

Xie, Q., Y. Hao, L. Tao, S. Peng, C. Rao, H. Chen, H. You, M. Q. Dong, and Z. Yuan. 2012. 'Lysine methylation of FOXO3 regulates oxidative stress-induced neuronal cell death', *EMBO Rep*, 13: 371-7.

Yamagata, K., H. Daitoku, Y. Takahashi, K. Namiki, K. Hisatake, K. Kako, H. Mukai, Y. Kasuya, and A. Fukamizu. 2008. 'Arginine methylation of FOXO transcription factors inhibits their phosphorylation by Akt', *Mol Cell*, 32: 221-31.

Yan, C., M. Takahashi, M. Okuda, J. D. Lee, and B. C. Berk. 1999. 'Fluid shear stress stimulates big mitogen-activated protein kinase 1 (BMK1) activity in endothelial cells. Dependence on tyrosine kinases and intracellular calcium', *J Biol Chem*, 274: 143-50.

Yan, L., J. Carr, P. R. Ashby, V. Murry-Tait, C. Thompson, and J. S. Arthur. 2003. 'Knockout of ERK5 causes multiple defects in placental and embryonic development', *BMC Dev Biol*, 3: 11.

Zhou, G., Z. Q. Bao, and J. E. Dixon. 1995. 'Components of a new human protein kinase signal transduction pathway', *J Biol Chem*, 270: 12665-9.

ACKNOWLEDGEMENTS

This long and not easy journey would have not been possible without the support of many people, which I would like to sincerely thank at this point.

First and foremost a great thank goes to Prof. Dr. Marc Schmidt, my first PhD supervisor. He happily welcomed me in his lab, first for my master's internship and later for my PhD. I really appreciate the trust he had in me, and I hope I could fulfil his expectations. I would like to thank him not only for providing the fundings for the project, but above all for the constant supervision, for answering to many questions, for being always available for explanations and help, and for the very constructive scientific exchange. In his lab I learnt how to be an excellent scientist, how to conduct experiments, and how to interpret the data. Thus, I can just thank him for having guided me through the PhD roller coaster.

I was lucky to have Prof. Dr. Elke Butt-Dörje and Dr. David Schrama as second and third supervisor, respectively. I want to thank them for the time they invested to mentor me and for the nice scientific discussions. I want to thank Elke for her always positive attitude and her encouraging and motivating words. Many thanks also to David for his constant assistance, even in the early night hours, and for letting me execute some of the experiments in his lab.

Essential for the success of my PhD has been the GSLS, a big family, where I always felt welcome. Thanks for funding my participation to congresses and for offering so many interesting workshops, which allowed me to improve my skill baggage. Above all I want to thank Dr. Blum-Oehler and Dr. Pleines-Meinhold for the precious guidance through the bureaucratical issues.

I also want to convey my thankful thoughts to Dr. Roland Houben and to the other group leaders of the Dermatology Department for their honest and helpful feedbacks given during our Friday seminars. I would like to mention Prof. Dr. med. Matthias Goebeler as well, for taking his time to join the seminars, for supporting me with suggestions and for funding my position between the grants. Speaking of fundings I want to thank the DFG and the IZKF institutions, which made possible to work on the project for almost five years.

Another person I would like to thank is Prof. Dr. Andreas Schlosser with his team. Thank you for the guidance during the optimisation of the HA-IP and for performing the MS analysis with my samples. The results brought me a big step further in my PhD path, allowed me to publish my first first-authorship paper and opened to interesting new research ideas.

I cannot absolutely forget the AG Schmidt lab members, many fantastic people with whom I daily shared my journey. It might sound predictable, but without their support I would not have reached this finish line. I did not find only colleagues, but also people I could count on in every moment. When the experiments landed in the rubbish, when the results were the best ever, when I needed some help with scraping a plate, when just a coffee or a good word was needed to

improve a bad day, when… they were there. Remarkably, I want to thank Christian, who concretely guided me in the lab from the first second I entered it. Thank for his patience, for the knowledge he shared with me and for the nice time we spent shoulder to shoulder at the bench. Helga also needs a special mention, as she supported me from the very beginning until she retired and made my path easier with all her technical expertise. Furthermore, I want to thank Andrea and Rupesh for the enormous work they did during the revision of the paper, making possible its publication, and Verena for her always light-hearted and happy mood and for infecting the colleagues with it. Last but not least, an ocean of thanks goes to Katharina: the one who walked the whole path side-by-side with me, investing all the energies she could. I cannot write how thankful I am, I guess I can only wrap it up in a very famous quote from her: "I Pinky, you Brain".

I want to also acknowledge all the other research people I met in the cellars of the Dermatology Department, especially the people from Kerstan's lab, Sonja, Bhavishya, and Simone. Having the possibility to ask for help at any time of the day and to talk to somebody during the boring waiting times was really a gift.

Next in the list I want to thank all my friends from Bagolino. The 700 km in between us do not make easy to maintain a friendship, and a pandemic neither helped. I can be just glad to have them as friends, because whenever I come back in Bagolino it always seems like I left just a day earlier. I would like to thank them for having accepted my decision to leave and for still being there. Alice, Chiara, Elisa, Lidia, Lodovica and Paola deserve a deeper thank: our more or less regular Zoom meetings help to kill the distance, are always a revitalizing wind and a moment of true happiness. And the same applies to the girlz from the Marianum university residence: Anna, Annagiulia, Francesca, Giulia, Laura, Martina e Vittoria.

During this long path there was one big polar light, which did not stop to shine and guided me. My big loud and chaotic Italian family: mamma Mariella, papà Giovita, Alessandra, Claudio, Massimo, Samuele, Tommaso, Cristian, Monica, Noemi and Riccardo. I will be never able to thank them enough for all the energy they provided me. Despite the distance and the rules of the pandemic, I could feel their hands holding mine for the whole time. A huge thank you to my grandparents: the good memories with them are imprinted in the soul and they will always be an example to follow. They all have always been, and they will always be my polar light and sunshine.

And finally, last but absolutely not the least: Jonas. A biologist, a friend, a motivator, a shoulder, an excellent cook, a private driver, a supporter, but above all my deepest love. Without him by my side, I would not be the person I am and the way to reach the PhD would have been way harder. I could count on him since the very first moment we met, and I know I can count on him for all the days of my life. Together with him I would like to thank his family: Dagmar, Ernst, Linda, and Malin. They accepted me since the beginning as new family member and their support and warmth have also helped me a lot while walking along this path, above all in the last years.

PUBLICATIONS LIST

• **Fusi L**, Paudel R, Meder K, Schlosser A, Schrama D, Goebeler M, Schmidt M. Interaction of transcription factor FoxO3 with histone acetyltransferase complex subunit TRRAP modulates gene expression and apoptosis. J Biol Chem. 2022 Mar;298(3):101714. doi: 10.1016/j.jbc.2022.101714. Epub 2022 Feb 11. PMID: 35151693; PMCID: PMC8914384.

• Paudel R, **Fusi L**, Schmidt M. The MEK5/ERK5 Pathway in Health and Disease. Int J Mol Sci. 2021 Jul 15;22(14):7594. doi: 10.3390/ijms22147594. PMID: 34299213; PMCID: PMC8303459.

• Adam C, **Fusi L**, Weiss N, Goller SG, Meder K, Frings VG, Kneitz H, Goebeler M, Houben R, Schrama D, Schmidt M. Efficient Suppression of NRAS-Driven Melanoma by Co-Inhibition of ERK1/2 and ERK5 MAPK Pathways. J Invest Dermatol. 2020 Dec;140(12):2455-2465.e10. doi: 10.1016/j.jid.2020.03.972. Epub 2020 May 4. PMID: 32376279.

CURRICULUM VITAE